الجمهورية الجزائرية الديمقراطية الشعبي

وزارة التعليم العالي والبحث العلمي

UNIVERSITÉ BADJI MOKHTAR - ANNABA
BADJI MOKHTAR – ANNABA UNIVERSITY

جامعة باجي مختار – عنابـــــــــــة

Faculty of Technology
Department of Mechanical Engineering
Science and Technology Domain
Major: Mechanical Engineering Specialization: Materials Engineering

DISSERTATION

Submitted in Partial Fulfillment of the Requirements for the Master's Degree

Thesis Title:

ANALYSIS OF STRESS-STRAIN BEHAVIOR AND MECHANICAL PROPERTIES ACROSS THE WALL OF AN HDPE-100 PIPE BASED ON STANDARDIZED TEST SPECIMENS

Presented by: *BOUGHAZI YOUSRA*

Supervisor: *Professor Chaoui Kamel — University: Badji Mokhtar Annaba*

Jury :

Pr. Hamadache Hamid	Professor	UBM Annaba	Examiner
Dr. Rahmaoui Fateheddine Zakaria	MCB	UBM Annaba	Examiner
Pr. Chaoui Kamel	Professor	UBM Annaba	Examiner

Academic Year: 2024/2025

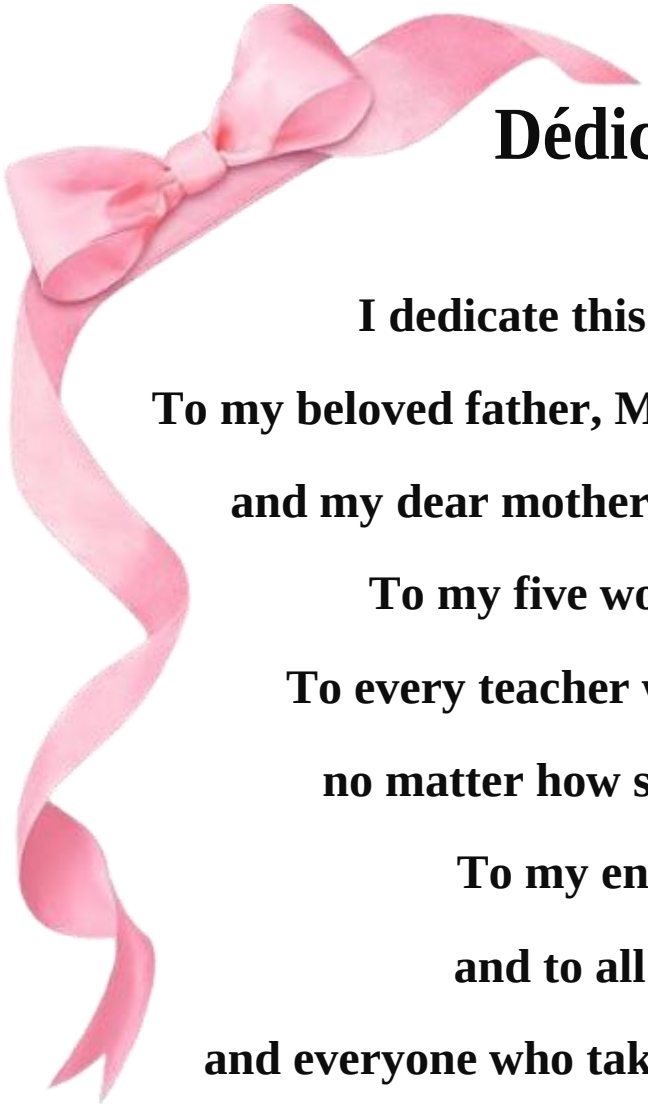

Dédicacions

I dedicate this work to myself,

To my beloved father, Mr. Abdelwahab Boughazi,

and my dear mother, Mrs. Anane Karima,

To my five wonderful sisters,

To every teacher who ever taught me

no matter how small the lesson is,

To my entire family,

and to all my friends

and everyone who takes the time to read this.

Acknowledgements

All praise and thanks are due to Allah, Lord of all worlds, who granted me success. Indeed, whoever doesn't thank Allah won't thank people.

I extend my sincere gratitude to all the esteemed professors **who taught me throughout my five years at the university. I'd like to especially thank my supervisor,** Professor Kamel Chaoui**, for overseeing my thesis completion so thoroughly and for allowing me to experience genuine scientific research.**

My thanks also go to SIDER El Hadjar Company **for their warm reception, assistance, and guidance. Special appreciation goes to the workers in the** AMM branch**, whose support made my practical work run smoothly, despite limited resources and unsuitable equipment.**

I must also acknowledge my father, Abdelwahab Boughazi**, who was a constant source of material and moral support, as well as my mother,** Anane Karima**.**

I thank my friend Allali Anfal **for her help with coordination, and the members of the** LR3MI lab **for their valuable guidance.**

Finally, I thank myself for all the efforts I've put in.

List of figures

Chapter I: Literature Review on HDPE-100

Chapter II: Preparation of Test Specimens and Experimental Methodology

Chapter III: Mechanical Behavior of HDPE under Aggressive Environment

CHAPTER I : **Literature Review on HDPE-100 Extruded Water Pipes**

Liste des tableaux

Table of Contents

CHAPTER I : Literature Review on HDPE-100 Extruded Water Pipes

Abstract.

The mechanical behavior and characteristics of High-Density Polyethylene (HDPE-100) pipes are thoroughly investigated experimentally and analytically in this thesis, with an emphasis on comprehending how the material reacts across the thickness of its walls and in harsh environmental settings. Standardized tensile samples and rectangular prism samples were painstakingly manufactured and tested in order to accomplish this. These samples were taken from an HDPE-100 water pipe in a variety of orientations (longitudinal and transverse) and layers (outer, middle, and inner). A set of reference (untreated) samples and samples that were immersed in IGEPAL solution, a realistic aggressive environment, for predetermined periods of seven and twenty-one days were included in the study. The experimental findings provided important new information. First off, even in the reference condition, differences in Young's modulus and stress-strain characteristics were noted in various orientations and across pipe wall layers, suggesting that the material's mechanical properties are inherently heterogeneous and most likely the result of manufacturing procedures. Second, and perhaps most importantly, the study showed that immersion in IGEPAL solution had a significant effect. After seven days of immersion, several samples showed a slow but discernible increase in Young's modulus. After 21 days, this increase became noticeably more noticeable in some samples, especially in the outer layers and in some orientations, where Young's modulus values increased drastically (e.g., reaching up to about 45 for some longitudinal outer samples). This significant rise indicates severe material hardening, which is frequently linked to a higher propensity for brittleness and a possible loss of ductility. The length of exposure, the orientation of the sample, and its location within the pipe wall were found to have a significant impact on the magnitude of this environmental effect. These results highlight how important it is to take into account HDPE-100 pipes' inherent heterogeneity as well as the material's vulnerability to environmental deterioration when designing, producing, and deploying these pipes. The long-term dependability and operational safety of HDPE pipe systems in harsh settings can be significantly impacted by the noted changes in mechanical properties. In order to guarantee the long-term performance of HDPE infrastructure, this research opens the door for better material selection, design optimization, and proactive maintenance techniques by giving engineers useful data and advancing our understanding of polymer material science in difficult applications.

الملخص

تقدم هذه المذكرة تحقيقاً تجريبياً وتحليلياً شاملاً في السلوك الميكانيكي وخصائص أنابيب البولي إيثيلين عالي الكثافة (HDPE-100)، مع تركيز خاص على فهم استجابة المادة عبر سمك جدارها وتحت ظروف بيئية عدوانية. لتحقيق ذلك، تم إعداد واختبار عينات شد قياسية وعينات متوازي مستطيلات بدقة. تم استخلاص هذه العينات من طبقات مختلفة (الخارجية، الوسطى، الداخلية) واتجاهات متعددة (طولية وعرضية) من أنبوب ماء مصنوع من HDPE-100وشملت الدراسة مجموعة من العينات المرجعية (غير المعالجة) وعينات تعرضت للغمر في محلول الإيجبال، وهو بيئة عدوانية ممثلة، لفترات زمنية محددة هي 7 و 21 يوماً.

كشفت النتائج التجريبية عن رؤى مهمة. أولاً، حتى في الحالة المرجعية، لوحظت اختلافات في خصائص الإجهاد–الانفعال ومعامل يونغ عبر طبقات جدار الأنبوب وفي الاتجاهات المختلفة، مما يشير إلى عدم تجانس متأصل في الخصائص الميكانيكية للمادة، والذي يرجح أن يكون ناتجاً عن عمليات التصنيع. ثانياً، والأهم من ذلك، أظهرت الدراسة تأثيراً عميقاً للغمر في محلول الإيجبال. فقد لوحظت زيادة تدريجية ولكن ملحوظة في معامل يونغ لبعض العينات بعد 7 أيام من الغمر. وتصاعدت هذه الزيادة بشكل كبير وملحوظ في عينات محددة بعد 21 يوماً، خاصة في الطبقات الخارجية واتجاهات معينة، حيث ارتفعت قيم معامل يونغ بشكل كبير (على سبيل المثال، وصلت إلى حوالي 45 لبعض العينات الطولية الخارجية). تشير هذه الزيادة الكبيرة إلى تصلب شديد للمادة، والذي غالباً ما يرتبط بفقدان محتمل للمطيليّة وزيادة في الميل نحو الهشاشة. وقد وُجد أن مدى هذا التأثير البيئي يعتمد بشكل كبير على مدة التعرض، وموقع العينة داخل جدار الأنبوب، واتجاهها.

تؤكد هذه النتائج على الحاجة الماسة لأخذ كل من عدم التجانس المتأصل لأنابيب HDPE-100 وقابلية المادة للتدهور البيئي في الاعتبار عند تصميم، تصنيع، وتطبيق هذه الأنابيب. يمكن للتغيرات الملحوظة في الخصائص الميكانيكية أن تؤثر بشكل حاسم على الموثوقية طويلة الأمد والسلامة التشغيلية لأنظمة أنابيب HDPE في البيئات العدوانية. يوفر هذا البحث بيانات قيمة للمهندسين ويساهم في فهم أعمق لعلم مواد البوليمرات في التطبيقات الصعبة، مما يمهد الطريق لتحسين اختيار المواد، وتحسين التصميم، واستراتيجيات الصيانة الاستباقية لضمان الأداء المستدام للبنية التحتية المصنوعة من HDPE.

Résumé

Cette thèse présente une investigation expérimentale et analytique approfondie du comportement mécanique et des propriétés des tubes en polyéthylène haute densité (HDPE-100), en mettant l'accent sur la compréhension de la réaction du matériau à travers l'épaisseur de sa paroi et dans des environnements agressifs. Pour ce faire, des échantillons de traction normalisés et des échantillons de prismes rectangulaires ont été méticuleusement fabriqués et testés. Ces échantillons ont été prélevés sur une conduite d'eau en HDPE-100 dans diverses orientations (longitudinale et transversale) et couches (externe, médiane et interne). L'étude a inclus un ensemble d'échantillons de référence (non traités) et des échantillons qui ont été immergés dans une solution d'IGEPAL, un environnement agressif réaliste, pendant des périodes prédéterminées de 7 et 21 jours. Les résultats expérimentaux ont fourni de nouvelles informations importantes. Tout d'abord, même dans la condition de référence, des différences dans le module d'Young et les caractéristiques contrainte-déformation ont été observées dans diverses orientations et à travers les couches de la paroi du tube, suggérant que les propriétés mécaniques du matériau sont intrinsèquement hétérogènes et très probablement le résultat des procédures de fabrication. Deuxièmement, et c'est peut-être le plus important, l'étude a montré que l'immersion dans la solution d'IGEPAL avait un effet significatif. Après sept jours d'immersion, plusieurs échantillons ont montré une augmentation lente mais discernable du module d'Young. Après 21 jours, cette augmentation est devenue nettement plus prononcée chez certains échantillons, en particulier dans les couches externes et dans certaines orientations, où les valeurs du module d'Young ont augmenté drastiquement (par exemple, atteignant environ 45 pour certains échantillons longitudinaux externes). Cette augmentation significative indique un durcissement sévère du matériau, qui est fréquemment lié à une propension plus élevée à la fragilité et à une perte possible de ductilité. Il a été constaté que la durée d'exposition, l'orientation de l'échantillon et son emplacement dans la paroi du tube avaient un impact significatif sur l'ampleur de cet effet environnemental. Ces résultats soulignent l'importance de prendre en compte l'hétérogénéité inhérente des tubes en HDPE-100 ainsi que la vulnérabilité du matériau à la détérioration environnementale lors de la conception, de la production et du déploiement de ces tubes. La fiabilité à long terme et la sécurité opérationnelle des systèmes de tuyauterie en HDPE dans des environnements difficiles peuvent être considérablement affectées par les changements observés dans les propriétés mécaniques. Afin de garantir les performances à long terme des infrastructures en HDPE, cette recherche ouvre la voie à une meilleure sélection des matériaux, à l'optimisation de la conception et à des techniques de maintenance proactives en fournissant aux ingénieurs des données utiles et en améliorant notre compréhension de la science des matériaux polymères dans des applications difficiles.

General Introduction

Because of their unique and varied qualities—which include lightness, flexibility, chemical resistance, and ease of processing—polymeric materials have completely transformed contemporary industry. High-Density Polyethylene (HDPE), and more especially the HDPE-100 grade, has become a popular and affordable option for many important engineering applications within this broad category. Because of their exceptional resistance to corrosion, flexibility, and capacity to tolerate both internal and external pressures, HDPE-100 pipes have become an essential part of everything from gas pipelines and chemical industries to drinking water distribution networks and sewage systems.

Despite these important benefits, HDPE-100 pipes' long-term performance and operational dependability in real-world settings remain problematic, necessitating a thorough comprehension of their mechanical behavior under varied circumstances. There are two main factors that drive this behavior: The first is the intrinsic variation in mechanical characteristics throughout the thickness of the pipe wall. The material's microstructure may exhibit gradients between the outer, middle, and inner layers as a result of manufacturing techniques including extrusion and cooling. These variations in microstructure might represent variations in the material's stiffness and ductility. Second, continuous exposure to aggressive service conditions, such as soil with a particular chemical makeup or groundwater that contains organic or inorganic compounds that can react with the polymer, can cause the material's mechanical properties to gradually change, which can compromise the integrity and lifespan of the pipe.

According to this viewpoint, comprehensive research is desperately needed to assess these coupled factors. The thorough experimental and analytical investigation presented in this thesis aims to pinpoint the exact mechanical behavior of HDPE-100 pipes. The effort is focused on the following main goals: (1) Determining the degree of internal property homogeneity or heterogeneity by analyzing the stress-strain characteristics and basic mechanical properties (like Young's modulus) of samples taken from various layers (outer, middle, and inner) and multiple orientations (longitudinal, transverse) across the pipe wall

(2) Evaluating the effects of exposure to IGEPAL (a detergent constituent) solution, which was chosen to depict a particular harsh environment pertinent to real-world pipe applications, on these mechanical characteristics following varying immersion times (7 and 21 days). In order to give a thorough and cohesive understanding of the material's behavior, the study used tensile testing on standardized tensile samples in addition to tests on rectangular prism samples.

This study intends to provide scientific data that advance our understanding of HDPE-100 pipe performance through its meticulous methodology and thorough analysis of the findings. This will help engineers and designers make better decisions about material selection, system design, and maintenance plans, increasing infrastructure reliability and promoting sustainable development in key industries.

Chapter I:

Literature Review on HDPE-100 Extruded Water Pipes

CHAPTER I : **Literature Review on HDPE-100 Extruded Water Pipes**

1. Introduction

High-density polyethylene (HDPE), particularly in its PE100 grade, is a semi-crystalline thermoplastic polymer widely used in industrial applications that require strong and durable materials. It stands out for its high rigidity, remarkable mechanical strength, and chemical stability, making it ideal for manufacturing pressure pipes for potable water, natural gas, and transportation of other fluids. The growing interest in HDPE-100 is due to its enhanced performance in slow crack growth (SCG) resistance and long-term creep resistance which are critical factors in ensuring longevity and reliability of pipeline networks [1].

Historically, polyethylene was first synthesized accidentally in 1933 by Eric Fawcett and Reginald Gibson at Imperial Chemical Industries (ICI) in England. This fortuitous discovery led to the industrial production of low-density polyethylene (LDPE) under high pressure. However, it wasn't until 1953 that German chemist Karl Ziegler, in collaboration with Erhard Holzkamp, succeeded in polymerizing ethylene at low pressure and temperature using organometallic catalysts, leading to HDPE [2]. This breakthrough enabled the production of linear polyethylene with higher density and superior mechanical properties.

The subsequent development of the Ziegler-Natta process, notably by Giulio Natta, revolutionized polyolefin production, allowing better control of polymer molecular structure. This innovation earned Ziegler and Natta the Nobel Prize in Chemistry in 1963 for their work on polymerization catalysts [3].

PE100, as an advanced grade of HDPE, was specifically designed to meet the strict requirements of pressure applications. It offers exceptional resistance to slow crack growth, increased toughness, and improved long-term performance under constant loading conditions [4]. These characteristics are essential to ensure the safety and durability of fluid transport infrastructures.

A deep understanding of the mechanical behavior of PE-100, especially its stress-strain response and through-thickness properties, is crucial for optimizing its implementation and predicting service life. Recent studies have highlighted the importance of microstructure, crystallinity, and molecular orientation induced by manufacturing processes on the material's mechanical performance [5-6]. However, given the critical role of PE-100 in demanding applications and the potential influence of manufacturing processes on the homogeneity of its mechanical properties across pipe walls, two fundamental questions arise: *(i)* How precisely do the stress-strain behavior and mechanical properties (*such as Young's modulus, tensile strength, and elongation at break*) vary through the thickness of a PE-100 pipe, and *(ii)* what are the implications of such variations for the structural integrity of the pipe and its long-term durability?

2. Chemical Structure and Morphology of HDPE-100

As shown in Figures I.1 and I.2, HDPE is a fundamental polyolefin polymer, structurally composed of repeating ethylene monomer units $(–CH_2–CH_2–)_n$ [7].

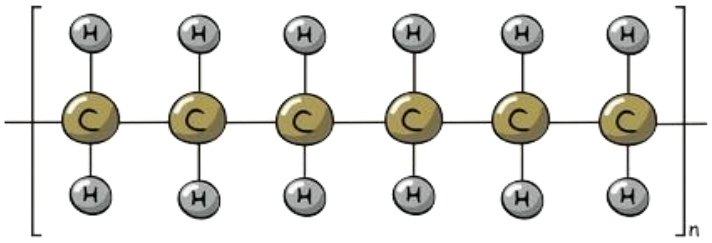

Figure I.1: Linear polyethylene structure [8].

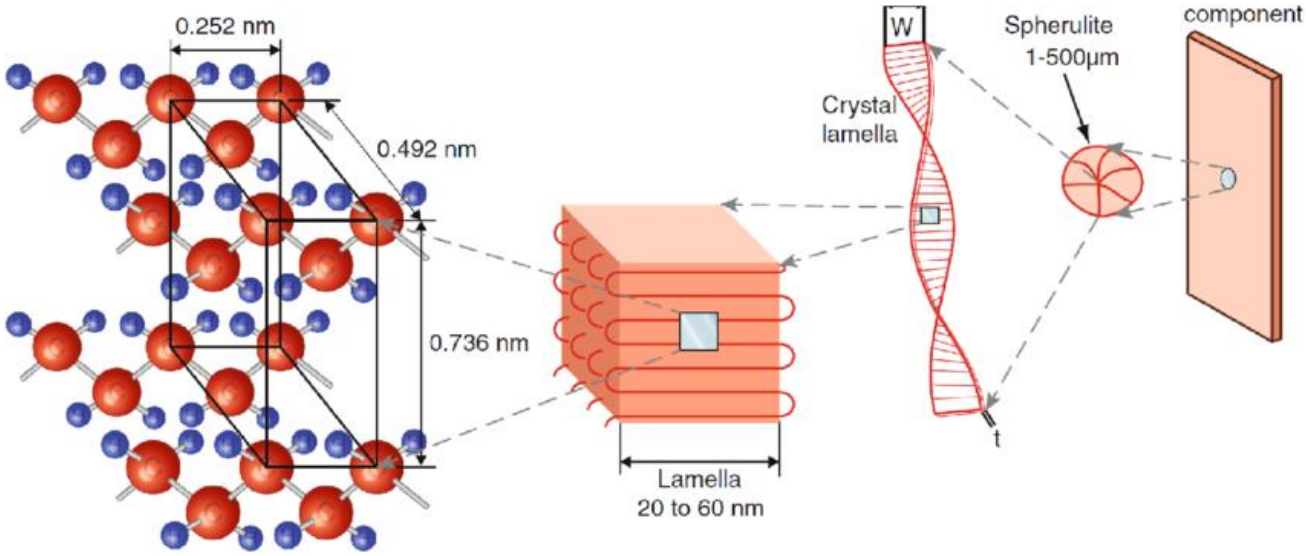

Figure I.2: Molecular structure schematic of high-density polyethylene (HDPE) [9].

The apparent simplicity of this molecular structure withholds the complexity of its physical behavior, especially in its semi-crystalline form, where the polymer chains are partially ordered into crystalline lamellae interspersed within an amorphous matrix. PE-100, an advanced grade of HDPE, is characterized by a high molecular weight distribution and a very low degree of long-chain branching [10]. These precise molecular architecture characteristics are crucial for the polymer's ability to form highly crystalline and mechanically robust structures, which confer upon it the renowned performance properties for which it is known. The production of PE100 typically involves the use of advanced catalyst systems such as new-generation Ziegler-Natta catalysts or metallocene catalysts. These catalysts enable exceptional control over the polymer's molecular

architecture, promoting the formation of linear macromolecules with uniform chain lengths (Figure I.3) .

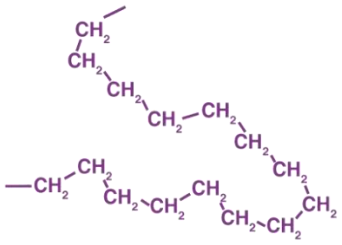

Figure I.3: High-density polyethylene polymer chain model [11].

This precise control leads to higher levels of crystallinity (often exceeding 70%) and narrower molecular weight distributions. These specific morphological features are essential for improving the material's resistance to slow crack growth (SCG) and enhancing its mechanical stability under continuous, long-term stresses, which are critical factors in high-performance pipe applications. From a morphological perspective, the microstructure of such material exhibits multiple, complex hierarchical levels. At the atomic level, the crystalline regions adopt an orthorhombic lattice structure [12].

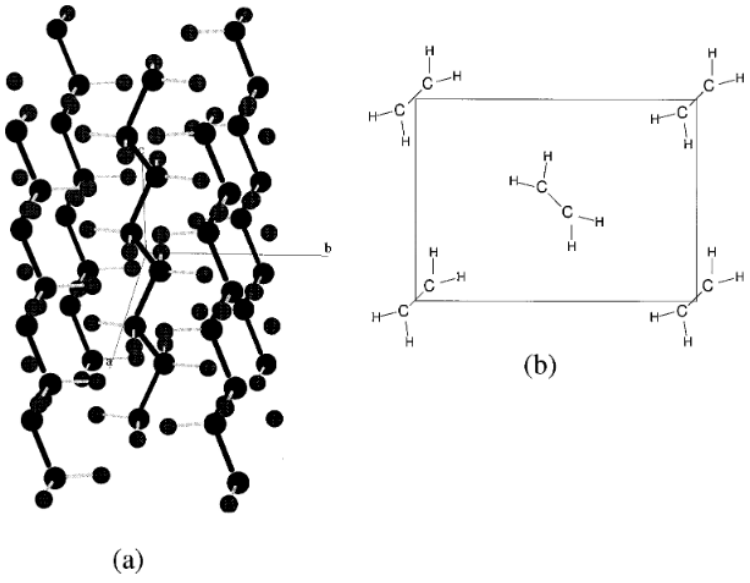

Figure I.4: Crystalline structure of polyethylene, (a) Side-view of orthorhombic structure, (b) Projection of unit cell on the [a-b] plane [12].

This structure is characterized by distinct unit cell parameters, with approximate values of a* = 7.4 Å, b* = 4.9 Å, and c* = 2.55 Å, where the c*-axis corresponds to the direction of the polymer chain. These crystalline domains, referred to as lamellae, form thin layers typically ranging from 10 to 20 nm in thickness. These lamellae are formed during the cooling phase of the manufacturing

process, as polymer chains repeatedly fold back upon themselves to minimize the system's free energy, leading to this crystalline arrangement. These lamellae interlink and are embedded within an amorphous phase composed of uncrystallized chain segments, molecular entanglements, free chain ends, and additives. This combination results in a two-phase system that fundamentally defines the material's overall mechanical response [13].

At the microscopic level, the crystalline lamellae organize radially to form larger superstructures known as spherulites. The diameters of these spherical domains can range from a few micrometers to several hundred micrometers, and they form during the solidification of the molten polymer, growing outwards from nucleation sites [13,14]. When examined under a polarized light microscope, these spherulites reveal a characteristic "Maltese Cross" pattern resulting from birefringence, which is a visual manifestation of the radial orientation of the lamellae. The size and perfection of these spherulites are significantly influenced by factors such as cooling rates, the polymer's molecular weight, the presence of nucleating agents, and the stresses applied during processing. For instance, rapid quenching or shear flow during the extrusion process can lead to the formation of smaller, more irregular spherulites and alter the orientation of the lamellae, directly contributing to anisotropy in mechanical properties across the pipe wall [14].

At the macroscopic scale, this morphological organization plays a crucial role in determining the pipe's behavior under mechanical loads. Regions with higher crystallinity, typically found closer to the outer pipe wall due to faster cooling rates, exhibit higher stiffness and greater yield strength . Conversely, the inner pipe wall often shows lower crystallinity, leading to higher ductility but reduced resistance to long-term failure mechanisms such as slow crack growth or creep rupture [15]. These structural gradients can be accurately measured using advanced techniques such as Differential Scanning Calorimetry (DSC, Figure I.5), X-ray Diffraction (XRD), and polarized optical microscopy. These measurements have been extensively correlated with variations in Young's modulus, tensile strength, and elongation at break across the pipe's cross-section [16].

In summary, the superior performance of PE100 stems not only from its chemical purity and molecular weight but also from its highly optimized crystalline morphology [17,18]. However, the very same manufacturing processes that impart these desirable features also introduce internal heterogeneities within the material. These variations must be carefully understood and managed to ensure uniform and reliable mechanical performance across the entire pipe wall [17]. Consequently, a detailed investigation into these morphological variations is essential to support

structural integrity assessments, failure predictions, and the development of more accurate design standards for critical HDPE piping systems.

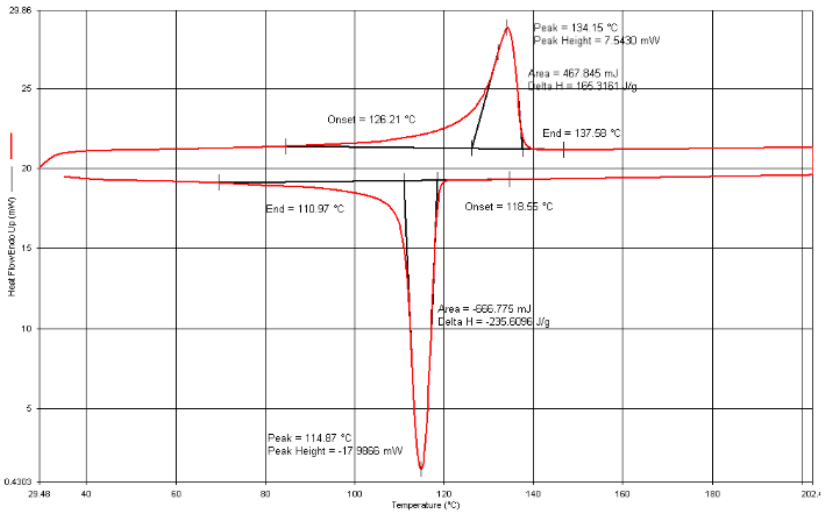

Figure I.5: DSC curve for sample-1 (High-Density Polyethylene) [19]**.**

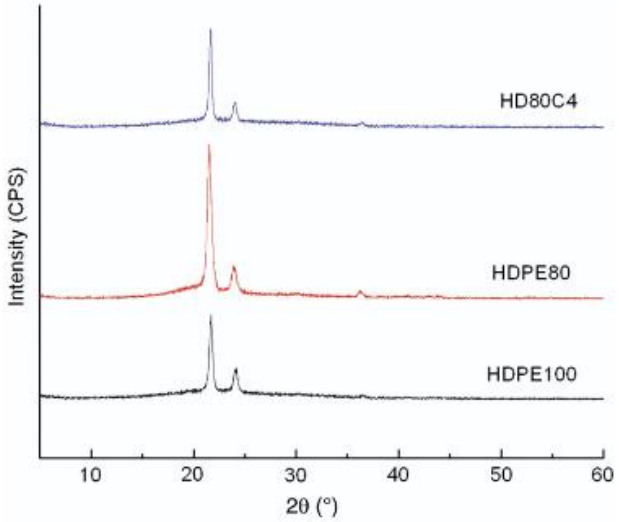

Figure I.6: X-ray diffraction (XRD) spectra of HDPE blends [20].

2. Classification by Density and Applications

Polyethylene is classified into 4 main categories based on density and branching (Table I.1):

1. LDPE (Low-Density PE): Highly branched, ρ: 0.910 – 0.925 g/cm³.
2. LLDPE (Linear LDPE): Short-chain branching, ρ: 0.915 – 0.925 g/cm³.
3. MDPE (Medium-Density PE), ρ : 0.926–0.940 g/cm³.
4. HDPE (High-Density PE): Linear structure, ρ ≥ 0.941 g/cm³ [21].

Table I.1: Classification and Properties of Polyethylene Types [22].

Type	Density (g/cm³)	Branching Structure	Crystallinity (%)	Key Applications
LDPE	0.910–0.925	Long, irregular branches	40–50	Packaging films
LLDPE	0.915–0.925	Short, uniform branches	50–60	Stretch wrap, containers
HDPE	≥0.941	Minimal branching	70–80	Pressure pipes, tanks

3. Mechanical Behavior and Stress-Strain Response of PE100

3.1 Stress-Strain Characteristics

Under uniaxial tensile loading at room temperature, PE-100 displays a typical three-stage stress-strain curve (Figures I.7 a-b):

1. Linear Elastic Region (up to yield), characterized by an elastic modulus (900–1100 MPa).
2. Yielding and Necking, Yield stress ranges from 22 to 26 MPa.
3. Strain Hardening and Failure, Elongation at break (>600%), indicating excellent ductility [23].

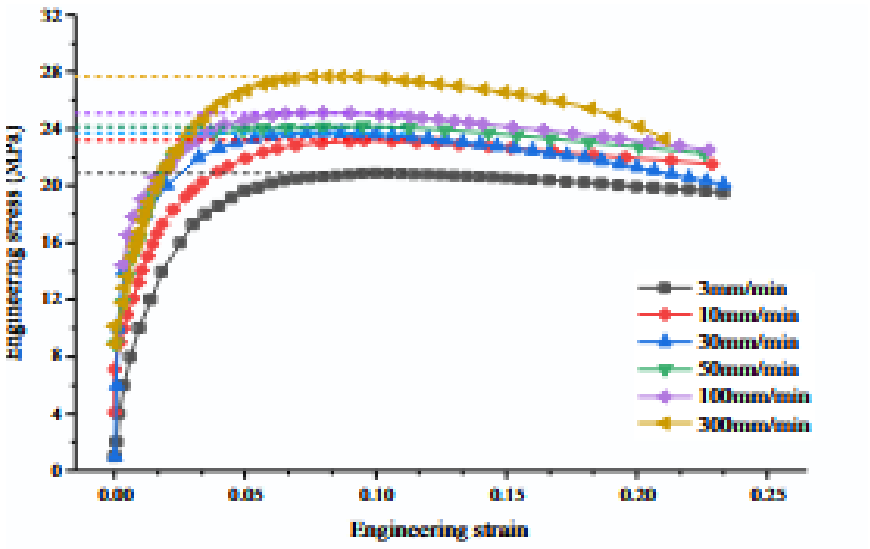

(A) Engineering stress-strain curve

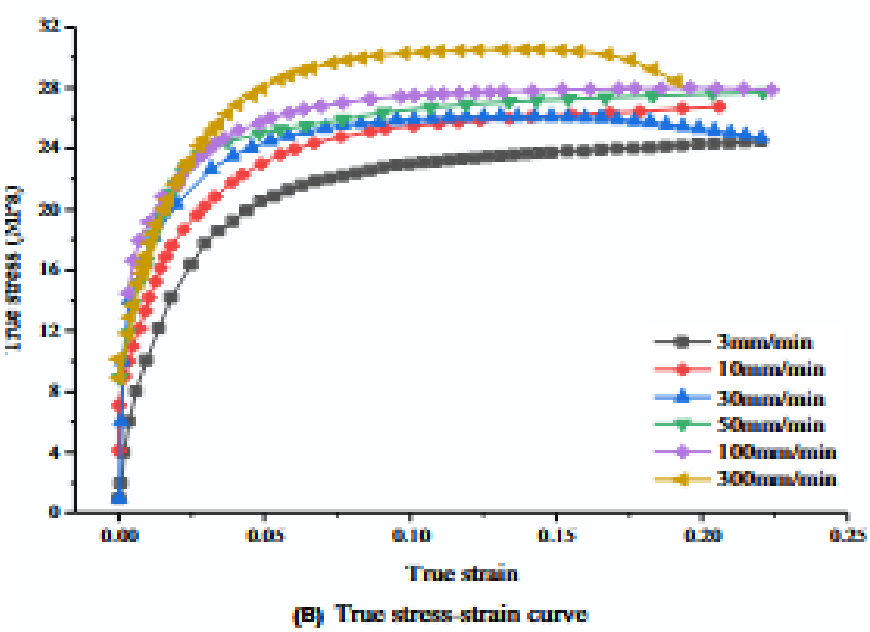

Figure I.7: Typical engineering (A) and true (B) stress-strain curves of PE-100 according to ISO 527-2 [24].

4. Influence of Strain Rate and Temperature

The mechanical response of PE100 is strongly strain-rate dependent:

- At low strain rates (~0.001 s^{-1}): PE100 behaves more ductile, with delayed necking.
- At high strain rates (>1 s^{-1}): Stress hardening is prominent, with earlier yielding and brittle failure modes.

Temperature variation also significantly alters tensile performance:

- Below 20°C: Both stiffness and yield stress increase (~2%/°C).
- Above 40°C: Yield stress decreases significantly (~0.5 MPa/°C), and the material becomes more compliant [25].

Table I.2: Influence of strain rate on tensile properties of PE-100 [26]

Strain Rate (s^{-1})	Yield Stress (MPa)	Elongation at Break (%)
0.001	22.1	640
0.1	25.5	610
1.0	28.2	580

5. Fatigue and Cyclic Behavior of PE-100

5.1 Fatigue Phenomena in Semi-Crystalline Polymers

Fatigue in polymers like PE100 is defined as the progressive and localized structural damage that occurs under cyclic loading. Unlike metals, fatigue in polymers is dominated not only by crack propagation but also by viscoelastic and plastic dissipation within the amorphous phases and at crystalline boundaries [27]. For PE-100, fatigue is generally assessed using S-N curves (stress amplitude vs. number of cycles to failure), with testing often following ISO 13479:2009 or ASTM D7791 standards. These curves typically show three regions:

- High-cycle fatigue (>10^5 cycles): Failure occurs at low stress levels due to crack growth.
- Low-cycle fatigue (<10^4 cycles): Dominated by plastic deformation and damage accumulation.
- Endurance limit: A threshold below which the material theoretically survives infinite cycles (though, this is rare in polymers).

5.2 Experimental Fatigue Response of PE-100

A comprehensive study by *Viebke et al.* reported that PE-100 under sinusoidal tensile fatigue (R = 0.1, 1 Hz) has a fatigue life ranging from 10^4 to 10^7 cycles depending on stress level. The crack growth rate under cyclic stress was characterized using Paris' Law, with the exponent “m” ranging between 3.8 and 5.2 [28].

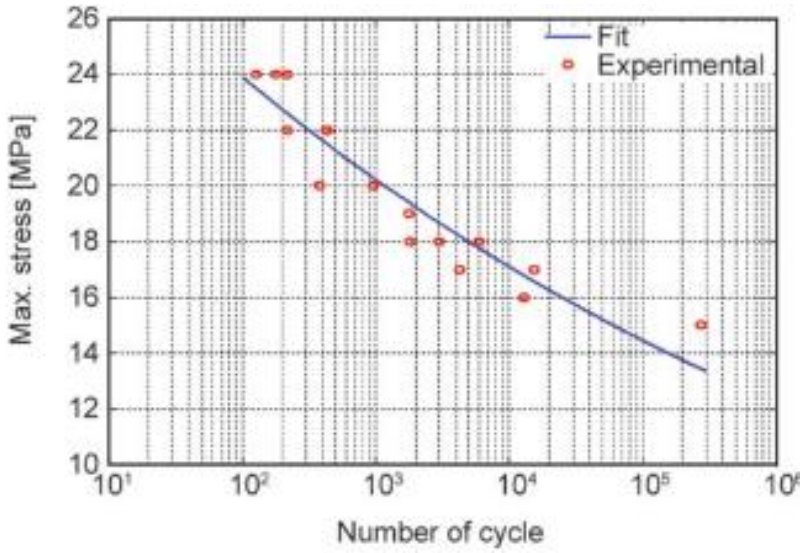

Figure I.8: S-N curve for PE100 under tension-tension fatigue [29].

Furthermore, fatigue resistance improves significantly with higher crystallinity, carbon black reinforcement and stress relaxation periods between cycles [30].

6. Creep and Time-Dependent Deformation

6.1 Creep Mechanisms

Creep is a time-dependent deformation under constant stress, which is especially critical in long-term applications like pressure pipes. For PE100, the creep behavior shows a primary, secondary, and tertiary stage, with eventual rupture under long-term stress at elevated temperatures [31].

The empirical relation is often expressed by the Andrade model:

$$\varepsilon(t) = \varepsilon_0 + At^n$$

where ε_0 is the instantaneous strain, A and n are material constants function of T° and load. For instance, at 20°C and 8 MPa, the time to rupture can exceed 100,000 hours, reflecting its long-term durability [32,33].

6.2 Factors Influencing Creep Performance

Creep resistance is affected by many factors:

- Temperature: Time-to-failure drops exponentially with temperature increase (Table I.3).
- Molecular weight: Higher Mw reduce chain mobility and increasing creep resistance.
- Additives: Antioxidants and crosslinking agents improve stability.

Table I.3: Effect of temperature on creep rupture time (at 8 MPa) [34].

Temperature (°C)	Time to Rupture (hrs)
20	>100,000
40	~45,000
60	~12,000
80	~2,000

6.3 Stress Relaxation Behavior.

Stress relaxation occurs when a polymer under constant strain gradually reduces internal stress over time. For PE100, this phenomenon is critical in applications requiring long-term dimensional stability, such as pipe fittings, flange seals, and compression joints [35].

6.4 Molecular Mechanisms of Stress Relaxation.

The relaxation process in semi-crystalline polymers like PE100 involves two primary mechanisms:

1. Chain Disentanglement: In the amorphous regions, polymer chains gradually slip past each other, redistributing stress through reptation motion.
2. Crystalline Phase Effects: The crystalline lamellae act as physical crosslinks, slowing relaxation by restricting chain mobility [36].

The stress decay typically follows a stretched exponential (KWW) function:

$$\sigma(t)=\sigma_0 \cdot e^{-(t/\tau)\,\beta}$$

Where:

- σ_0: Initial stress (MPa).
- τ: Average relaxation time (s).
- β: Stretching exponent ($0 < \beta \leq 1$), reflecting material heterogeneity.

For PE100 at 23°C, τ ranges from 10^2 to 10^4 seconds, depending on molecular weight distribution and crystallinity [37].

6.5 Experimental Characterization

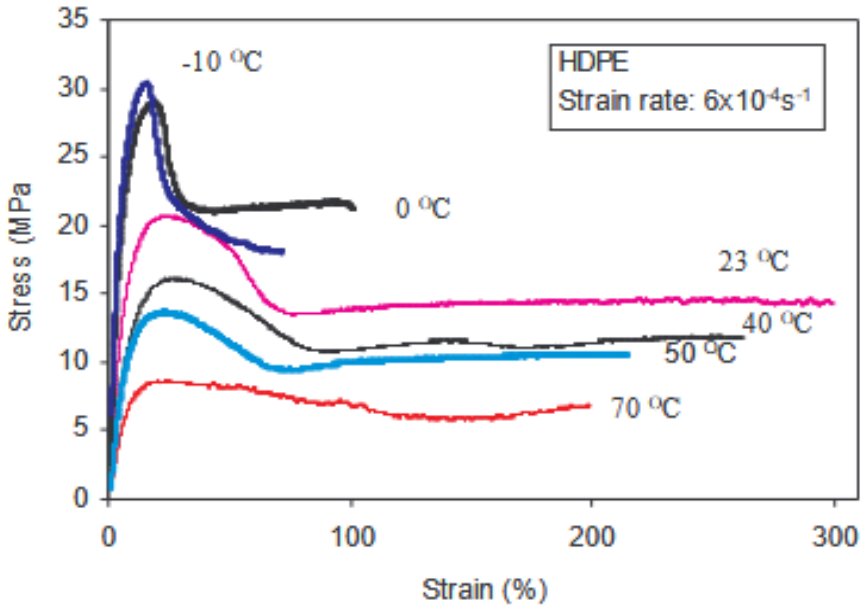

Figure I.9: shows stress relaxation curves for PE100 at different temperatures, highlighting the thermo-viscoelastic nature of the material.

Key observations include:

At T > 50°C: Stress decays exponentially due to increased free volume and chain mobility ($\tau\tau$ drops to ~10^2 s).

At T < 0°C: Relaxation slows dramatically ($\tau\tau > 10^5$ s), mimicking elastic behavior.

Table 4: Residual stress in PE100 after 24 hours under constant strain [38].

Temperature (°C)	Residual Stress (% of σ_0)
-20	85%
23	18%
60	5%

6.6 Engineering Implications

1. Design Considerations:
    - Joints subjected to constant strain (e.g., bolted connections) require periodic retightening.
    - Residual stresses after relaxation must be accounted for in FEA simulations [39].
2. Material Optimization:
    - High crystallinity grades (PE100 RC) extend τ by 30-50%.
    - Carbon nanotube additives (1-3 wt%) enhance stress retention through nanoscale reinforcement [40].

7. Fracture Toughness and Crack Propagation in PE100

7.1 Slow Crack Growth (SCG) Resistance

High-density polyethylene grade PE100 demonstrates superior resistance to slow crack growth (SCG), a critical property for ensuring the long-term integrity of pressure pipes. This resistance stems from two key factors:

1. Molecular Architecture:
    - Linear polymer chains with minimal long-chain branching.
    - High molecular weight (Mn > 120,000 g/mol).
2. Processing-Induced Morphology:
    - Uniform crystalline lamellae thickness (12–18 nm).
    - Optimal tie molecule density (15–20 chains/μm^3) [41].

7.2 Standardized Testing Methods

SCG performance is quantified using:

1. Full Notch Creep Test (FNCT)
    - Conducted per ISO 16770 at 80°C in surfactant solution.
    - Measures time-to-failure under constant tensile stress.
2. Notched Pipe Test (NPT)

- Standardized by ISO 13479 for full-scale pipe evaluation.
- Simulates real-world stress concentrations [42].

7.3 Crack Propagation Kinetics

The relationship between crack growth rate (da/dN) and stress intensity factor range (ΔK) follows:

$$\frac{da}{dn} = C(\Delta K)m$$

Material Constants for PE100:

Table 5: Data compiled from multiple FNCT studies [43-44].

Parameter	Value	Measurement Conditions
CC	1.1×10^{-10}	FNCT, 80°C, 4 MPa
mm	4.8	R = 0.1, 1 Hz

7.4 Environmental Degradation Factors

7.4.1 Environmental Stress Cracking (ESC)

Environmental Stress Cracking (ESC) is one of the most common causes of polymer failure. The main reason for this is the complexity of the phenomenon, which includes aspects such as chemical compatibility, liquid diffusion, and crack initiation and propagation. Although both crystalline and amorphous polymers are susceptible to Environmental Stress Cracking (ESC), amorphous polymers are particularly sensitive because their structures are relatively open and prone to fluid penetration. Once the fluid penetrates the polymer, it dissolves locally, thereby promoting cracking and fissuring of the polymer.

7.4.2 Aging of PE

HDPE resins are frequently chosen for manufacturing structures and products for technical uses (geomembranes, pipes, tanks, and parts). Given that these products are regularly used in unfavorable environments, it is necessary to evaluate the resulting consequences of such contact (sorption, diffusion, permeability, or solubility) and also to assess the Environmental Stress Cracking Resistance (ESCR) in terms of degradation or aging mechanisms depending on the service operation. In service, both sides of the pipeline (external and internal) are exposed to different environments characterized by unstable and aggressive conditions such as temperature, operating pressure, humidity, chemical concentration, and external soil load.

In general, plastics exhibit excellent resistance to many forms of chemical attack and are better than many metals, especially when faced with weak acids or alkaline solutions. However, they are

attacked by strong acids and oxidizers. Thermoplastics can also be dissolved by various organic solvent compounds. As molecular weight increases, the solubility of the diffusant in the polymer also influences permeability. Solubility generally reduces permeability [48].

7.4.3. Influencing Factors on Buried Pipes:

The multiple advantages of fluid transport through HDPE pipes have directed research towards studies of HDPE pipe degradation and their service life, as well as their manufacturing processes with the aim of optimizing operating conditions from extrusion to installation. The deterioration of pipes in operation under the influence of internal factors, as well as the evolution of their physicochemical properties during aging, is induced by external environmental factors. thesis highlighted the heterogeneity between the two wall surfaces of an HDPE-100 pipe. She found that the internal surface exhibits better morphological and structural properties, which gives it better mechanical behavior than the external surface. In the case of HDPE aged in TM, the curves of the two surfaces are dispersed, and the gap between the inner and outer surface increases with the absence of the hardening plateau [49]. Pipelines easily degrade depending on several parameters such as air and water permeability, and humidity. Various factors can influence pipeline degradation, including air and water permeability, humidity, soil salinity, as well as acidity or alkalinity and conductivity or resistivity of the surrounding medium. For example, a soil that is both humid, poorly aerated, and acidic proves to be particularly corrosive, thus affecting the material's integrity in several ways, both chemically and physically.

SCG accelerates under specific environmental conditions:

Table I.6: Environmental Acceleration Factors [50, 51].

Condition	Crack Growth Rate Multiplier	Mechanism
2 ppm Chlorinated H_2O	3.2×	Oxidative chain scission
5% Surfactant	4.7×	Surface energy reduction
pH < 4	2.1×	Acidic hydrolysis

8. Environmental Degradation and Aging Effects in PE-100

8.1 UV-Induced Photo-Oxidation

While PE100 is primarily utilized in buried piping systems, its above-ground applications necessitate rigorous evaluation of UV stability. Exposure to ultraviolet radiation (290–400 nm) initiates Norrish Type I/II reactions, leading to:

- Chain scission in amorphous regions.
- Carbonyl group formation (detectable via FTIR at 1715 cm^{-1}).
- Surface embrittlement (reduction in elongation at break from >600% to <50% within 6 months) [52].

Mitigation Strategies:

- Carbon black additives (2–3 wt%): Absorb 99% UV radiation ($\lambda < 400$ nm).
- Hindered amine light stabilizers (HALS): Scavenge free radicals, extending service life by 8–10× [53].

8.2 Chlorine and Oxidative Degradation

PE100's performance in potable water systems is compromised by oxidative disinfectants through Fickian diffusion-controlled mechanisms:

Table I.7: Data from accelerated aging tests at 60°C [54]

Disinfectant	Diffusion Coefficient (m^2/s)	Critical Concentration (ppm)
Free Chlorine	1.2×10^{-13}	2.0
Chlorine Dioxide	3.8×10^{-13}	0.5

Degradation Outcomes:

- 35% reduction in SCG resistance after 1,000 hours at 1 ppm ClO_2.
- 50% loss in tensile strength after 5 years at 2 ppm free chlorine [55].

Protection Methods:

- Co-extruded barrier layers (EVOH or PA11).
- Phenolic antioxidants (0.1–0.3 wt%).

8.3 Thermal Aging and Autoxidation

Thermal degradation above 80°C follows autoxidation kinetics:

$$\frac{d[POOH]}{dt} = k_p[ph][poo] - k_t[pooh]^2$$

Where: [POOH]: Hydroperoxide concentration and K_p, K_t: Propagation/termination rate constants. Typical oxidation induction time (OIT) data is shown in Table I.8:

Tableau I.8: ISO 11357-compliant measurements [56]

Condition	OIT (min)	Molecular Weight Drop (%)
Virgin PE100 (200°C)	25.4 ± 2.1	-
Aged 1 year @ 110°C (air)	4.2 ± 0.5	38
Aged 2 years @ 90°C (N_2)	18.7 ± 1.8	12

8.4 Comparative Performance of PE100 with Other Polyolefins

The evaluation of PE100 in comparison with other common thermoplastics such as unplasticized polyvinyl chloride (PVC-U) and polypropylene-random copolymer (PP-R) provides important insights into its mechanical and chemical advantages. PE100 offers a superior balance of flexibility, mechanical strength, and long-term stability under various service conditions.

From a density perspective, PE100 is significantly lighter (0.955 g/cm³) than PVC-U (1.38 g/cm³), facilitating easier handling and lower transport costs. Its elastic modulus (~1000 MPa) is lower than PVC-U (3000 MPa), yet higher than PP-R (1200 MPa), placing it in an intermediate zone that favors both ductility and dimensional stability [57].

In terms of impact resistance, PE100 demonstrates an Izod value of 85 kJ/m², far exceeding PVC-U's 4 kJ/m² (Charpy) and PP-R's 35 kJ/m², making it more suitable for applications involving external stresses and ground movement. Creep resistance is another critical criterion in long-term pipe performance, where PE100 consistently outperforms PVC-U and exhibits better crack growth resistance compared to PP-R, despite the latter's superior thermal stability (maximum service temperature of 90°C versus 60°C for PE100) [58]. The following Table provides a comparative overview of key material properties:

Table I.8: Summary of some Properties of PE-100 Compared to PVC-U and PP-R

Property	PE100	PVC-U	PP-R
Density (g/cm³)	0.955	1.38	0.90
Elastic Modulus (MPa)	1000	3000	1200
Impact Resistance	85 (Izod)	4 (Charpy)	35 (Izod)
Max. Service Temp (°C)	60	60	90
Creep Resistance	High	Low	Moderate
Chemical Resistance	Excellent	Good	Excellent

The data of Table I.8 is adapted from ISO 4427, ISO 1452, and ISO 15874 standards [59].

9. Applications of PE100

PE100 has established its position as a leading material in numerous sectors due to its outstanding combination of mechanical, chemical, and economic properties.

9.1 Pressure Piping Networks

PE100 is extensively used in municipal water supply and natural gas distribution systems. Its ability to endure internal pressure, resist corrosion, and adapt to ground shifts makes it ideal for long-term infrastructure. According to the Plastic Pipe Institute (PPI), PE100 pipelines can provide service life exceeding 100 years under normal operational conditions [60]. Electrofusion and butt fusion welding technologies allow for seamless joints, virtually eliminating the risk of leakage and reducing maintenance requirements [61].

9.2 Industrial Applications

Industries such as mining, chemical processing, and geothermal energy systems utilize PE100 for its high resistance to abrasion, thermal fatigue, and aggressive chemicals. In mining, it handles slurry transport efficiently due to its wear resistance. In geothermal applications, PE100 endures thermal cycling without compromising structural integrity. It is also well suited for chemical transport lines where resistance to acids, alkalis, and solvents is required [62].

9.3 Non-Pressure Applications

Beyond pressure systems, PE100 is utilized in non-pressure environments where longevity, durability, and environmental resistance are essential:

- Cable conduits: Provide robust protection for power and communication lines.
- Sewage and drainage systems: Benefit from PE100's non-stick surface and resistance to biological fouling.
- Agricultural irrigation: Relies on UV-stabilized PE100 for long-term performance in open-field conditions [63].

This broad range of applications underscores the material’s exceptional versatility across varied operational contexts [64].

Chapter II

Preparation of Test Specimens and Experimental Methodology

1. Introduction:

This chapter illustrates the different stages of sample preparation from a high-density polyethylene (PE-100) pipe used for potable water transport, along with the experimental methodology for mechanical testing. The primary objective is to study the evolution of stress-strain behavior across the pipe wall, specifically focusing on each of its layers: the outer, middle, and inner layers. The ultimate objective is to investigate any differences in properties behavior due to structure heterogeneities induced by manufacturing process. A precise manufacturing protocol was adopted, followed by a rigorous review of dimensions and surface quality. This approach considers both the requirements of industrial standards and the technical constraints associated with available resources.

2. Tube Material Description

The tube used in this study is HDPE-100 which is specifically designed for the transportation and distribution of drinking water. It is manufactured by K-PLAST Co. (Sétif, Algeria) [2]. It shows the following specifications (as depicted in Figure III.1):

- Manufacturer: K-PLAST SETIF – Algeria.
- Material Type: PE-100 – Drinking Water.
- Outer diameter (OD): 200 mm.
- Thickness (t): 11 mm.
- Nominal Pressure (PN) : PN10.
- Standard Dimension Ratio (SDR) : SDR 17.6.

Figure II.1: HDPE-100 Pipe Used for Sample Preparation

3. Cutting and Preliminary Preparation Process

The machining operations are carried out at the AMM Unit of SIDER Co. [3]. The pipe is divided into three sections using a circular power saw. This operation is carried out precisely, without generating heat in the cutting area, to protect the material and its structure, especially at the edges (overheating is checked with hand contact at the end of cutting)**.**

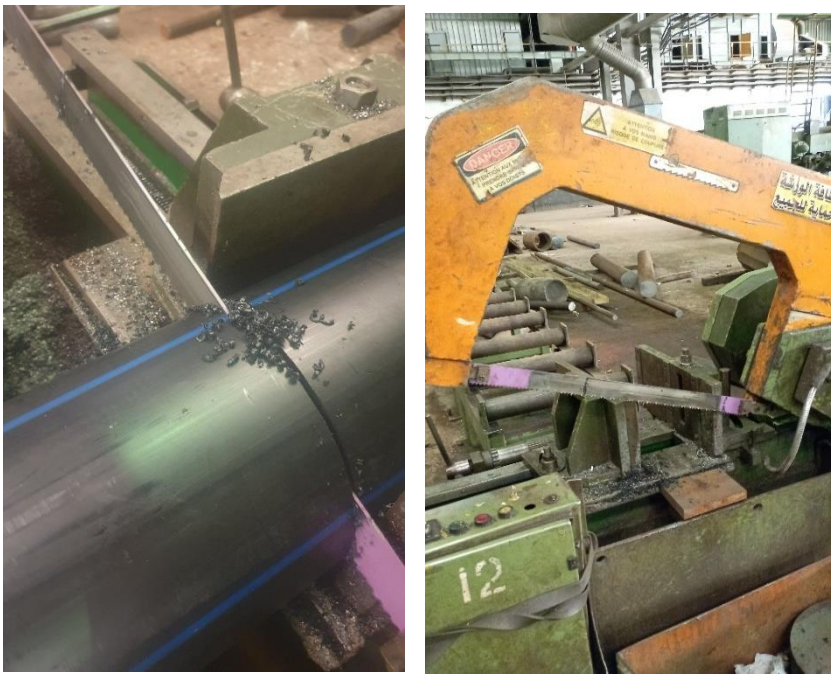

Figure II.2: Illustrates the Cutting Saws and the Pipe Cutting Process (ring and ring opening).

Figure II.3: The three pipes pieces obtained after cutting (similar cylinders)

Subsequently, each segment underwent a smoothing process using a lathe and a high-speed steel cutting tool on both sides. This was done to remove any imperfections resulting from the cutting and to achieve a clean final length of 2500 mm.

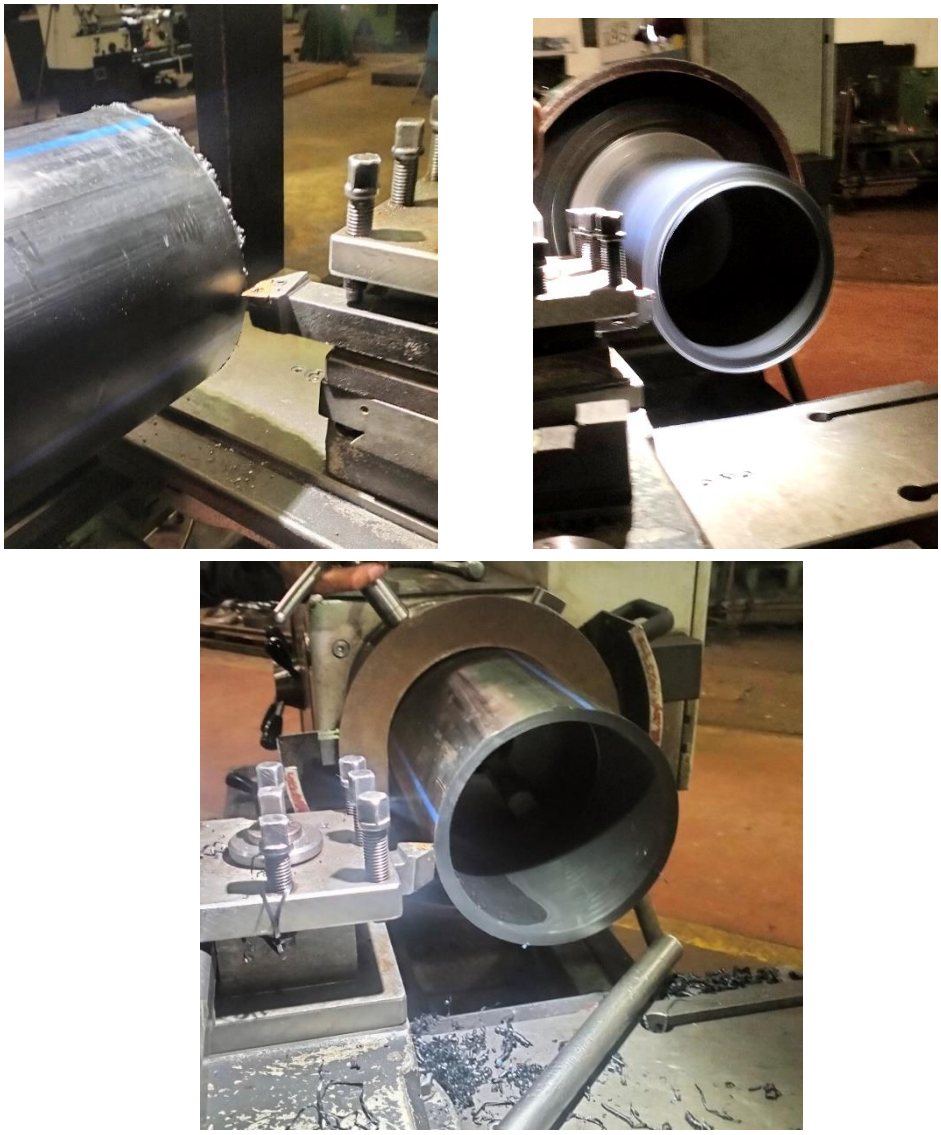

Figure II.4: Illustrates the surface smoothing process

Figure II.5: Surface smoothing tool

Waste generated during this stage (sawdust, threads, scraps, chips) is collected in separate bags, with the origin of each batch (piece 1, 2, 3) clearly identified. These by-products will be studied later as part of a sub-study specifically on the deformation of particles produced by cutting.

4. Methodology for Layer Preparation

A gradual manufacturing approach was adopted, based on removing specific layers from the pipe wall, working from the outside to the inside. Many previous studies have set the best machining parameters for HDPE pipes [4-8]. The goal was to obtain three types of samples representing:

Outer Layer: 4 mm ± 0.1
Middle Layer: 4 mm ± 0.1
Inner Layer: 4 mm ± 0.1

Figure II.5: The three obtained pipes (inner, middle, outer layers)

5. Preparing the Outer Layer (Boring operation)

The polyethylene pipe was inserted into a metallic cylinder (envelope) with an exact outer diameter of 200 mm. This metallic pipe section was then securely fixed onto a conventional 16D20 lathe. A high-speed steel (HSS) cutting tool was used with a cutting depth of 2 mm. This procedure was executed in two stages to achieve the desired thickness [6-8]. Since PE-100 does not require it, no cooling agents are used.

The plastic chips generated from this stage are collected in bags and classified with a serial number indicating the layer and the original pipe section.

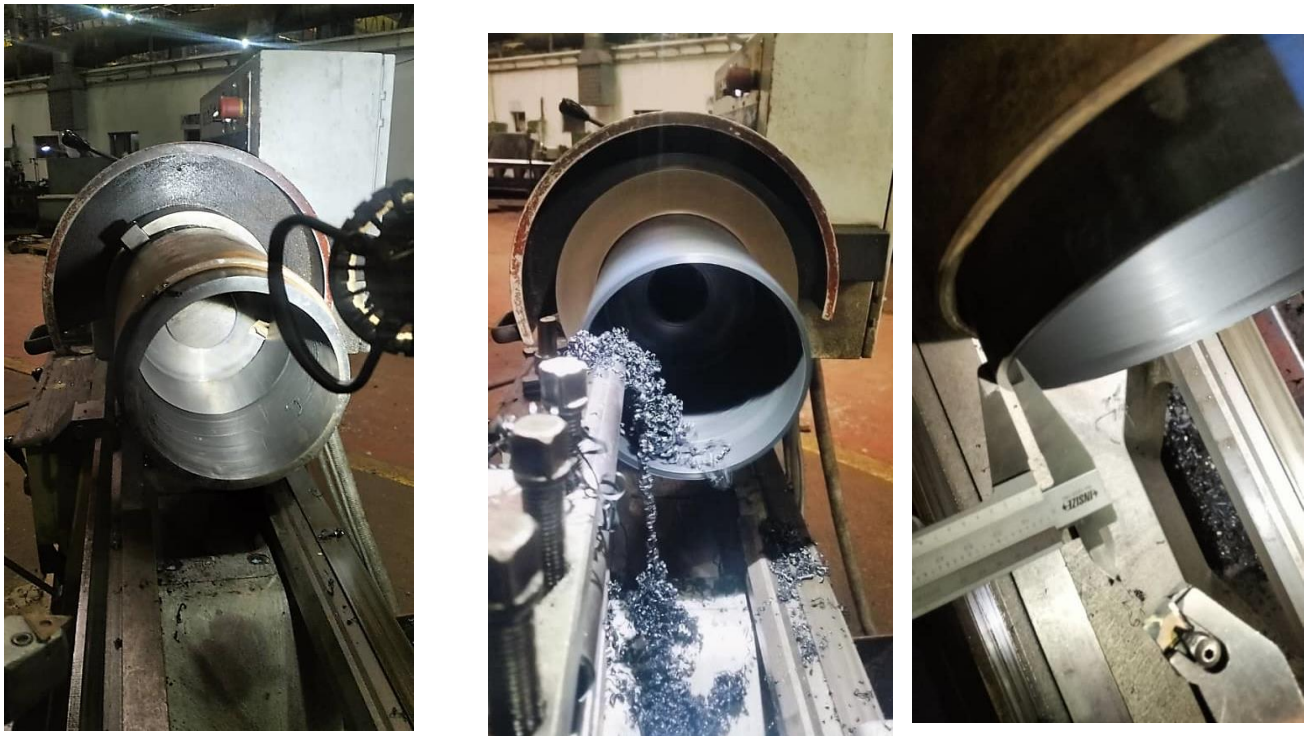

Figure II.6: Boring Process

6. Machining the Inner Layer (turning)

Again, another metallic pipe is placed inside the polyethylene pipe to prevent deformation. A specially mounted internal boring tool was used to perform the internal hollowing process. A 2 mm thick layer is removed from the inner surface under the same conditions as the previous stage, with the chips collected in the same manner.

Figure II.7: External Turning Process

7. Machining the Middle Layer (turning and Boring)

In this stage, the remaining wall thickness was adjusted to reach the target value of 4 mm in thickness. To achieve this, a gradual material removal process was performed from both sides:

- Removal of 1 mm thick layer from the Inner Surface: Using the specialized internal boring tool, a 1 mm deep layer was removed from the inner surface of the remaining cylinder.
- Removal of 1 mm thick layer from the Outer Surface: Subsequently, the outer surface underwent a 1 mm removal process using the high-speed steel (HSS) cutting tool.

This alternating process (removing from the inside, then from the outside) is repeated with precision and care, and a continuous thickness verification, until the exact desired thickness of 4 mm is achieved for the middle layer [4,7,8-10]. The shavings generated from this process were collected and classified in the same manner as in the previous stages.

TableII.1: Lathe Operating Parameters for Pipe Layers

Operation		Cutting Speed (m/min)	Rotational Speed
Surface Dressing		600	3 /1
Turning	Outer layer	1000	6/3
	Middle layer	1000	6/3
	Inner layer	1000	6/3

Figure II.8: Turning Tool

Figure II.9: Boring Tool

8. Pipe Displacement Monitoring after slitting

Once we had successfully obtained the three distinct pipe cylinders (outer, middle, and inner), we moved on to preparing for slitting and for displacement monitoring.

8.1 Marking and Surface Preparation

To prepare for cutting and to facilitate accurate observation, we began by using adhesive tape and a pencil to precisely mark the intended cut locations on the pipe's surface. We then meticulously covered the entire pipe surface with adhesive tape to serve as a clean, uniform background for displacement observation. Furthermore, specific reference points were established to ensure clear tracking: one side of the cut was marked with a single point, while the opposite side received two points. This clear distinction allowed us to unambiguously monitor displacement from both sides of the cut.

8.2 Sectioning and Observation Period

Next, we carefully transported the three prepared pipe sections to a research center. To prevent any localized heating that might alter the material's structural integrity, we used saws at a very low cutting speed. Then, every cylinder was longitudinally slit on one side (Fig. 10).

Figure II.10: Pipe Cutting Process with Automatic Saw

Following this sectioning, we initiated continuous displacement monitoring for a period of one week [10-12]. All observations regarding the progression of displacement were carefully recorded throughout this period and photographed at each step (Figs. 11-13).

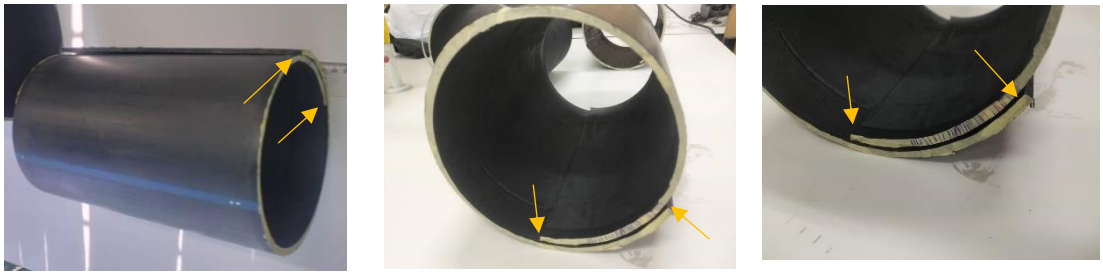

Figure II.11: Outer Layer Displacement

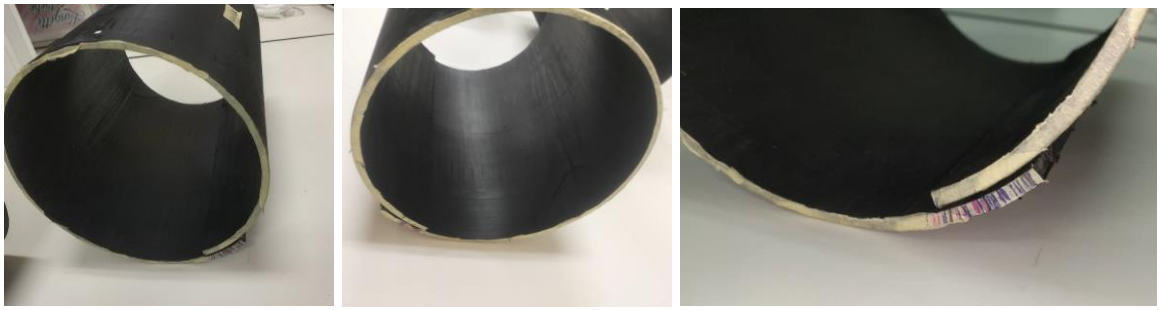

Figure II.12: Middle Layer Displacement

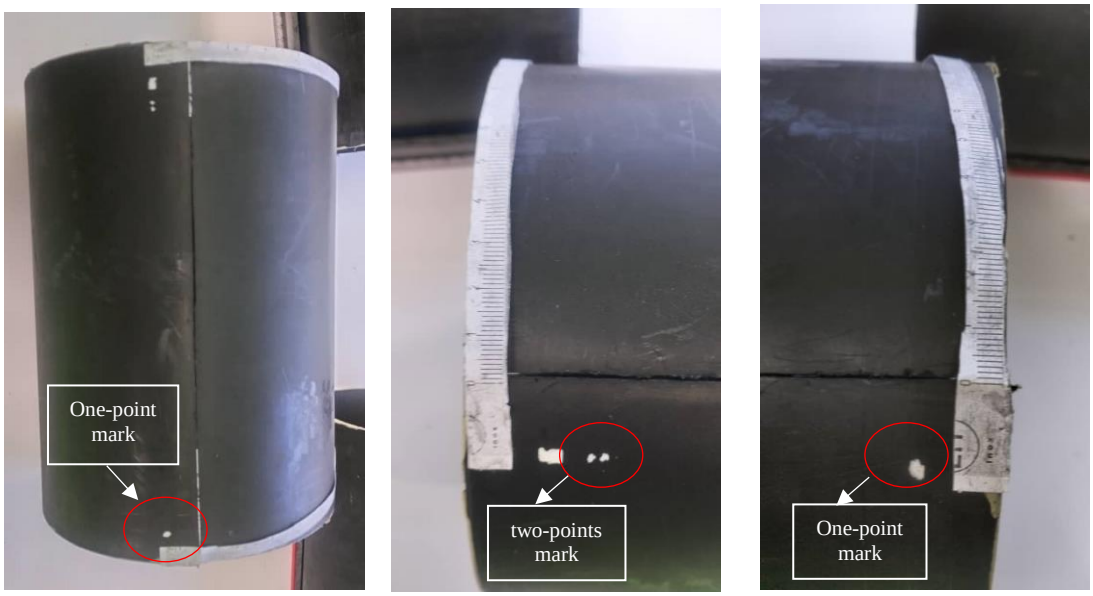

Figure II.13: Inner Layer Displacement

9. Preparation of Tensile Test Specimens

After concluding the displacement monitoring, we consulted with our supervising professor and decided to prepare specimens for tensile testing according to a specific standard. The Standard

Protocol involves specimen's preparation in compliance with the dimensions outlined in ASTM D-638 (specifically Type IV specimens, as depicted in the accompanying image). This is a well-established standard for determining the tensile properties of plastic materials [9].

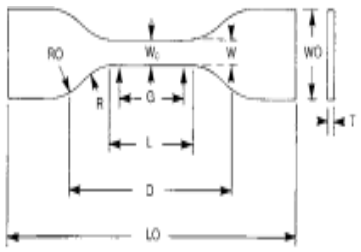

TYPE IV

Specimen Dimensions for Thickness, *T*, mm (in.)[A]

Dimensions (see drawings)	7 (0.28) or under		Over 7 to 14 (0.28 to 0.55), incl	4 (0.16) or under		Tolerances
	Type I	Type II	Type III	Type IV[B]	Type V[C,D]	
W—Width of narrow section[E,F]	13 (0.50)	6 (0.25)	19 (0.75)	6 (0.25)	3.18 (0.125)	±0.5 (±0.02)[B,C]
L—Length of narrow section	57 (2.25)	57 (2.25)	57 (2.25)	33 (1.30)	9.53 (0.375)	±0.5 (±0.02)[C]
WO—Width overall, min[G]	19 (0.75)	19 (0.75)	29 (1.13)	19 (0.75)	...	+ 6.4 (+ 0.25)
WO—Width overall, min[G]	...	...	...	...	9.53 (0.375)	+ 3.18 (+ 0.125)
LO—Length overall, min[H]	165 (6.5)	183 (7.2)	246 (9.7)	115 (4.5)	63.5 (2.5)	no max (no max)
G—Gage length[I]	50 (2.00)	50 (2.00)	50 (2.00)	...	7.62 (0.300)	±0.25 (±0.010)[C]
G—Gage length[I]	...	...	...	25 (1.00)	...	±0.13 (±0.005)
D—Distance between grips	115 (4.5)	135 (5.3)	115 (4.5)	65 (2.5)[J]	25.4 (1.0)	±5 (±0.2)
R—Radius of fillet	76 (3.00)	76 (3.00)	76 (3.00)	14 (0.56)	12.7 (0.5)	±1 (±0.04)[C]
RO—Outer radius (Type IV)	...	...	...	25 (1.00)	...	±1 (±0.04)

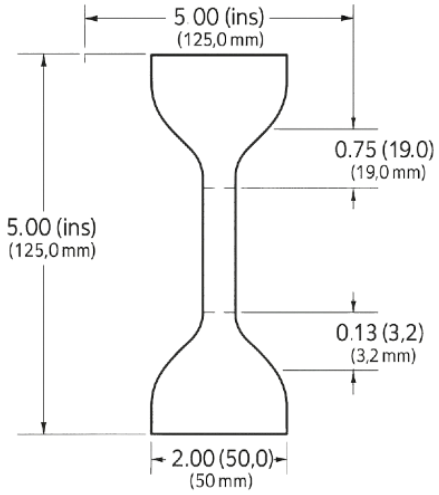

Figure II.14: ASTM D638 Type IV Tensile Test Specimen Dimensions and schematic [1].

10. Cutting Procedure:

The cutting of these specimens was performed in the Rubber Workshop laboratory of AMM Unit (SIDER Co.). The samples are punched (cut in a specified form, Fig. 14) from the pipe

material (machined cylinders) in two different orientations: L (longitudinally) and T or (tangentially) [8,13]. This operation is done using a specific specimen die (Fig. 15) and forming machine (press) for rubber cutting (Fig. 16).

Figure II.15: The die used to cut the specimens

Figure II.16: The hydraulic press (used to cut the specimens)

11. Post-Cutting Refinement and Identification:

Once the initial cutting was complete, we carefully removed any excess material or minor imperfections from the edges of the specimens by hand. Finally, to keep track of every sample, we assigned each one a unique alphanumeric code (Figs. 17-18).

Figure II.17: Specimens L and T. **Figure II.18:** Coding method (ex: specimen ATI1).

11.1 Specimen Coding System:

A standardized coding system is implemented for all specimens to ensure clear identification and traceability. The coding is as follows:

- **A**: This letter indicates the **non-immersed (control) specimens**, serving as the reference samples not exposed to the ARKOPAL/IGEPAL immersion.
- **V**: This indicates specimens that were **immersed** in the ARKOPAL/IGEPAL solution.
- **T**: Denotes that the specimen was cut tangentially.
- **L**: Denotes that the specimen was cut longitudinally.
- **X**: Indicates specimens immersed for 7 days.
- **Y**: Indicates specimens immersed for 21 days.
- **1 to 6 (or 5 or 4)**: This simply represents the individual specimen number within its specific group.

Each specimen is meant for property characterization operations and immersion preparation in aggressive environments. Following the preparation of the tensile test specimens, each sample underwent a meticulous characterization process to ensure accuracy in subsequent analyses.

11.2 Initial Measurements:

Each specimen was subjected to multiple measurements for critical dimensions:

- We measured the **weight** three times (Fig. 19).
- We measured the **thickness** three times.
- And we measured the **width** three times. These multiple measurements were performed to obtain reliable average values for each dimension.

Figure II.19: Weighing L and T Specimens with a High-Precision Balance

11.3 Immersion Protocol:

A specific immersion protocol was established, agreed upon for each layer of the pipe (outer, middle, and inner) following previous studies [8,14]. For each layer, we prepared three distinct groups of specimens:

- A **Longitudinal Group**: Comprising specimens cut longitudinally.
- A **Tangential Group**: Comprising specimens cut tangentially.
- A **Non-Immersed (Control) Group**: These specimens did not undergo the immersion process and would serve as a reference for comparison.

The 2 immersed groups (L and T) were then further subdivided based on immersion duration. One set of specimens from each layer (O; M; I) and orientation (L; T) was designated for **7 days of immersion**. Another set was designated for **21 days of immersion**.

11.4 Immersion Medium Preparation:

Glass containers designated for specimen immersion were prepared by thoroughly cleaning them to remove any impurities, followed by complete drying. The immersion agent selection is a known aggressive liquid used as detergent commercially called (IGEPAL or ARKOPAL). This substance is known to have a significant impact on PE pipes. Also, it is commercially available in the product VIGOR (Fig. 20).

Figure II.20: The Solution Used for Specimen Immersion

Figure II.21: Glass Containers Used for Specimen Immersion

12. Preparation for Testing and Testing Procedure

Before conducting the tensile tests, we carried out several crucial preparation steps for each specimen to ensure accurate and reliable results. First, we prepared the specimen surface where the machine grips would hold it. This involved **roughening both ends of the sample**. This

roughening was essential to prevent any slippage of the specimen within the testing machine's grips during the test. Next, we precisely **marked the midpoint of each side of the specimen**. From this midpoint, we measured and marked **twenty millimeters on both ends** – these were the sections that the machine grips would firmly hold. This left a precise **sixty-five millimeters in the middle of the specimen** as the gauge length, which is the section that would undergo deformation and be measured during the test. With the specimens meticulously prepared, we proceeded with the tensile testing (Fig. 22). The sequence was as follows:

1. We first performed the **tensile test on the non-immersed (control) specimens**.
2. Following this, we proceeded to test the **aged specimens**. Before testing aged ones, we **re-weighed them** to account for any changes in mass. We then repeated the same surface preparation steps (roughening and marking) as for the non-immersed samples.
3. Upon completion of these tests, we obtained the necessary data and results for analysis [8,13,14].

Figure II.22: Specimens Undergoing Preparation for Tensile Testing

13. Fabrication of Parallelepiped Samples

To prepare the standardized parallelepiped samples, a 500 mm section of the PE pipe was carefully readied. The pipe segment was then securely mounted onto a lathe. Using a 4 m/min cutting speed, the pipe was precisely cut into rings 24 mm wide (Fig. 23).

Figure II.23: Ring Cutting Process on the Lathe

Subsequently, four of these rings were carefully transferred to a milling workshop. Each ring was then securely clamped onto a milling machine. With a rotational speed of 215 revolutions per minute (RPM) and a feed rate of 355 mm/min, the rings were meticulously cut to form individual samples. Following the milling process, these samples underwent final adjustment to achieve the required dimensions: 24 mm in length and 1 mm in width, forming the final parallelepiped geometry [15-17].

Figure II.24: Fabrication of Parallelepiped Samples Using a Milling Machine

14. Characterization of Parallelepiped Samples and Immersion Protocol

After fabricating the parallelepiped samples, each was assigned a code, and an immersion protocol was agreed upon with the supervising professor to evaluate their behavior in various environments (Fig. 25).

Figure II.25: Image of Parallelepiped Sample Coded 60, Illustrating Obtained Dimensions

14.1 Initial Measurements:

Before immersion, each parallelepiped sample was weighed three times to obtain an accurate initial weight. The thickness was also measured three times and the width three times for each sample to ensure dimensional accuracy.

14.2 Immersion Protocol:

The cut samples (longitudinally and tangentially from the different layers) were divided for immersion into three different chemical and environmental media to assess their impact on the material:

- Bleach water
- Demineralized water
- VIGOR (containing IGEPAL or ARKOPAL): The latter is a solution known for its strong effect on high-density polyethylene (HDPE) pipes used for water transport, especially in a natural aquatic environment.

The samples were immersed in groups, typically six samples per group, directly within the containers of the substances themselves, and the immersion periods varied as follows: **7 days, 14 days, 21 days, and 28 days.** Additionally, a non-immersed (control) group of each type was designated for comparison (Fig. 26).

BLEACH WATER **DEMINERALIZED WAT** **VIGOR LIQUID**

Figure II.26: Immersion of Parallelepiped Samples

14.3 Weight Monitoring During Immersion:

During the specified immersion periods (7, 14, 21, 28 days), groups were randomly withdrawn from their immersion media. Upon withdrawal of each group, the samples were re-weighed three times to record any changes in mass due to liquid absorption or degradation. All these observations and data were meticulously recorded to obtain the results.

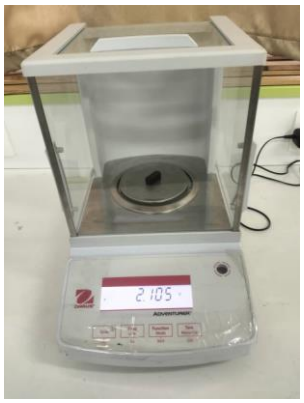

Figure II.27: Weighing Parallelepiped Samples with a Sensitive Balance

Chapter III :

Mechanical Behavior of High-Density Polyethylene (HDPE) Pipes Under Aggressive Environmental Influence

1. Introduction:

The mechanical behavior of high-density polyethylene (HDPE) pipes, which are essential parts of water transportation networks and other industrial uses, is thoroughly examined in this chapter. The purpose of the study is to assess how well these pipes function in challenging environmental circumstances, paying special attention to the impact of exposure to Igepal solution. This solution was selected because it reflects a particular harsh environment (such corrosive soil or groundwater with a certain chemical composition) that HDPE pipes could experience in real installation sites, which is an important consideration when evaluating their dependability and lifespan. A thorough examination of mechanical properties is provided in this chapter.

Based on tests conducted on rectangular prism samples and standard tensile samples that were both taken from HDPE pipes. Reference (unexposed) samples and samples immersed in Igepal solution for varied lengths of time (7 and 21 days) are among the samples used. To give a thorough grasp of how these variables impact the material's stiffness and resistance to deformation over time, the results are presented taking into account the variation of samples in terms of their extraction from the particular water pipe and their distribution within its layers (outer, middle, and inner).

2. Examination of Residual Deformation in Cut Ends and Layers

The exact findings of the residual deformation measured in the pipe after the initial sawing procedure are shown in this section. To evaluate the temporal and spatial nature of the deformation, the displacement of the pipe was carefully monitored over a period of several days. Measurements were taken from two separate cut ends, clearly marked P• and P••, as well as from three different layers inside the pipe wall: the inner, middle, and outer layers. These deformations will be graphically depicted in the following representations, and then the patterns, layer differences, and comparisons between the two cut ends will be thoroughly examined. Residual Deformation, mm/mm, for the middle layer from the P• side is graphically represented in Figure III.1.

Additionally, the following formulas and laws were applied:

aw for calculating Eps (Diameter Strain):

$$\text{Eps} = \frac{\text{OD New} - \text{P(OD)}_{\,mm}}{\text{P(OD)}_{\,mm}}$$

$$P(OD)_{mm} = D0 * 3.14$$

$$Pnew = P(OD)_{mm} - Pnew_{mm}$$

$$OD\ New = Pnew/3.14$$

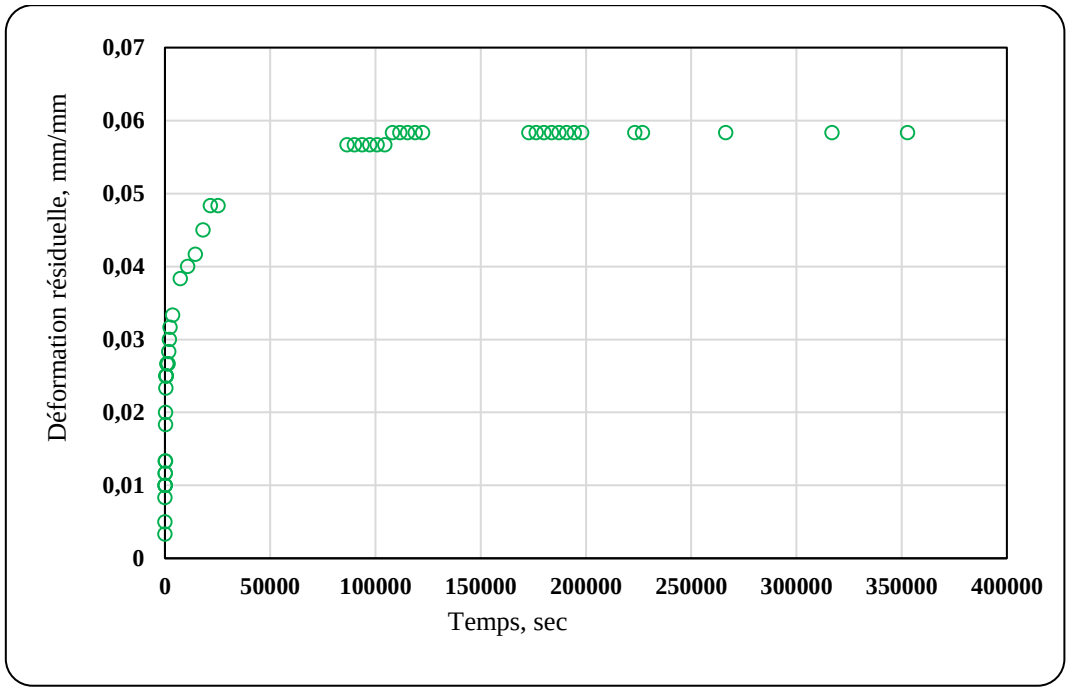

Figure III.1: Graphical representation of Residual Deformation, for the middle layer from the P• side.

Examination of the Two Curves in Graphics:

General Curve Description: This curve shows how time (sec) on the horizontal axis and residual deformation (mm/mm) on the vertical axis relate to one another. Following the initial sawing operation, this graph shows the evolution of residual deformation in the pipe's middle layer as measured from end P•.

Behavior of Deformation:

Initial Stage (Rapid Increase): There is a noticeable and quick rise in residual deformation during the first-time frame, which is roughly 0 to 20,000 seconds. Beginning at a value around zero, the deformation progressively increases to about 0.048 mm/mm. This early rise is a reflection of the material's instantaneous reaction to residual cutting-related stresses, such as

thermal stresses produced during sawing and mechanical stresses brought on by material removal.

Stabilization Stage: The residual deformation stabilizes at a value of roughly 0.057 to 0.059 mm/mm after about 100,000 seconds, when it becomes almost constant. In terms of residual deformation over time, this stabilization shows that the material has achieved an equilibrium condition, also known as a quasi-static state. After a significant amount of time, the material in the middle layer from the P• side retains the permanent distortion, which is represented by the ultimate stabilized value of residual deformation.

Figure III.2 shows the middle layer's residual deformation, expressed graphically as mm/mm from the P•• side.

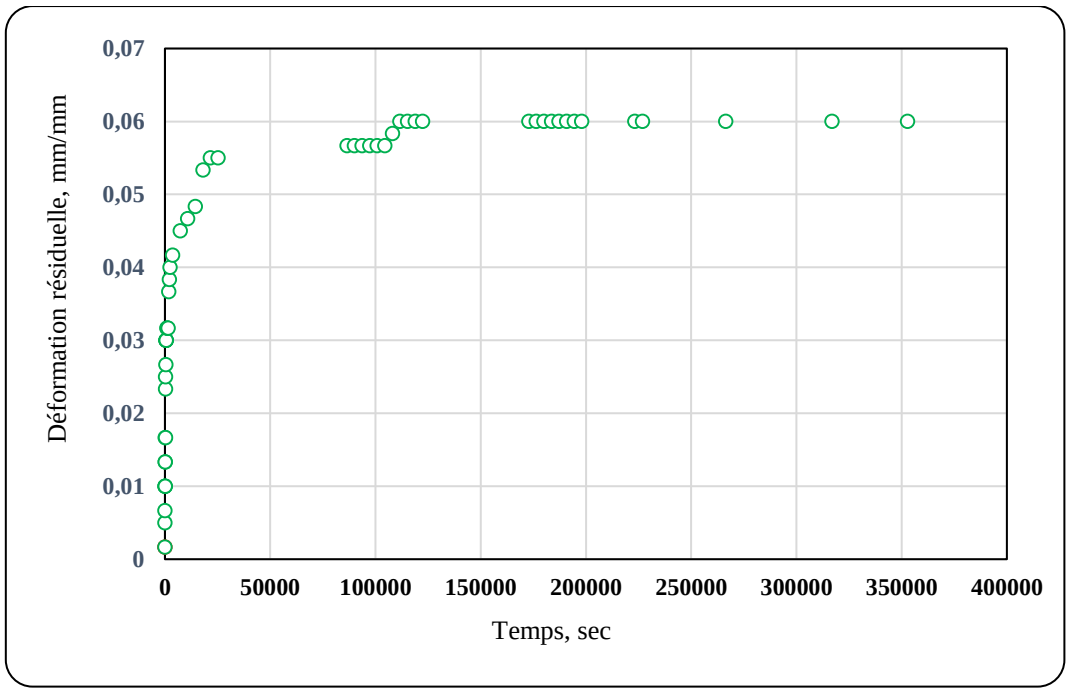

Figure III.2: Graphical representation of Residual Deformation, mm/mm, for the middle layer from the P•• side.

General Curve Description: This curve also shows how time (sec) on the horizontal axis and residual deformation (mm/mm) on the vertical axis relate to one another. Measured from end P••, this graph shows the progression of residual deformation in the pipe's middle layer. **Behavior of Deformation:** Looking at the given curve, we can observe that it behaves precisely like Figure III.1. After roughly 100,000 seconds, the deformation stabilizes at a value between 0.057 and 0.059 mm/mm, after a sharp increase from roughly 0 to 20,000 seconds.

Comparing and analyzing both curves together (Middle Layer):

Exact Correspondence: The most important finding is that Figure III.1 and Figure III.2 are exactly the same. This same response clearly implies that the middle layer of both pipe ends (P• and P••) had almost equal residual deformations as a result of the initial sawing process. Evidence of Uniformity: This consistency in the two ends' deformation behavior is a good sign that the cutting procedure was reliable and well-managed. It suggests that at both pipe cut ends, the middle layer encountered mechanical and thermal conditions that were remarkably similar. This could involve the efficiency of pipe clamping along its length, saw blade quality, feed rate, and cutting speed uniformity.

Reaching Stabilization: Following the removal of the cutting forces, both curves show that the residual deformation eventually stabilizes, indicating that residual stresses have subsided and the material has reached equilibrium. The middle layer's permanent distortion is represented by this stable value.

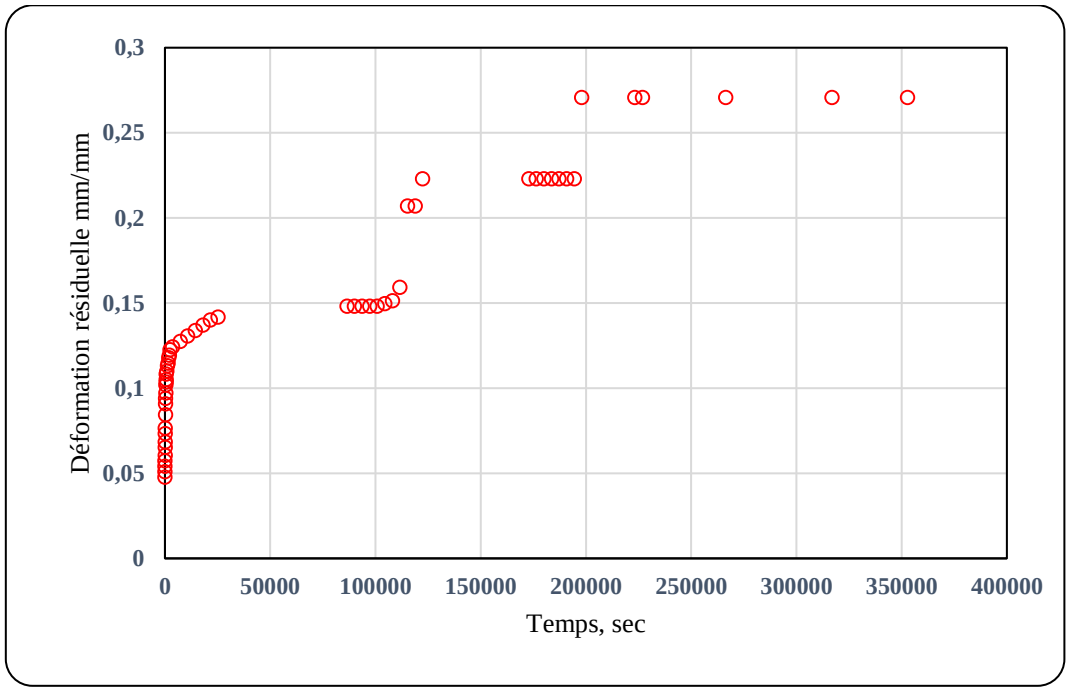

Figure III.3: Graphical representation of Residual Deformation, mm/mm, for the outer layer from the P• side

Examination of the Two Curves in Graphics:

Residual Deformation, mm/mm, for the outer layer from the P• side is graphically represented in Figure III.3.

Description of the General Curve: The relationship between time (seconds) on the horizontal axis and residual deformation (mm/mm) on the vertical axis is depicted by this curve. Following the initial sawing operation, this graph shows the evolution of residual deformation in the pipe's outer layer as measured from end P•.

Behavior of Deformation (outer layer):

Initial Stage (Sharp and Rapid Increase): The residual deformation increases sharply and quickly during the first time period (about 0 to 15,000 seconds), rising from around 0.05 mm/mm to roughly 0.14 mm/mm. The outer layer's direct and robust reaction to the high mechanical and thermal stresses brought on by the saw blade's direct contact with the pipe's surface is reflected in this abrupt increase.

Multiple Gradual Stabilization Stages: The curve displays several stabilization or gradual, sporadic increase stages after this first spike. At initially, the deformation settles within a range of 0.14 to 0.15 mm/mm. The deformation then jumps again at around 100,000 seconds, reaching about 0.15 mm/mm and then rising to about 0.16 mm/mm. Around 110,000 seconds later, the deformation increases once again to over 0.21 mm/mm before leveling off at about 0.22 mm/mm.

Third Jump and Final Stabilization: The residual deformation experiences a final jump at 200,000 seconds, reaching a value of 0.26 to 0.27 mm/mm. From there, it stays quite constant until the measurement period ends at 350,000 seconds.

Final Deformation Value: From the P• side, the outer layer's final stabilized residual deformation value is roughly 0.26 to 0.27 mm/mm.

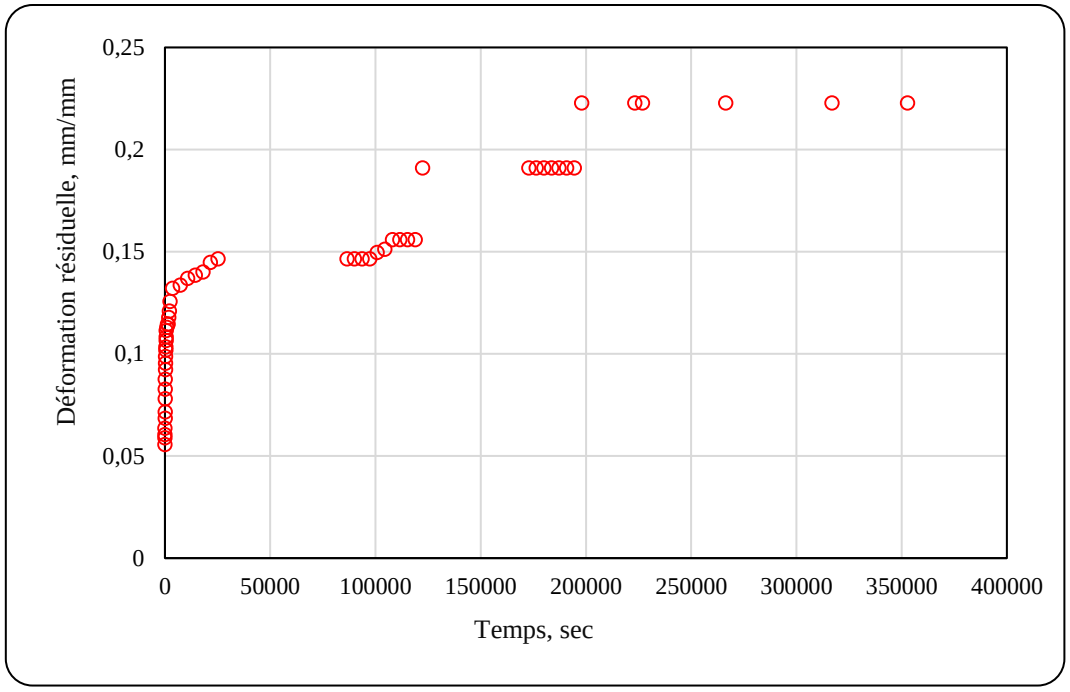

Figure III.4: Graphical representation of Residual Deformation, mm/mm, for the outer layer from the P•• side.

Residual Deformation, mm/mm, for the outer layer from the P•• side is graphically represented in Figure III.4.

General Curve Description: This curve also shows how time (seconds) on the horizontal axis and residual deformation (mm/mm) on the vertical axis relate to one another. The progression of residual deformation in the pipe's outer layer, as measured from end P•• following the initial sawing operation, is depicted in this graph.

Behavior of Deformation:

First Stage (Sharp and Rapid Increase): As in Figure III.3, this stage starts with a sharp and quick rise in residual deformation, which starts at around 0.05 mm/mm and reaches roughly 0.145 mm/mm in the first time period.

Several Gradual Stabilization Stages: An first stabilization at roughly 0.145 to 0.15 mm/mm comes next. Around 100,000 seconds later, there is another jump, this time with the deformation increasing to roughly 0.155 mm/mm and subsequently to 0.19 mm/mm. The deformation then increases to over 0.22 mm/mm at 170,000 seconds and then levels off at around 0.22 mm/mm.

Third Jump and Final Stabilization: The residual deformation experiences a final jump after around 180,000 seconds, reaching a value between 0.225 and 0.23 mm/mm. From there, it stays very constant until the measurement period ends at 350,000 seconds.

Final Deformation Value: From the P•• side, the outer layer's final stabilized residual deformation value is roughly 0.225 to 0.23 mm/mm.

Analysis and Comparison of Both Curves (Figures III.3 and III.4):

Greater Deformation Values: According to both curves, the residual deformation values in the outer layer are substantially greater (up to around 0.27 mm/mm) than in the previously examined intermediate layer (between 0.057 and 0.059 mm/mm). This demonstrates that the outer layer experiences higher mechanical and thermal stresses, resulting in more persistent deformations, because it is the region most directly exposed to the cutting tool interaction.

Multi-Stage Behavior: The two curves show a multi-stage pattern of fast growth, jumps, and then steady stabilization. This implies that the outer layer's stress relaxation and deformation redistribution process is more intricate, gradual, and may involve several deformation mechanisms.

Minor Variation in Final Values: Although the overall pattern is comparable, there are minor variations between the two ends' final stabilized residual deformation values. For the P• side, the outer layer stabilizes at about 0.26 to 0.27 mm/mm, while for the P•• side, it stabilizes at around 0.225 to 0.23 mm/mm.

The Difference's Implications: Despite being small, this discrepancy suggests a tiny variation in the material reaction or cutting conditions between the pipe's two ends in the outer layer. These differences may be explained by:

- slight variations in saw blade edge wear where the cut enters and exits.
- little variations in the pipe clamping pressure or feed rate at each end.
- slight variations in the material characteristics of the pipe along its length.
- vibrations caused by the saw that may not be exactly the same at both ends.

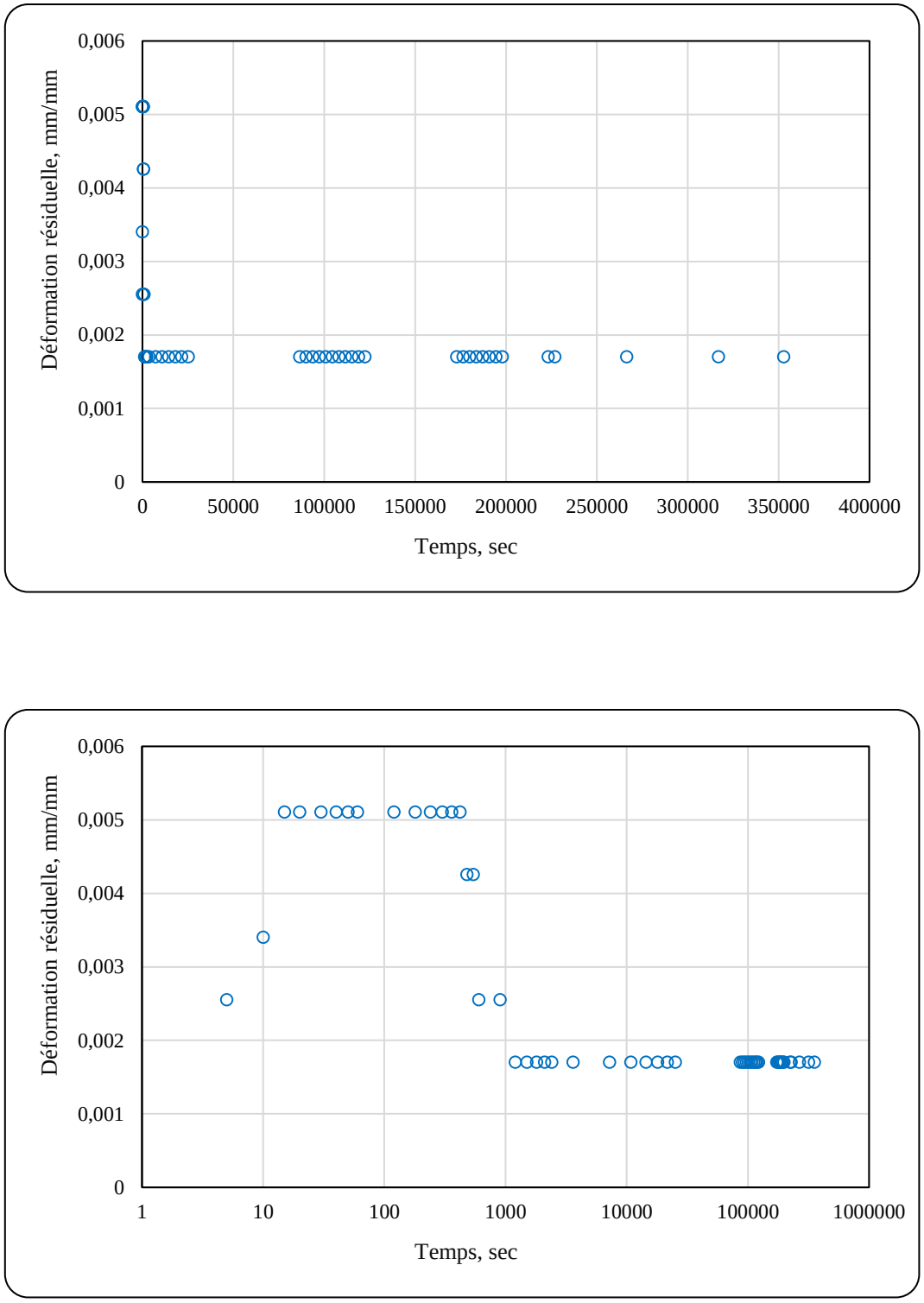

Figure III.5: Graphical representation of Residual Deformation, for the inner layer from the P• side as a function of time (upper: linear scale, lower: Log Scale).

Analysis of the Two Curves in Graphics:

Residual Deformation, mm/mm, for the inner layer from the P• side is graphically represented in Figure III.5.

General Curve Description: This curve shows how time (seconds) on the horizontal axis and residual deformation (mm/mm) on the vertical axis relate to one another. Following the initial sawing operation, this graph shows the evolution of residual deformation in the pipe's inner layer as measured from end P•.

Deformation Behavior: A characteristic behavior is seen in the very first time period (about 0 to 10,000 seconds), where the deformation begins at a very high value (around 0.005 mm/mm around time zero) and then swiftly and sharply drops over the first few thousand seconds. After that, the deformation rapidly settles to a very low value of about 0.0016 mm/mm.

Long-Term Stabilization Stage: For the duration of the remaining measurement time (up to around 350,000 seconds), the residual deformation stays constant at a value of about 0.0016 mm/mm.

Final Deformation Value: From the P• side, the inner layer's final stabilized residual deformation value is roughly 0.0016 mm/mm.

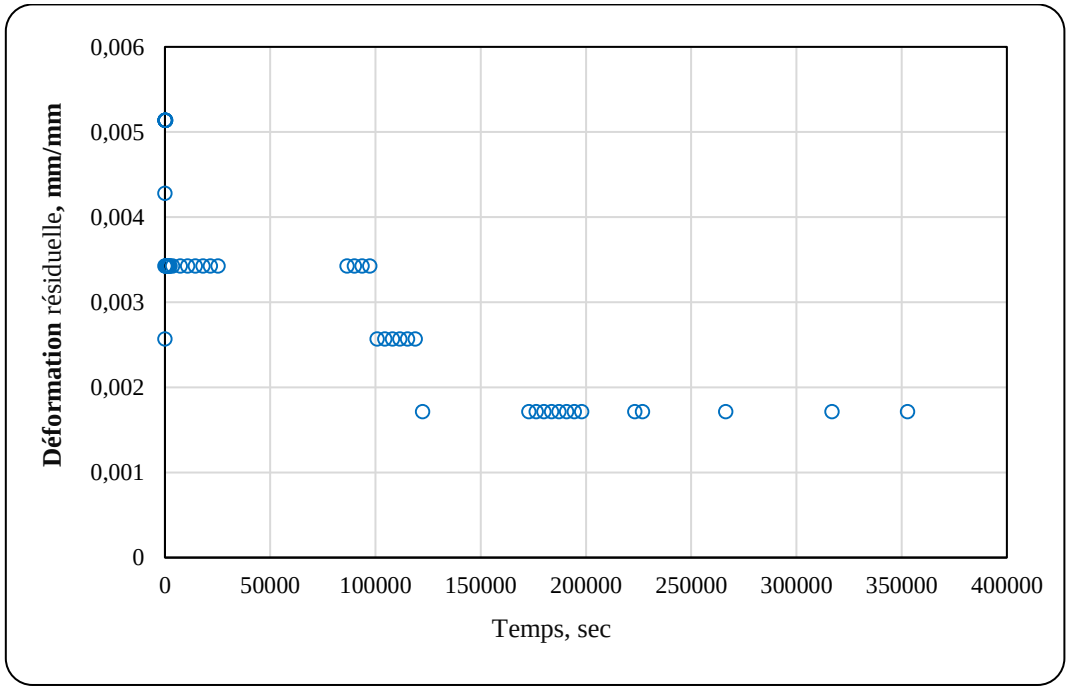

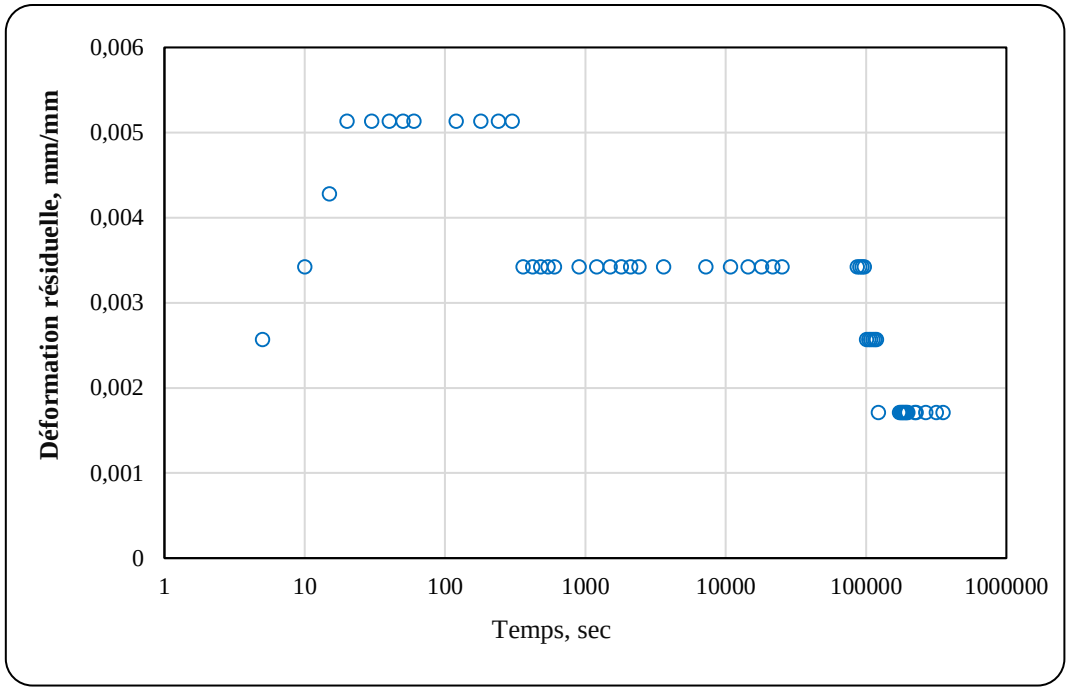

Figure III.6: Graphical representation of Residual Deformation for the inner layer from the P•• side as a function of time (upper: linear scale, lower: Log Scale).

2. Residual Deformation, mm/mm, for the inner layer from the P•• side is graphically represented in Figure III.6.

General Curve Description: This curve also shows how time (seconds) on the horizontal axis and residual deformation (mm/mm) on the vertical axis relate to one another. The evolution of residual deformation in the pipe's inner layer, as measured from end P•• following the initial sawing operation, is depicted in this graph.

Transformational Behavior:

Initial Decrease and Quick Stabilization with Jumps: The deformation begins at a high value (around 0.005 mm/mm close to time zero) and rapidly lowers during the initial time period (about 0 to 10,000 seconds). After a brief period of stabilization at around 0.0034 mm/mm, there is a noticeable jump at 90,000 seconds, and the deformation increases to about 0.0034 mm/mm once more.

Stages of Lower and Intermittent Stabilization: Following this jump, the deformation stabilizes at around 0.0025 mm/mm. This is followed by another jump at about 160,000 seconds, where it stabilizes at a very low value of about 0.0016 mm/mm. After that, the distortion stays at this level throughout the duration of the measurement (about 350,000 seconds).

Final Deformation Value: From the P•• side, the inner layer's final stabilized residual deformation value is roughly 0.0016 mm/mm.

Analysis and Comparison of Curves (Figures III.5 and III.6):

Generally Low Deformation Values: In comparison to the previously examined middle and outer layers, both curves show extremely low residual deformation values in the inner layer, peaking at about 0.005 mm/mm and stabilizing at 0.0016 mm/mm. This suggests that the forces brought on by the sawing process have a much smaller impact on the inner layer because it is located farthest from the cutting tool's direct interaction zone.

Achieving the Same End Stabilization Value: Although the curves' starting and intermediate behaviors differ, they both ultimately arrive at the same end stabilized residual deformation value, which is roughly 0.0016 mm/mm. This implies that, in terms of permanent deformation, the inner layers of both ends (P• and P••) reach the same final equilibrium state.

Variations in How People Relax:

A steep beginning decline is followed by a quick and ongoing stability at the end value, as seen in Figure III.5 (P• side).

But before reaching the final value, Figure III.6 (P•• side) shows a more complicated pattern with many jumps and brief stabilizing stages. The following factors may be responsible for these variations in the relaxation pathway:

* slight differences in the initial distribution of tension at each end of the pipe.

variations in the two sides' tiny mechanical rearrangements or stress relaxation systems.

Asymmetric cutting circumstances have minor effects on how stress spreads to the inner layer.

In conclusion, the inner layers of both ends (P• and P••) stabilize at the same low residual deformation value, even though the initial deformation path varies. This suggests that the internal sections of the pipe eventually experience a comparable, modest degree of permanent deformation as a result of the cutting operation, even though it may result in minor variations in the dynamics of stress relaxation. This pattern is said to be advantageous for the pipe's interior integrity.

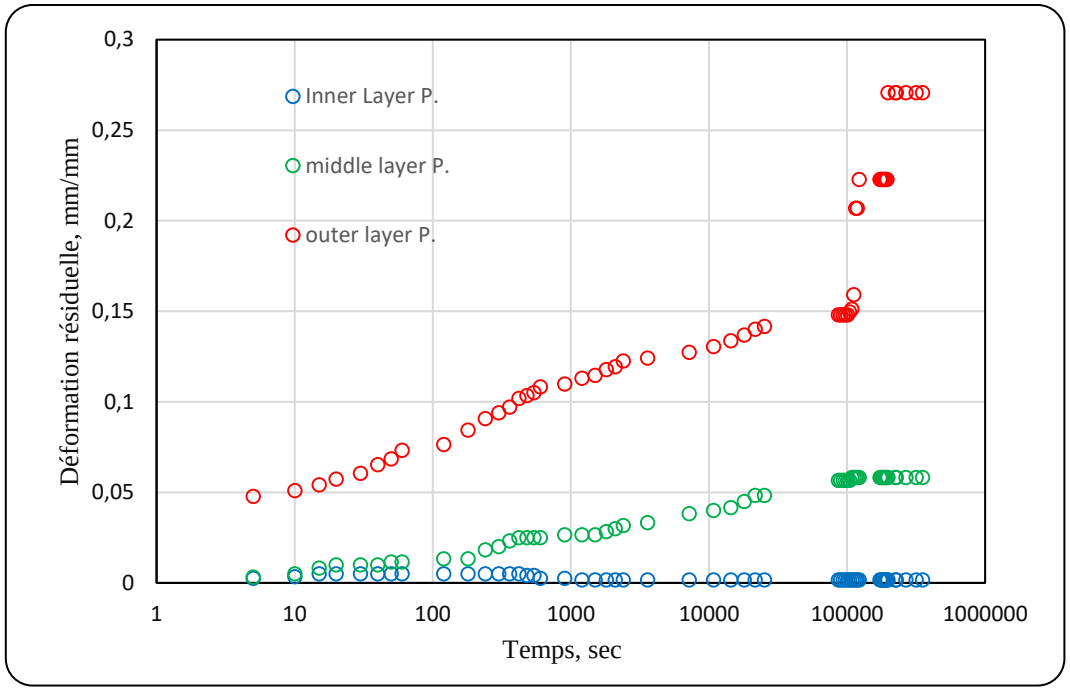

Figure III.7: Graphical representation of Residual Deformation, for the Inner, Middle, and Outer layers from the P• side.

Residual Deformation, mm/mm, for the Inner, Middle, and Outer layers from the P• side is graphically represented in Figure III.7.

A distinct gradient in residual deformation over the pipe's thickness from the P• side can be seen in this combined curve.

The inner layer (blue) is the least impacted by cutting, as seen by its lowest deformation values, which stabilize at a very low level (near zero).

The middle layer, or green, exhibits intermediate deformation values that first gradually grow before stabilizing at a level above the inner layer.

The Red outer layer shows the highest residual deformation values, with a notable

Its direct exposure to the highest stresses during the cutting process is shown in its rise and complex behavior (jumps and stability). The image shows a predicted material reaction to sawing, confirming that residual stresses are mostly localized in the surface layers and drastically decrease towards the interior.

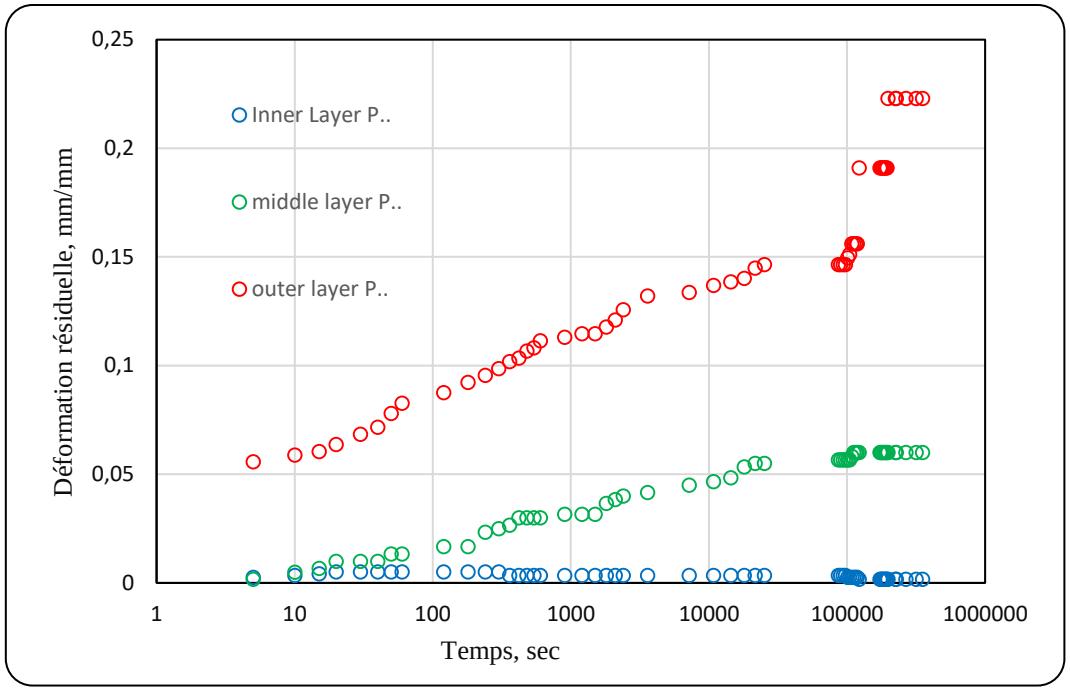

Figure III.8: Graphical representation of Residual Deformation, mm/mm, for the Inner, Middle, and Outer layers from the P•• side.

Residual Deformation, mm/mm, for the Inner, Middle, and Outer layers from the P•• side is graphically represented in Figure III.8. From the P•• side, this combined curve displays a comparable gradient in residual deformation across the pipe's thickness.

The inner layer (blue) shows the least amount of deformation and stabilizes at a very low level, indicating that the cutting process has had the least impact on it. The middle layer, or green, exhibits intermediate deformation values that first gradually grow before stabilizing at a level above the inner layer. With a notable increase and complex behavior (jumps and stability), the outer layer (red) shows the highest residual deformation values, indicating direct exposure to the highest stresses.

Figure III.7 (P• side) and Figure III.8 (P•• side) are compared:

The gradient between the three layers has the same general pattern when comparing Figure III.8 and Figure III.7: the outer layer exhibits the most deformation, followed by the middle layer, and finally the interior layer with the least distortion. This consistency, which reflects the homogeneity of the cutting operation and stress distribution over the thickness of the pipe at both cut ends, shows a general uniformity in the pipe's response to the cutting process throughout both its P• and P•• sides.

3. Graphical Analysis of Immersion Effect on Properties of Parallelepiped Samples

The experimental findings about the immersion impact on parallelepiped samples in different fluids are shown and examined in this section. The purpose of these tests is to investigate the effects of mineral water, Igepal, and bleach (Javel) on the percentage change in mass (Δm%) of parallelepiped samples. Samples for these metrics were selected at random for each of the following time periods: seven, fourteen, and twenty-one days. In order to discover behavioral patterns and the influence of each factor, a full study of the observed changes in Δm% over time and under the influence of each solution will be conducted after the graphical representations of these changes are shown in this section.

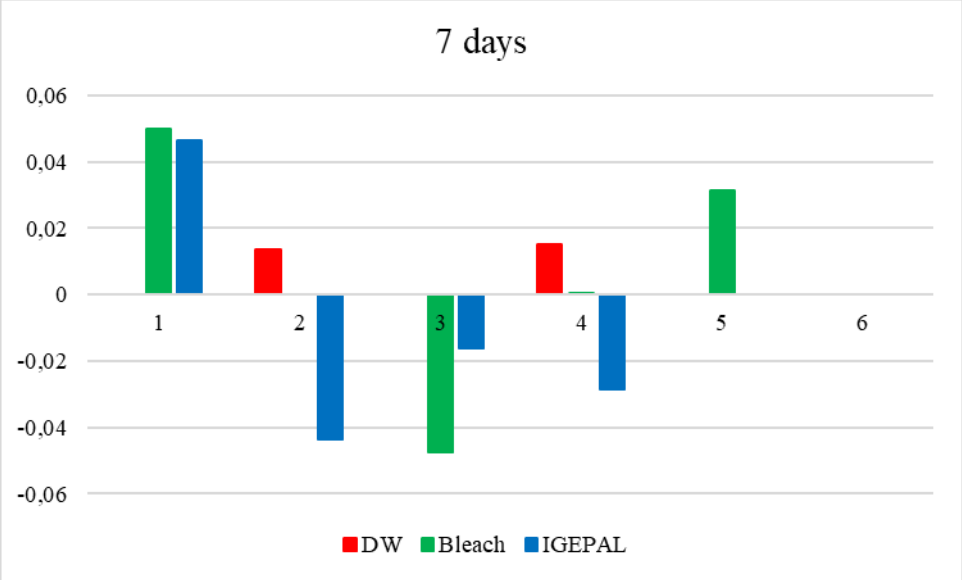

Figure **III.9**: Comparison of the Effect of Immersion Solutions (Distilled Water, Bleach, and Igepal) on the Percentage Change in Mass (Δm%) for Parallelepiped Samples after 7 Days of Immersion.

The impact of three distinct solutions—Igepal (IGEPAL), Bleach (BLEACH), and Distilled Water (WD)—on the percentage change in mass (Δm%) for parallelepiped samples following a seven-day immersion period is clearly compared in this bar chart. Six data points, numbered 1 through 6, are represented by the horizontal axis (Titre de l'axe), and they may represent various samples or experimental batches.

Important Points to Note:

Diverse Reaction to Solutions: The samples' reactions to the three solutions' effects on Δm% are diverse.

Blue bars of distilled water: Samples submerged in distilled water show the largest percentage change in mass values for the majority of locations. At point 2, for example, Δm%

approaches 145%, and at point 6, it approaches 140%. This implies that, in these circumstances, distilled water may alter sample mass the most.

Bleach (Green Bars): At most locations, samples submerged in bleach exhibit Δm% values that are lower than those of pure water, ranging from roughly 100% to 120%. But at point 4, the bleach's Δm% value is somewhat more than the distilled water's.

Igepal (Red Bars): In most situations, samples submerged in Igepal exhibit Δm% values that fall somewhere between distilled water and bleach. They display higher values than the other answers at certain points, like points 1 and 4.

Variations Between Points: For every solution, there are notable variations in the Δm% values between points 1 and 6. Variations in concentration or other variables not included on the horizontal axis might be the cause of this variance, as could variations in the samples themselves or sub-experimental settings for each point.

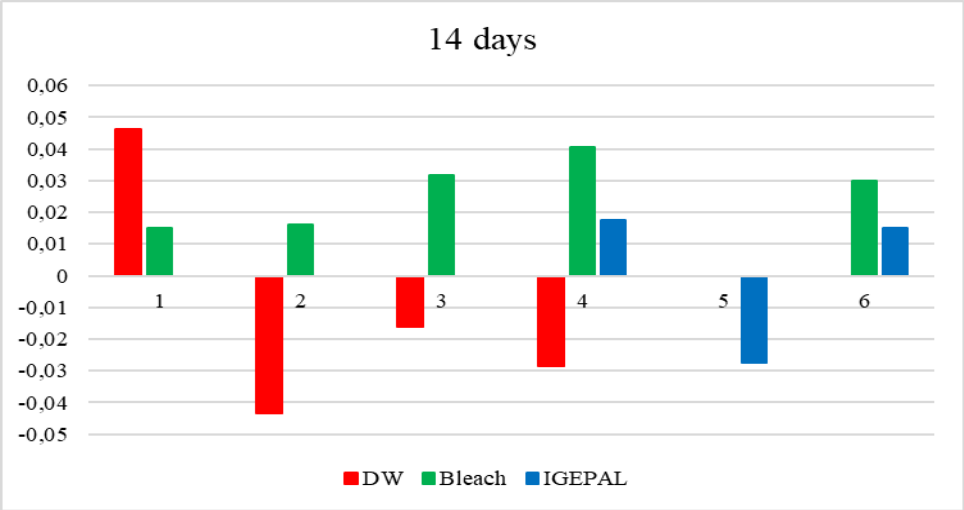

Figure III.10: Comparison of the Effect of Immersion Solutions (Mineral Water, Bleach, and Igepal) on the Percentage Change in Mass (Δm%) for Parallelepiped Samples after 14 Days of Immersion.

Figure III.10 compares how the percentage change in mass (Δm%) for parallelepipeds after 14 days of immersion is affected by the immersion solutions (mineral water, bleach, and Igepal). This bar graph compares the impact of Igepal (IGEPAL), mineral water (WD), and bleach (BLEACH) on the percentage change in mass (Δm%) for parallelepiped samples following a fourteen-day prolonged immersion period. Six data points (numbered 1 through 6) that reflect various samples or experimental circumstances are represented by the horizontal axis.

Important Points to Note:

Diverse Effect of Solutions: Following 14 days of immersion, the samples exhibit a range of reactions to the three solutions.

Mineral Water (Blue Bars): The Δm% readings of samples submerged in mineral water vary greatly between the sites. Their scores drastically drop at other locations like point 2 (about 91%) and point 5 (approximately 92%), although recording reasonably high values at point 1 (approximately 133%), and point 4 (approximately 112%).

Bleach (Green Bars): At point 4, the highest value in this figure, bleach is shown to produce the largest mass change (about 145%).

Igepal (Red Bars): Igepal records high Δm% values at points 2 (about 128%) and 5 (approximately 142%), indicating a considerable effect at certain locations. Additionally, igepal values and bleach coincide at other locations, as point 6 (around 119%).Persistent variations: The Δm% values for each solution continue to exhibit distinct variations across the various points (1-6), highlighting the variation in sample responses or individual situations.

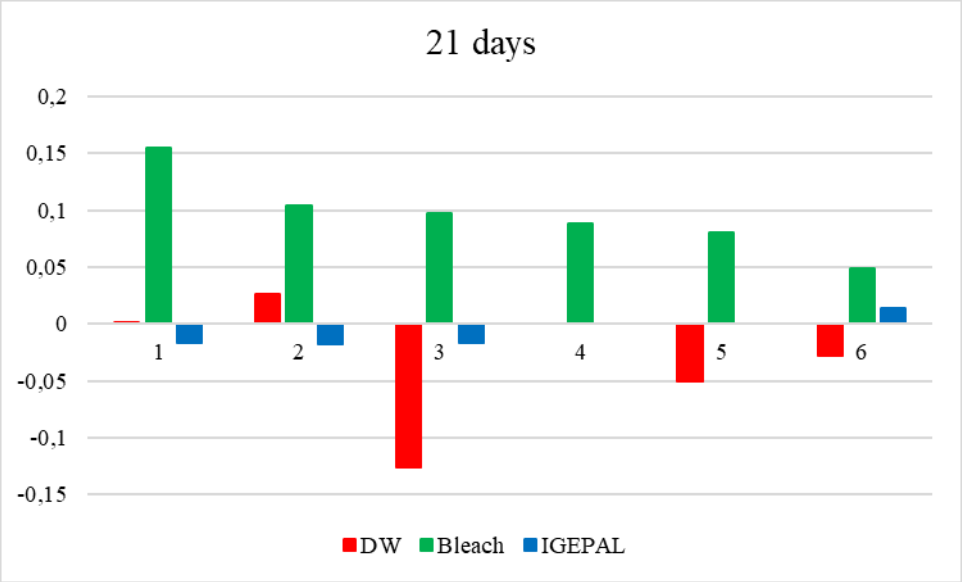

Figure III.11: Comparison of the Effect of Immersion Solutions (Mineral Water, Bleach, and Igepal) on the % Change in Mass (Δm%) for Parallelepiped Samples after 21 Days of Immersion.

The impact of three different immersion solutions—mineral water, bleach, and igepal—on the percentage change in mass (Δm%) for parallelepipeds following 21 days of immersion is compared in Figure III.11.

The impact of Mineral Water (WD), Bleach (BLEACH), and Igepal (IGEPAL) on the percentage change in mass (Δm%) for parallelepiped samples following a lengthy 21-day immersion time is depicted in this bar chart. Six data points (numbered 1 through 6) that reflect various samples or experimental circumstances are shown on the horizontal axis.

Important Points to Note:

Diverse Reaction to Solutions: Even after 21 days of immersion, the samples still show a range of reactions to the three solutions.

Blue Bars Mineral Water: The samples submerged in mineral water exhibit the highest Δm% values at multiple sites, including point 6 (about 139%), point 2 (approximately 160%), and point 3 (approximately 153%). In this figure, these values rank among the highest.

Bleach (Green Bars): In most places where mineral water is high, samples submerged in bleach exhibit lower Δm% values than mineral water; nevertheless, in certain places, they record greater values than Igepal. Their values fall between roughly 93% and 117%, with point 1 (roughly 117%), and point 4 (almost 128%), having the highest percentages.

Igepal (Red Bars): At point 6, Igepal records high Δm% values (about 141%), which are at or near the mineral water values. Additionally, it displays noteworthy values at point 1 (around 99%).

Inter-point Fluctuations: It is confirmed that the reaction is not consistent across all samples or situations by the pattern of distinct fluctuations in Δm% values for each solution between the various points (1-6).

. **Comparison between 7 Days, 14 Days, and 21 Days of Immersion:**

To provide a comprehensive understanding of the immersion effect, a comparative analysis across the three time periods (7, 14, and 21 days) for Figures III.9, III.10, and III.11 is crucial. This comparison highlights the dynamic and non-linear evolution of the percentage change in mass (Δm%) under the influence of different solutions.

General Patterns and Important Findings:

Non-Linear Evolution of Δm%: The most notable finding is that, for every solution or particular sample point, the change in mass (Δm%) does not rise or fall linearly with immersion time. Rather, there is a considerable variation in the values. Mineral Water (WD) at point 2, for instance, had a high Δm% at first (about 145% at 7 days), then dropped significantly (approximately 91% at 14 days), before rising quickly once again to reach the highest recorded value (approximately 160% at 21 days). This points to intricate interaction mechanisms that change over time, possibly involving time-dependent processes like initial absorption or degradation.

Shifting Dominance of Solutions: As immersion time increases, so does each solution's relative ability to alter mass.

Although it frequently results in a high Δm% in the first seven days, the effects of mineral water (WD) vary greatly at 14 days and then reappear as a potent inducer of mass change at certain places at 21 days.

Bleach (BLEACH): Throughout all periods, bleach exhibits significant Δm% values (about 138% at 7 days, approximately 145% at 14 days, and approximately 128% at 21 days),

demonstrating its constant strong effect. This is especially evident at point 4. This suggests that, for this particular sample condition, the impact on mass change over time is constant or even growing.

Igepal (IGEPAL): Igepal's impact varies as well. For example, it significantly increased from 7 days (about 118%) to 14 days (approximately 142%) at point 5, but subsequently reduced at 21 days (approximately 106%). This implies that under some circumstances, its maximum effect may be attained or exceeded by 14 days.

Sample-Specific Variability: Across all three time periods, the consistent fluctuation in Δm% values across points 1 to 6 for *each* solution implies that individual sample characteristics or subtle variations in experimental conditions for those specific points play a significant role in the observed mass changes. This suggests that the response is not only solution- and time-dependent but also potentially sample-dependent.

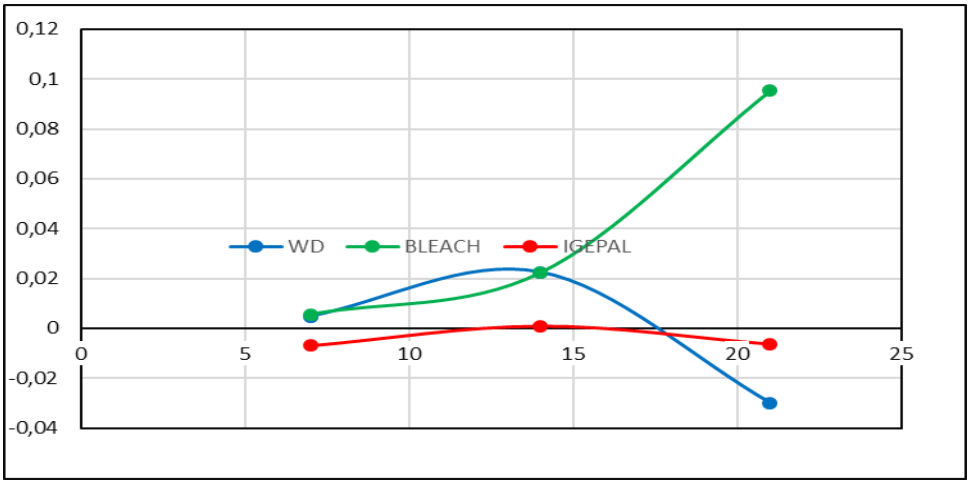

Figure III.12: Evolution of Percentage Change in Mass (Δm%) for Parallelepiped Samples with Immersion Time in Mineral Water, B leach, and Igepal Solutions.

The percentage change in mass (Δm%) for parallelepipeds as a function of immersion time in mineral water, bleach, and igepal solutions is shown in Figure III.11.

For parallelepiped samples submerged in three distinct solutions (mineral water, bleach, and igepal) for extended periods of time (7, 14, and 21 days), this line graph offers a thorough summary of the evolution of the percentage change in mass (Δm%). The dynamics of the effect may be compared thanks to this figure, which clearly shows how Δm% varies over time for each solution.

Important Points to Note:

Non-Linear Evolution: Neither of the three solutions exhibits a straightforward linear trend of Δm% growth or decline over time. This suggests that there are several steps of absorption,

degradation, or chemical reaction involved in the complicated interaction between the samples and the solutions.

Mineral Water (Blue Line): The Δm% value of samples submerged in mineral water is rather high at 7 days (about 122%), then drastically drops at 14 days (approximately 102%), before slightly increasing at 21 days (approximately 103%). This implies that before reaching a condition close to equilibrium, the first effect may involve quick absorption, stability, or even mass loss.

Bleach (Green Line): At 7 days, the bleach's Δm% value is approximately 116%. At 14 days, it slightly increases to approximately 118%, and at 21 days, it decreases to approximately 109%. In the medium term, bleach behaves more steadily than the other two solutions, with a minor decrease towards the end.

Gepal (Red Line): Igepal exhibits distinct behavior; it begins with a Δm% value (about 115% at 7 days), drops at 14 days (roughly 108%), and then sharply rises to the top of the solutions at 21 days (roughly 123%). This suggests that Igepal's long-term effects may be more noticeable.

Relative Effect Changes Over Time: It is evident that the solution with the highest or lowest Δm% changes as the immersion time increases. For instance, mineral water was nearly at the top after seven days. Igepal (for the average) and bleach (for the peak in the 14-day specific figure) had greater sway at 14 days. Igepal, however, occasionally outperforms bleach and mineral water at 21 days.

4. Effect of Immersion and IGEPAL Absorption on the Tensile Behavior of HDPE

This section presents and analyzes the tensile behavior of HDPE samples following their immersion in IGEPAL. The purpose of this investigation is to assess how IGEPAL absorption and immersion affect the samples' mechanical characteristics. To evaluate the reaction over time, samples were prepared for immersion in IGEPAL for two different time periods: seven days (7 days) and twenty-one days (21 days).

Each sample was weighed three times before and after immersion for each time period in order to measure the absorption. The amount of IGEPAL ingested was determined by calculating the percentage change in mass (ΔM) for each sample based on these measures. This relationship is used to determine ΔM:

$$\Delta M(\%) = ((Mt - M0)/M0) \times 100$$

Where: The mass of the sample at time t (either seven or twenty-one days) following immersion is denoted by Mt. The sample's initial mass prior to immersion is denoted by M0.

Bar charts are used to visually portray these data in order to compare and show absorption levels under various settings. Tensile test results and stress-strain curves are then presented, and they will be examined in light of the observed absorption.

Tensile Behavior of Longitudinal HDPE Samples After 7 Days of IGEPAL Immersion:

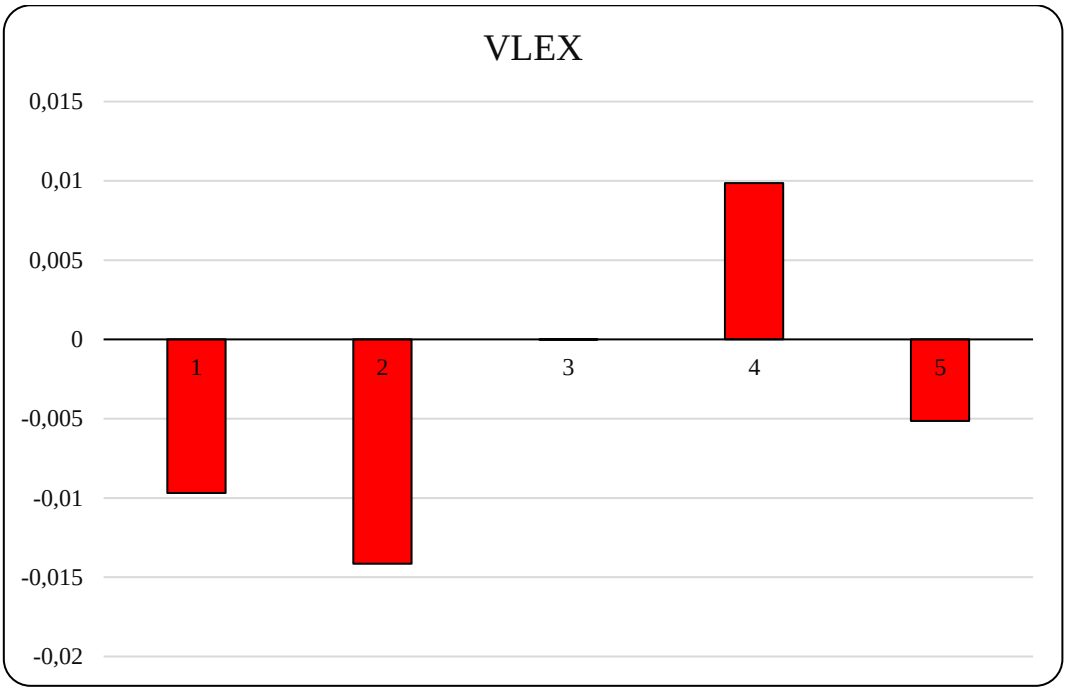

Figure III.13: Percentage Change in Mass (ΔM) for Longitudinal Outer Layer HDPE Samples After 7 Days of IGEPAL Immersion

Figure (III.12) demonstrates that, with the exception of sample 4, which shown a minor rise, the majority of the longitudinal outer layer HDPE samples showed a loss in mass (negative ΔM) following 7 days of IGEPAL immersion. This variation implies that the outer layer's reaction to IGEPAL absorption/desorption or its constituent parts is diverse, i.e. probably antioxidants or pigments or stabilizing agents are being dissolved.

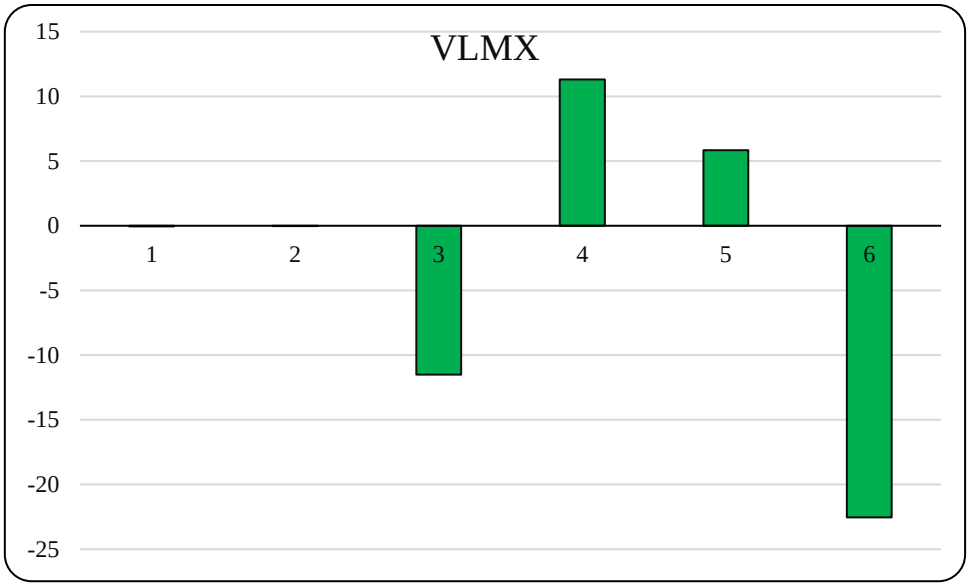

Figure III.14: Percentage Change in Mass (ΔM) for Longitudinal Middle Layer HDPE Samples After 7 Days of IGEPAL Immersion

Following seven days of IGEPAL immersion, the longitudinal middle layer HDPE samples showed more variability in mass change (ΔM) than the outside layer, as seen by ure (Y). Samples 4 and 5 had a noticeable mass gain, whereas samples 3 and 6 had a large mass loss. Some samples, such as 1 and 2, exhibited very little or no change. This implies that the middle layer's reaction to immersion varies, with some samples absorbing IGEPAL and others losing a significant amount of mass.

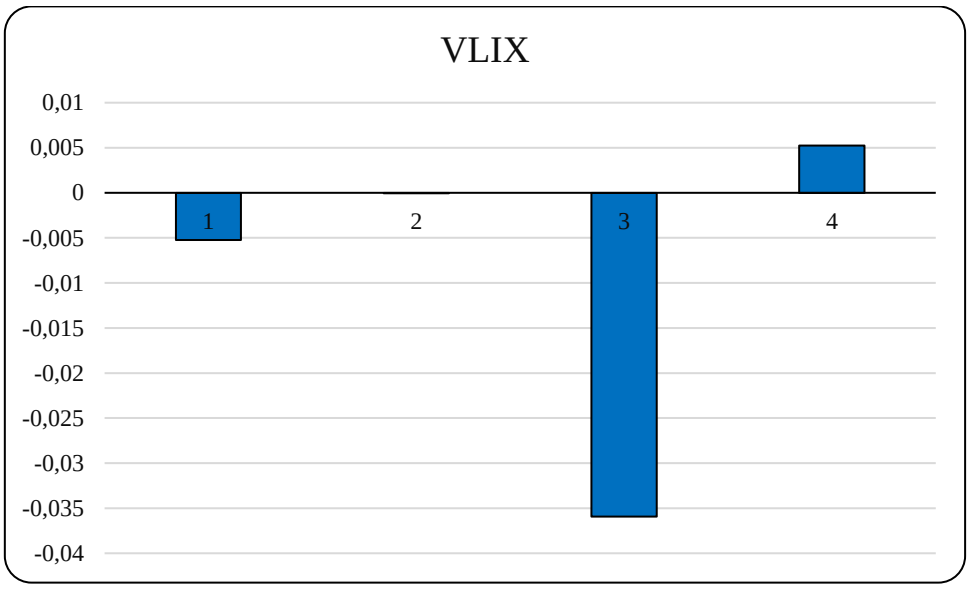

Figure III.15: Percentage Change in Mass (ΔM) for Longitudinal Inner Layer HDPE Samples After 7 Days of IGEPAL Immersion

Following seven days of IGEPAL immersion, Figure (Z) shows that longitudinal inner layer HDPE samples showed a modest gain in mass (negative ΔM) in sample 4, but a large mass drop (negative ΔM) in the majority of samples, particularly sample 3. This implies that under these circumstances, the inner layer tends to lose more mass, which could be a sign of component leaching or a particular interaction with IGEPAL.

Tensile Behavior of Transverse HDPE Samples After 7 Days of IGEPAL Immersion

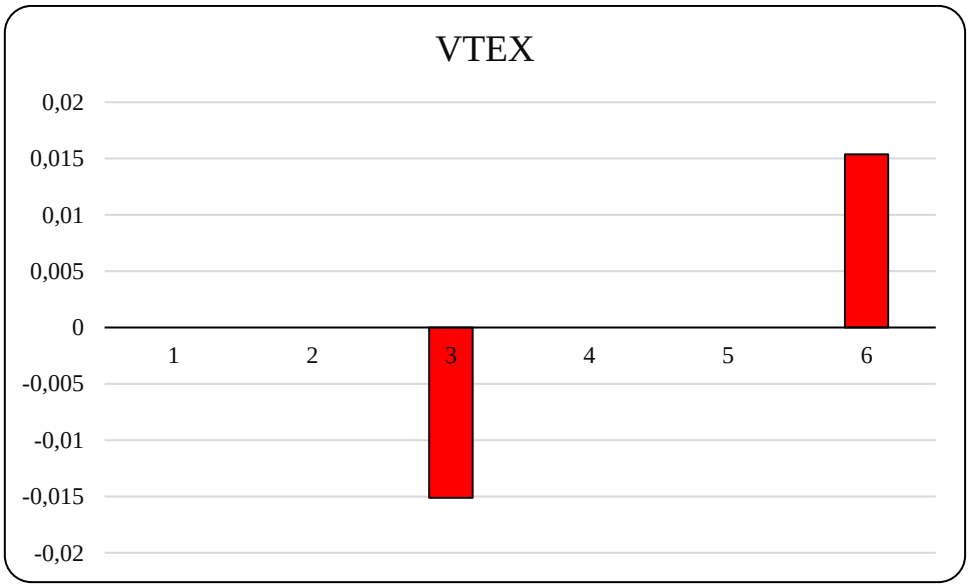

Figure III.16: Percentage Change in Mass (ΔM%) for Transverse Outer Layer HDPE Samples After 7 Days of IGEPAL Immersion

Following seven days of IGEPAL immersion, transverse outer layer HDPE samples showed diversity in mass change (ΔM), as shown in figure (A). Sample 3 recorded a substantial mass drop, while sample 6 showed a considerable mass rise. The majority of samples (1, 2, 4, and 5) showed no change. This variation points to a diverse reaction of the transverse outer layer to immersion circumstances.

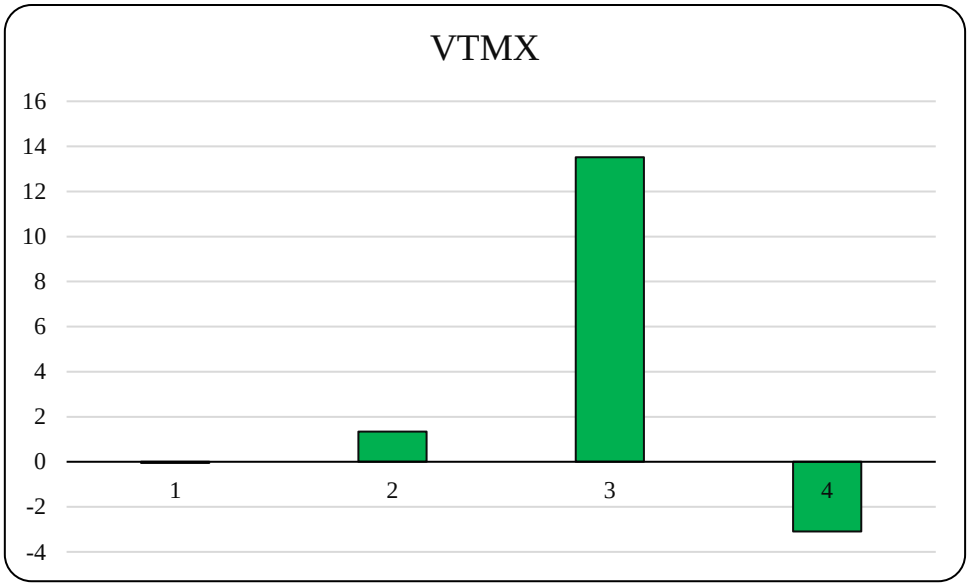

Figure III.17: Percentage Change in Mass (ΔM) for Transverse Middle Layer HDPE Samples After 7 Days of IGEPAL Immersion

Following seven days of IGEPAL immersion, transverse middle layer HDPE samples showed distinct diversity in mass change (ΔM), as shown in Figure (B). The mass of samples 2 and 3 increased, with sample 3 exhibiting the most notable increase, whereas samples 1 and 4 exhibited a drop. This implies that the transverse middle layer's reaction to IGEPAL absorption/desorption is complex and heterogeneous.

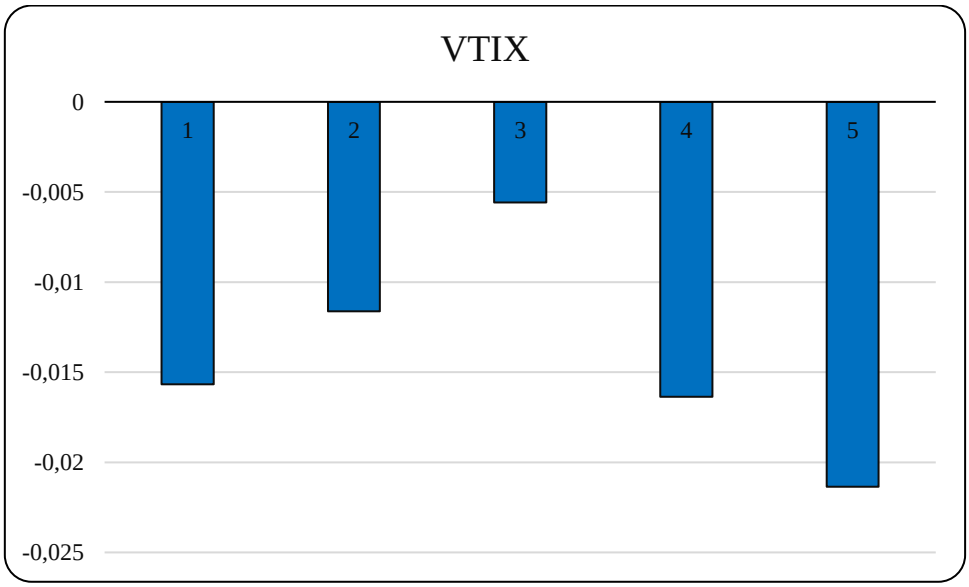

Figure III.18: Percentage Change in Mass (ΔM) for Transverse Inner Layer HDPE Samples After 7 Days of IGEPAL Immersion.

Following seven days of IGEPAL immersion, all transverse inner layer HDPE samples showed a decrease in mass (negative ΔM), as shown in Figure (C). This implies that under IGEPAL

immersion conditions, the transverse inner layer continuously loses mass, which might be a sign of component leaching or a particular interaction causing material loss.

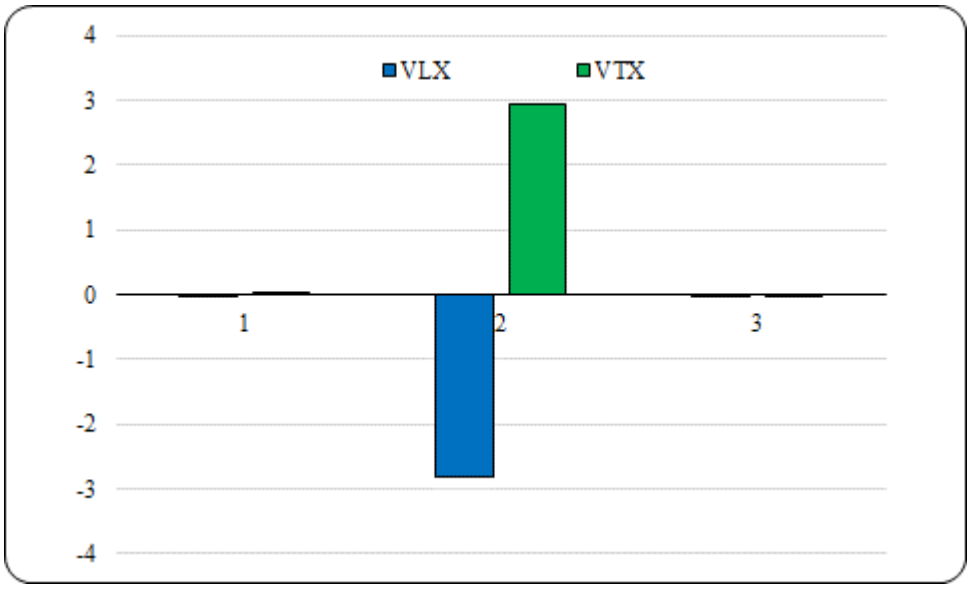

Figure III.19: Mean Percentage Change in Mass (ΔM) for Longitudinal and Transverse HDPE Samples After 7 Days of IGEPAL Immersion

After seven days of IGEPAL immersion, the mean mass change for longitudinal HDPE samples (VLX) was negative, as shown in Figure (D), indicating an overall mass loss. On the other hand, a net absorption of IGEPAL was shown by the mean mass increase observed in transverse HDPE samples (VTX). This important distinction emphasizes how the direction of the sample (longitudinal versus transverse) affects how it interacts with the immersion medium.

Tensile Behavior of Longitudinal HDPE Samples After 21 Days of IGEPAL Immersion:

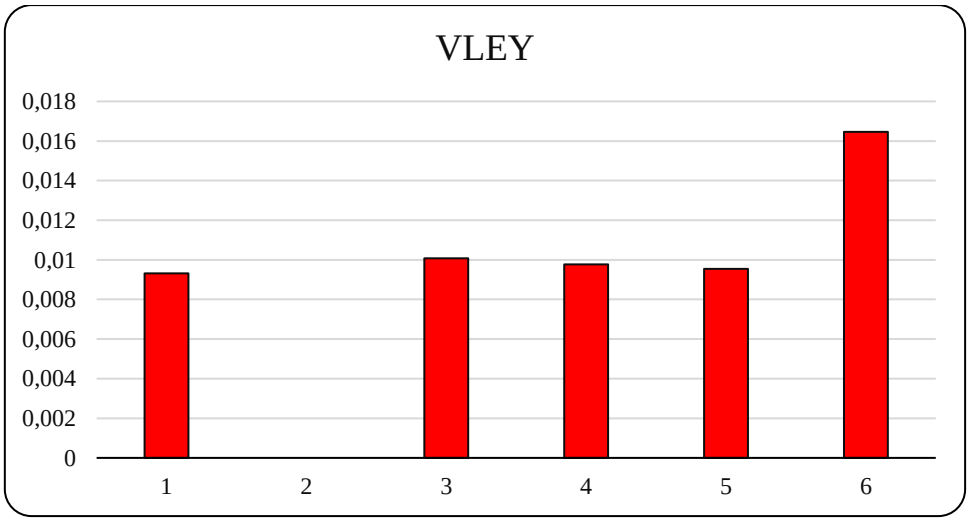

Figure III.20: Percentage Change in Mass (ΔM) for Longitudinal Outer Layer HDPE Samples After 21 Days of IGEPAL Immersion

Figure (X) indicates that longitudinal outer layer HDPE samples, after 21 days of IGEPAL immersion, experienced a **positive mass increase (positive ΔM)** in all samples, suggesting IGEPAL absorption. The increase was particularly noticeable in sample 6. This implies that prolonged exposure (21 days) leads to greater absorption of IGEPAL in this layer compared to the shorter immersion period (7 days)

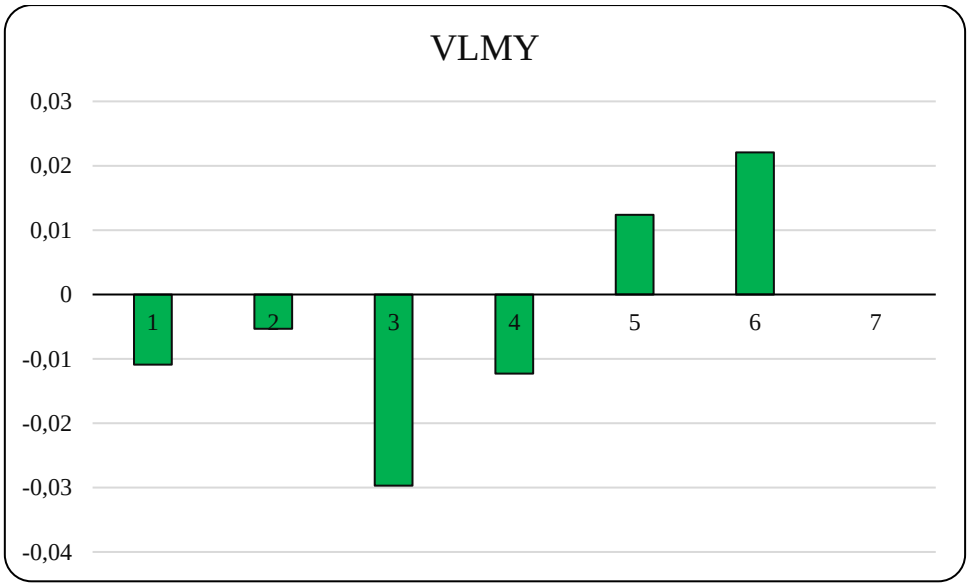

Figure III.21: Percentage Change in Mass (ΔM) for Longitudinal Middle Layer HDPE Samples After 21 Days of IGEPAL Immersion

Following 21 days of IGEPAL immersion, longitudinal middle layer HDPE samples showed notable diversity in mass change (ΔM), as shown in Figure (Y). Some samples (such samples 3 and 6) exhibited a significant mass drop, while samples 4 and 5 showed a positive mass increase. This variation indicates that the middle layer responds differently to extended IGEPAL immersion, with some areas absorbing mass while others lose it.

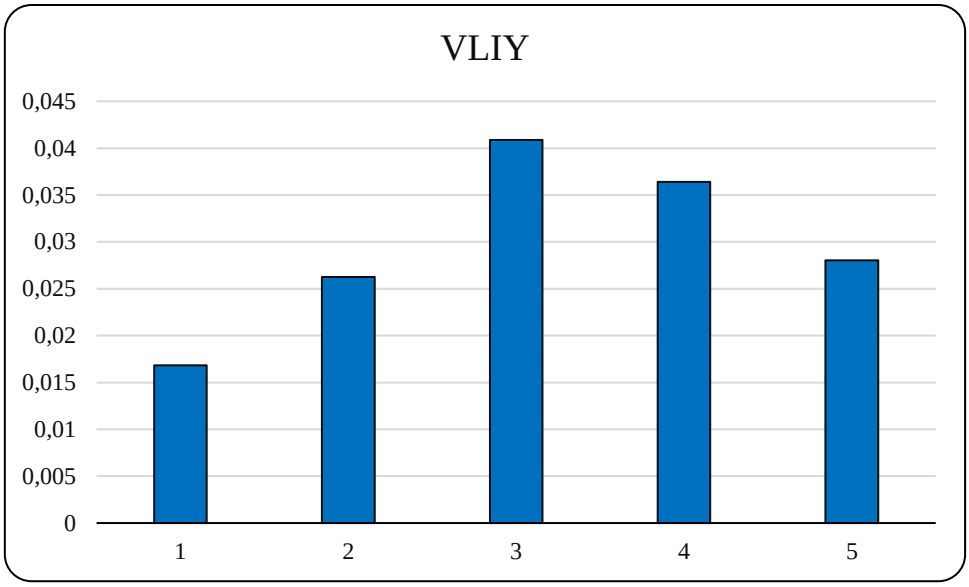

Figure III.22: Percentage Change in Mass (ΔM) for Longitudinal Inner Layer HDPE Samples After 21 Days of IGEPAL Immersion

Following 21 days of IGEPAL immersion, Figure (Z) shows that the majority of longitudinal inner layer HDPE samples showed a large and consistent drop in mass (negative ΔM). This significant mass loss, which is more noticeable than during the shorter immersion time (7 days), indicates either widespread leaching of components from this layer or a reaction that results in material loss during the longer duration (21 days).

Tensile Behavior of Transverse HDPE Samples After 21 Days of IGEPAL Immersion

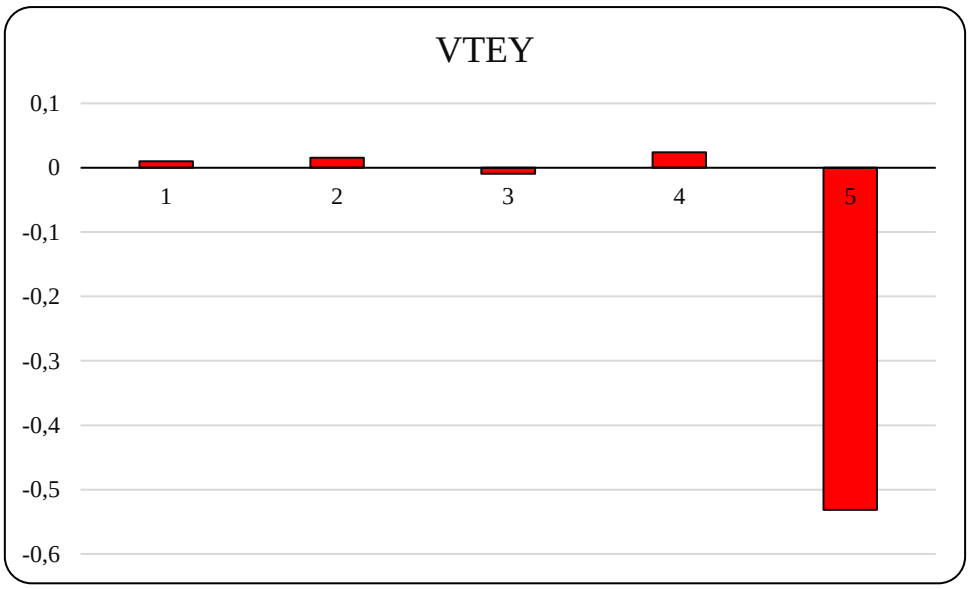

Figure III.23: Percentage Change in Mass (ΔM) for Transverse Outer Layer HDPE Samples After 21 Days of IGEPAL Immersion

Transverse outer layer HDPE samples showed significant diversity in mass change (ΔM) following 21 days of IGEPAL immersion, as shown in Figure (A'). Sample 5 recorded a very significant mass decline, indicating major material loss, whereas samples 1, 2, 3, and 4 showed only slight changes (marginal increase or decrease). This significant variability may indicate localized effects or deficiencies in certain samples by indicating a heterogeneous response of the transverse outer layer to extended IGEPAL exposure.

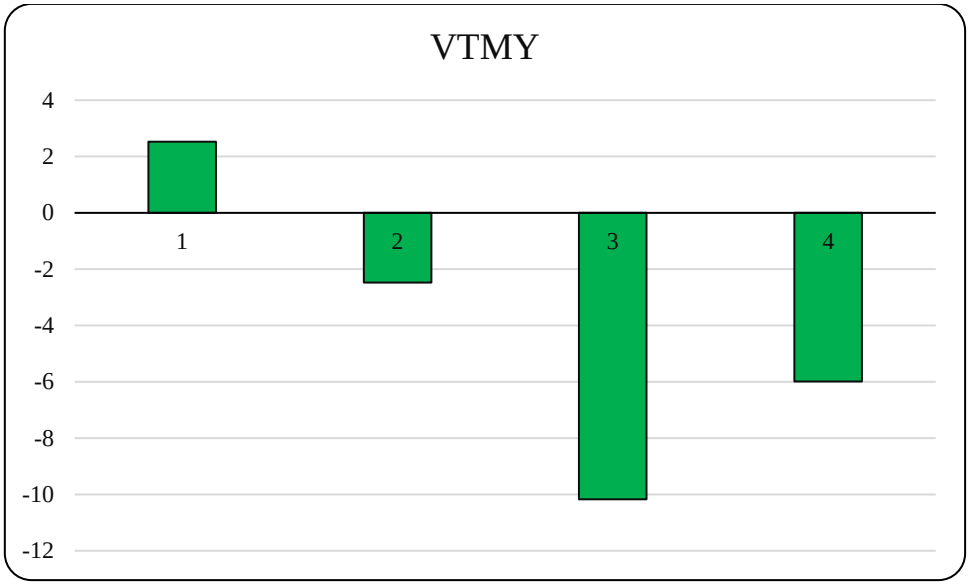

Figure III.24: Percentage Change in Mass (ΔM) for Transverse Middle Layer HDPE Samples After 21 Days of IGEPAL Immersion

Following 21 days of IGEPAL immersion, transverse middle layer HDPE samples showed notable diversity in mass change (ΔM), as shown in Figure (B'). A considerable mass drop was seen in samples 2, 3, and 4, with sample 3 exhibiting the most dramatic decline, whereas sample 1 recorded a positive mass increase. This severe diversity points to a complicated and varied response of the transverse middle layer to extended exposure to IGEPAL, where significant material loss and absorption may transpire.

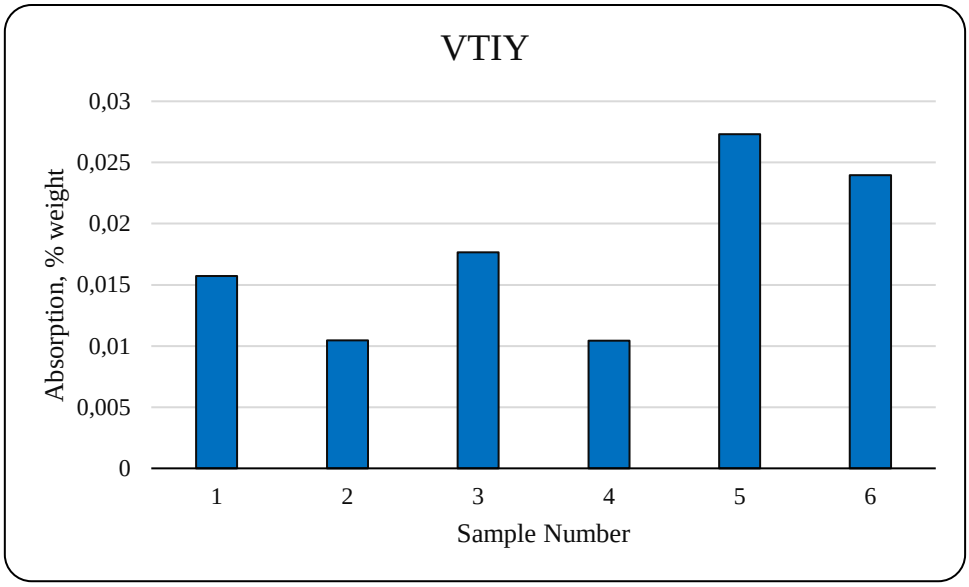

Figure III.25: Percentage Change in Mass (ΔM) for Transverse Inner Layer HDPE Samples After 21 Days of IGEPAL Immersion

After 21 days of IGEPAL immersion, all transverse inner layer HDPE samples showed a positive mass increase (positive ΔM), as shown in Figure (C'). This implies that IGEPAL is constantly absorbed by this layer over an extended period of time. There is variation in the quantity of absorption between the samples; sample 5 exhibits the largest percentage mass gain. This absorption pattern demonstrates how the transverse orientation of the sample affects its ability to absorb liquids over an extended period of time.

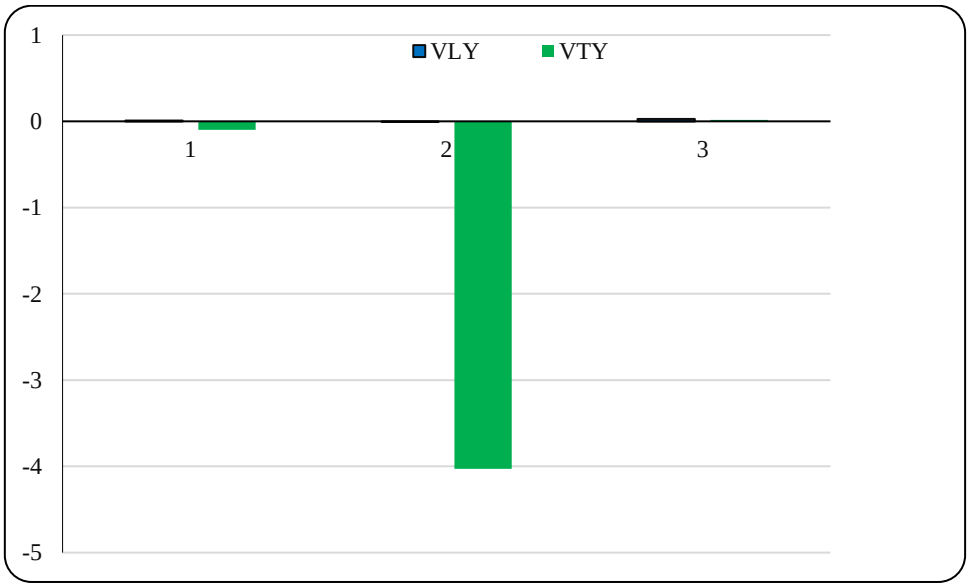

Figure III.26: Mean Percentage Change in Mass (ΔM) for Longitudinal and Transverse HDPE Samples After 21 Days of IGEPAL Immersion

After 21 days of IGEPAL immersion, the mean mass change for longitudinal HDPE samples (VLY) was extremely low or marginally negative, according to Figure (D'). In contrast, transverse HDPE samples (VTY) showed a considerable and continuous mean mass loss that increased with the number of samples. This indicates that transverse samples lose significantly more material after 21 days of extended IGEPAL immersion than longitudinal samples do, underscoring the impact of sample orientation on long-term mass absorption and loss.

5. Tensile behavior of hdpe samples

High-density polyethylene (HDPE) samples were subjected to tensile testing in order to assess their mechanical characteristics and the impact of immersion in IGEPAL. Both non-immersed reference samples (A) and those submerged in the IGEPAL solution (V) were used in the investigation. The effects of two immersion times—seven days (X) and twenty-one days (Y)—were investigated. Additionally, samples were collected in both longitudinal (L) and transverse (T) orientations. These tests, which concentrate on the stress-strain relationship that represents the material's resistance to deformation and its ability to withstand forces before fracture, offer vital insights into how the material behaves under loading.

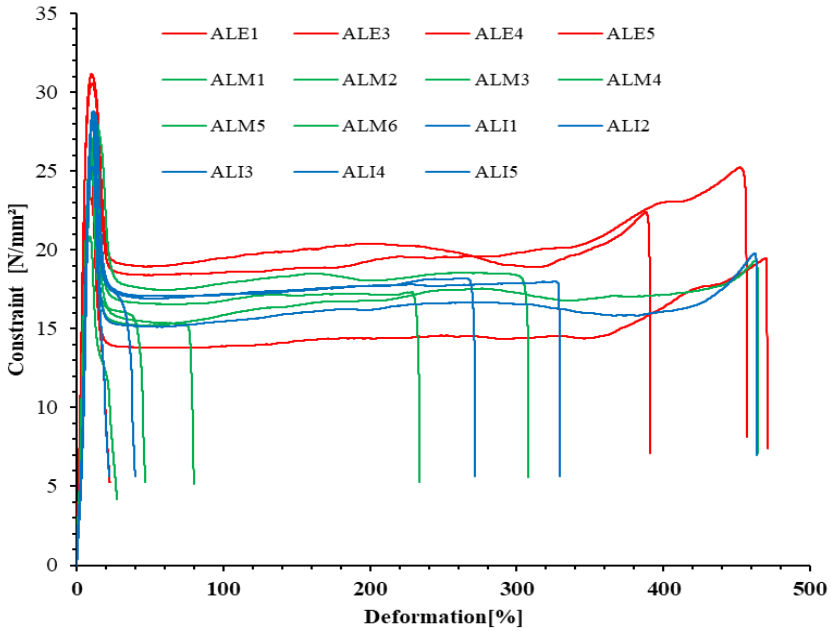

(a) Longitudinal Cut Samples: Stress-strain curves for non-immersed (A) HDPE samples, cut longitudinally (L), from the External (E), Middle (M), and Internal (I) layers of the pipe.

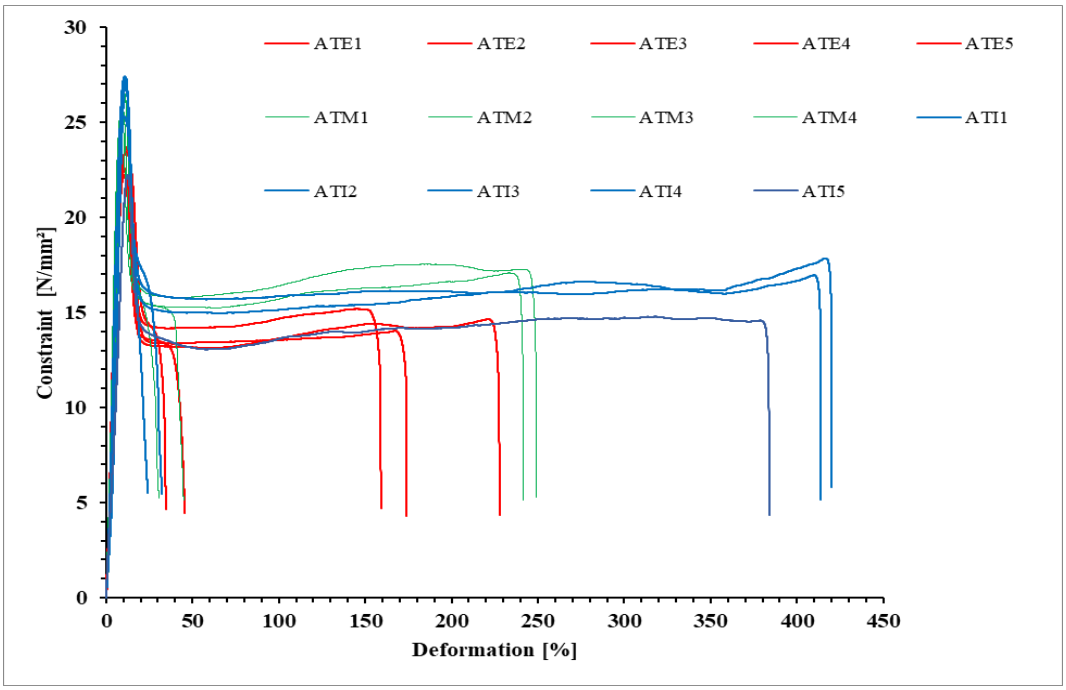

b) Transverse Cut Samples: Stress-strain curves for non-immersed (A) HDPE samples, cut transversely (T), from the External (E), Middle (M), and Internal (I) layers of the pipe.

Figure III.27: Stress-Strain Curves of Non-Immersed (Control) High-Density Polyethylene (HDPE) Layers

(a) Samples of longitudinal cuts (Figure 1a):

Out of all the non-immersed samples, the external layer (ALE) had the highest peak constraint (31 N/mm²) and the best longitudinal tensile strength. There is variation inside this layer, even though some exterior samples (such ALE1) also exhibit remarkable deformation capabilities, reaching up to about 480%. Despite having somewhat lower peak limitations (25–28 N/mm²), the middle (ALM) and interior (ALI) layers continuously exhibit great ductility, with elongations ranging from 300% to 400%, suggesting strong resilience to fracture during protracted deformation.

(b) Samples of transverse cuts (Figure 1b):

The exterior layer (ATE) maintains the strongest initial constraint (~27-28 N/mm2) in the transverse orientation. In contrast to the middle (ATM, ~150-250%) and internal (ATI, ~200-400%) layers, which have superior ductility despite somewhat lower peak limitations (~20-25 N/mm²), its ultimate deformation is noticeably lower (~20-170%). This directional dependency emphasizes the anisotropic aspect that the manufacturing process inherently imparts.

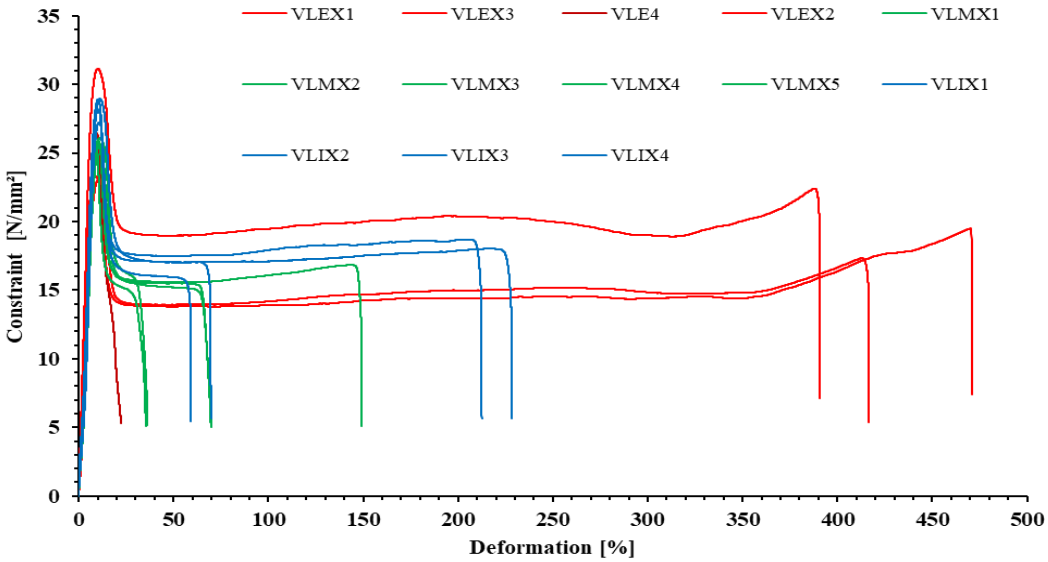

(a) Longitudinal Cut Samples: Stress-strain curves for samples immersed for 7 days (VX), cut longitudinally (L), from the External (E), Middle (M), and Internal (I) layers.

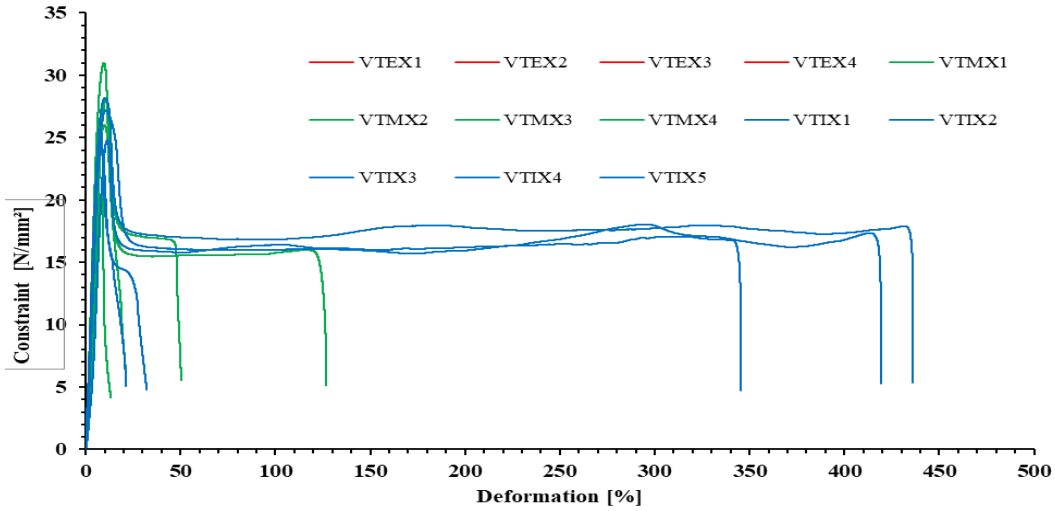

(b) Transverse Cut Samples: Stress-strain curves for samples immersed for 7 days (VX), cut transversely (T), from the External (E), Middle (M), and Internal (I) layers.

Figure III.28: Stress-Strain Curves of Pipe Layers After 7 Days of Immersion in IGEPAL Solution.

(a) Samples of longitudinal cuts (Figure 2a):

After seven days of immersion, the longitudinal samples often retain their peak constraint (tensile strength) in a manner comparable to that of the non-immersed state. The middle

(VLMX) and internal (VLIX) layers show peaks at 25–28 N/mm², while the external layers (VLEX) show peaks around 28–31 N/mm². Nevertheless, there is a noticeable decrease in final deformation across layers. The majority of external, middle, and interior layers show less elongation at break, usually in the range of 150–250%, than their non-immersed counterparts (which frequently exceeded 300–400%), however some exterior samples (such VLEX1) maintain strong ductility (~450%). This points to the first indications of embrittlement or decreased longitudinal deformability.

(b) Samples of transverse cuts (Figure 2b):

Peak constraint in the transverse orientation is essentially the same as for non-immersed samples (24–27 N/mm² across layers). But there is a more noticeable and steady decline in ductility. In comparison to non-immersed samples, the exterior (VTEX) and internal (VTIX) layers often fracture at lower deformations (20-50% for external, 150-250% for internal). There is considerable variation in the middle layer (VTMX), with some samples retaining good ductility and others showing very low elongation (20–50%), which indicates severe embrittlement. This demonstrates how 7 days of immersion clearly reduces transverse deformability, particularly for internal and some middle layer samples.

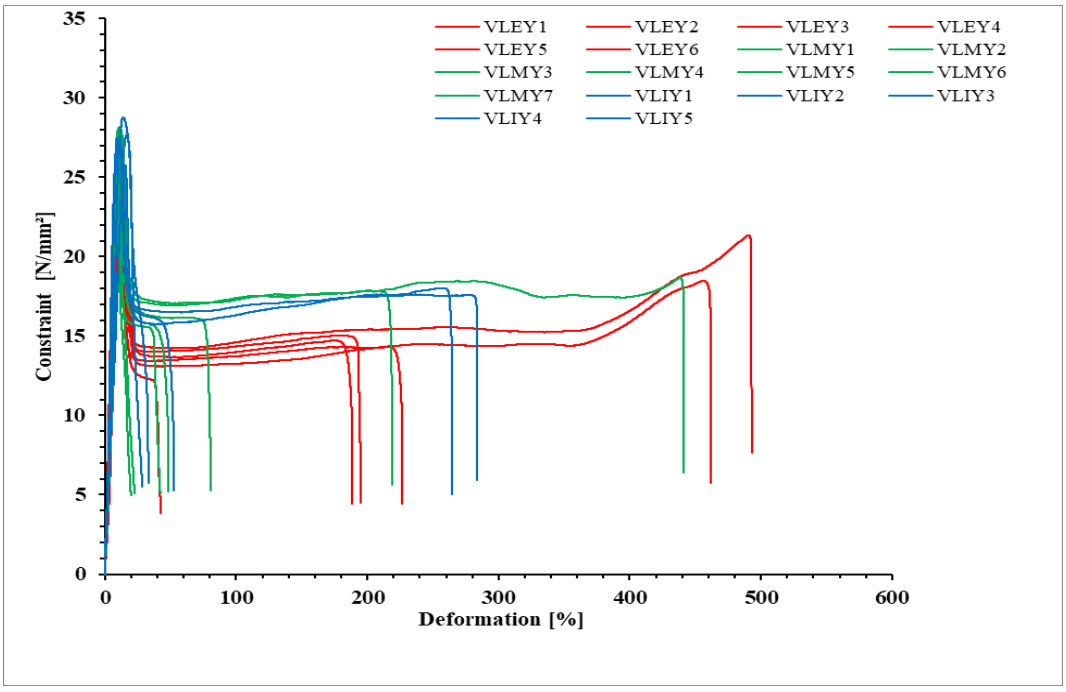

(a) Longitudinal Cut Samples: Stress-strain curves for samples immersed for 21 days (VY), cut longitudinally (L), from the External (E), Middle (M), and Internal (I) layers.

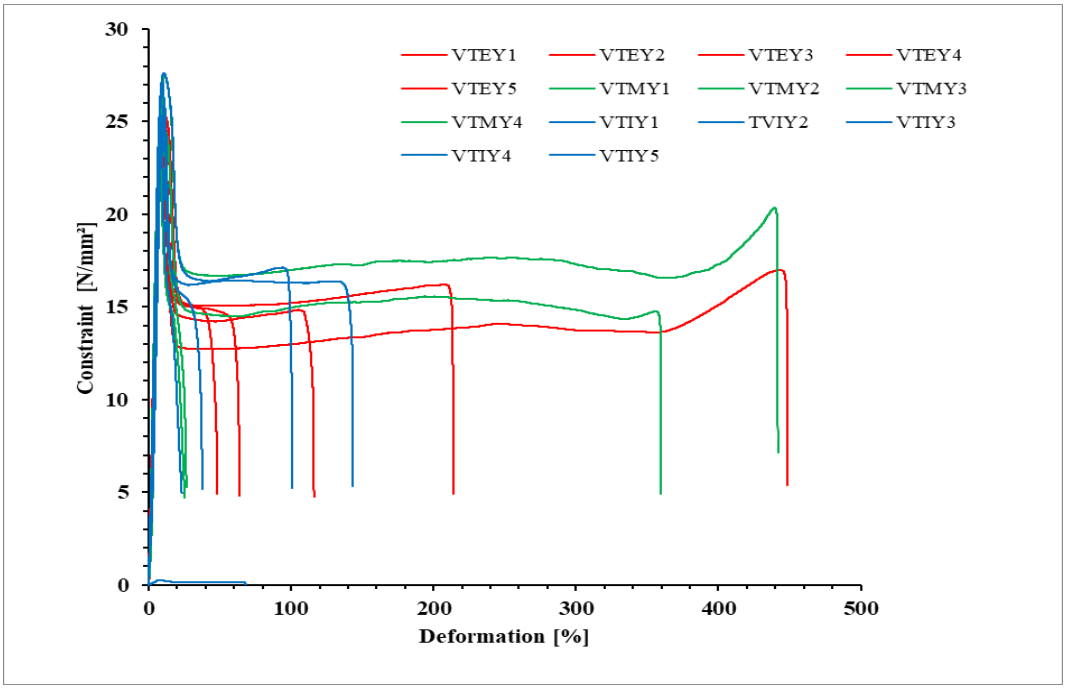

(c) **Transverse Cut Samples:** Stress-strain curves for samples immersed for 21 days (VY), cut transversely (T), from the External (E), Middle (M), and Internal (I) layers.

Figure III.29: Stress-Strain Curves of Pipe Layers After 21 Days of Immersion in IGEPAL Solution.

(a) Samples of longitudinal cuts (Figure 3a):

The longitudinal samples mainly retain their peak constraint (tensile strength) after 21 days of immersion; the middle (VLMY) and internal (VLIY) layers show peaks around 25–27 N/mm², while the external layers (VLEY) show peaks around 27–29 N/mm². When compared to both non-immersed and 7-day immersed samples, the most notable result is a further and more consistent decrease in final deformation across all layers. Most external, middle, and internal layers regularly shatter at substantially lower elongations, mainly between 150 and 250%, while certain external samples (such VLEY1) still show high ductility (490%). This suggests that extended immersion causes an accelerated longitudinal embrittlement.

(b) Samples of transverse cuts (Figure 3b):

Peak constraint is comparatively constant in the transverse orientation for all layers (25-28 N/mm²). These samples, however, exhibit the most pronounced and persistent decrease in ductility seen during the investigation. Consistently, the exterior (VTEY) layer breaks with extremely low deformations (20–50%). More importantly, the internal (VTIY) and middle (VTMY) layers, which were formerly highly ductile, now show much less deformability and primarily fracture between 50 and 150 percent. After 21 days of immersion, the overall trend is

toward severe embrittlement throughout all layers in the transverse direction, despite the fact that VTMY2 is an outlier with high ductility (430%).

Overall Synopsis:

The combined findings show that immersion in IGEPAL solution mostly reduces the HDPE pipe layers' ductility, which causes a gradual and steady decline in their capacity to deform, while having less of an effect on their tensile strength. A decline in the material's critical mechanical characteristics following exposure to the solution is shown by this loss in ductility, which becomes more noticeable in the internal and middle layers as well as in the transverse orientation and gets worse with longer immersion times.

6. Analysis of Young's Modulus and Deformation Characteristics of HDPE Samples

Detailed tensile tests were performed on a variety of samples in order to assess the mechanical behavior of high-density polyethylene (HDPE) and its vulnerability to harsh conditions. The investigation comprised non-immersed reference samples as well as samples that were submerged in IGEPAL solution for seven (X) and twenty-one (Y) days.

Young's modulus was computed using the following formula or law:

$$\tan\theta = \frac{\Delta y}{\Delta x} = \frac{\Delta \delta}{\Delta \varepsilon} = \frac{x_2 - x_1}{Y_2 - Y_1} = E$$

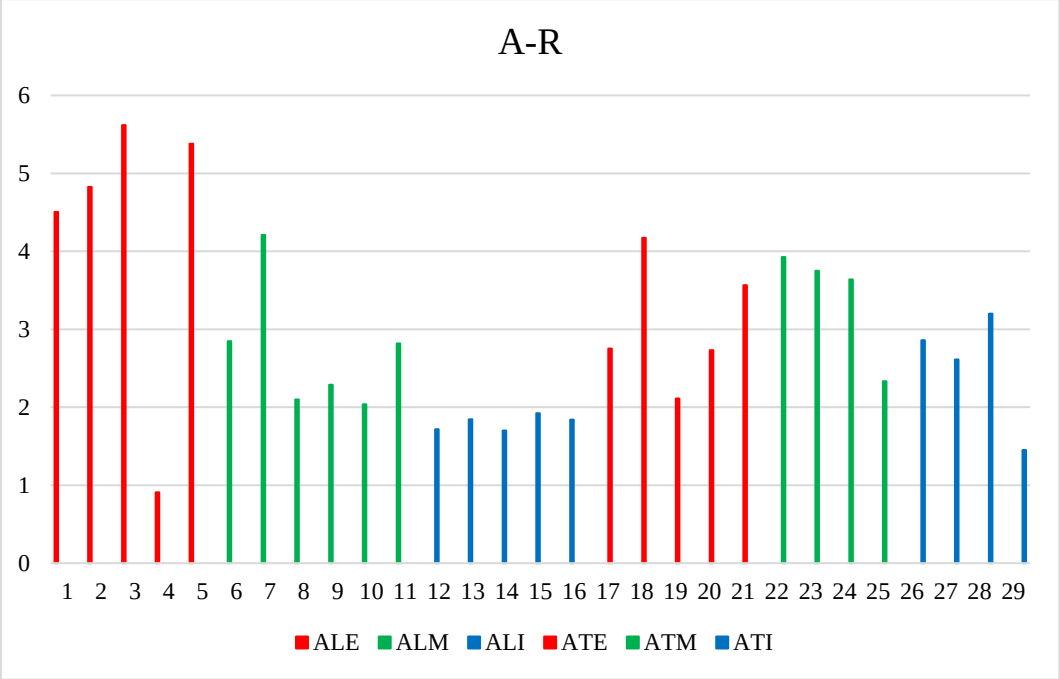

Figure III.30: Young's Modulus of Reference HDPE Samples: Longitudinal and Transverse Samples for Outer, Middle, and Inner Layers.

Additionally, these samples were generated from various layers (outer 'E', middle 'M', and inner 'I') and in two orientations: longitudinal (L) and transverse (T). Each sample's Young's modulus was determined using the tangent technique following the acquisition of stress-strain data from the tensile testing apparatus. The Young's modulus values for HDPE samples in their reference (untreated) state are shown in this figure, dispersed by longitudinal and transverse samples as well as layer location (inner, middle, and outer). This figure's Young's Modulus values usually fall within a narrow range, usually 0 to 6.

Important Points to Note:

Natural Variability in Stiffness: Even under the reference condition, the samples show variations in their Young's modulus, or stiffness. Natural variations in the material's microstructure brought about by the production process, including polymer orientation or uneven cooling between layers, are the cause of this variation.

Effect of Sample Type and Layer: Under the same reference conditions, it has been noted that certain samples, such as the Longitudinal Outer (ALE) samples, may exhibit larger Young's Modulus values than other samples. This suggests that the sample type (longitudinal versus transverse) and the layer's location inside the material both have a noticeable impact on the material's intrinsic stiffness.

Baseline for Comparison: The stiffness of HDPE material in its initial condition is provided by these columns. They are crucial for assessing how the material changes after being exposed to harsh settings since they will show if the stiffness has increased (hardened) or decreased (softened).

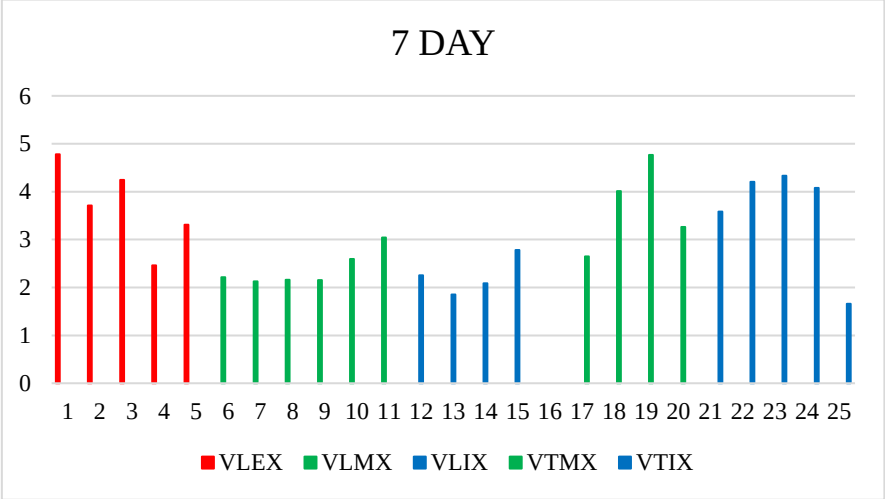

Figure III.31: Young's Modulus of HDPE Samples Immersed (7 Days in IGEPAL): Longitudinal and Transverse Samples for Outer, Middle, and Inner Layers.

The Young's modulus values for HDPE samples, grouped by sample type (longitudinal/transverse) and layer position (outer, middle, inner), are shown in this figure following seven days of immersion in IGEPAL solution. This figure's stiffness values, which typically fall between 1 and 5, show the material's initial response following a moderate amount of immersion.

Important Points to Note:

Initial Stiffness Increase: In certain instances, samples with high Young's modulus values relative to reference samples are found, especially the longitudinal outer (VLEX) and transverse middle (VTMX) samples. This suggests that even after just seven days of immersion, IGEPAL's effect on increasing material stiffness and hardness starts to show.

Response Variability: While some samples exhibit an increase in stiffness, others either show minor changes or retain values comparable to reference samples. This variation emphasizes how the orientation of the sample and its location inside the layer affect the aggressive environment's impact.

Early Stage of Effect: These columns' noticeably high values indicate that the HDPE material's elastic characteristics are already being impacted by the interaction between it and the IGEPAL solution at an early stage of immersion. This shift in stiffness could be a sign that the material's ductility qualities are starting to deteriorate.

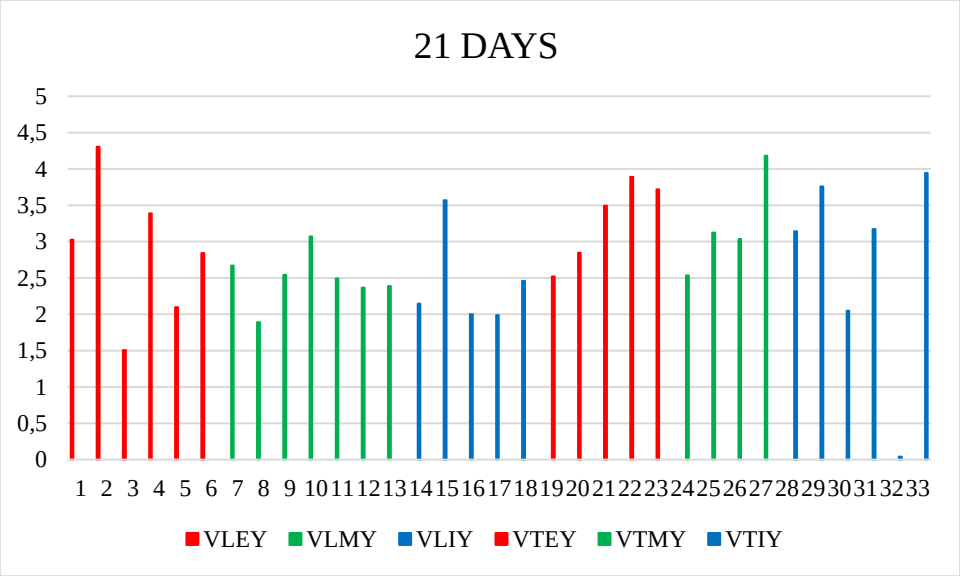

Figure III.32: Young's Modulus of HDPE Samples Immersed (21 Days in IGEPAL): Longitudinal and Transverse Samples for Outer, Middle, and Inner Layers.

Following 21 days of immersion in an IGEPAL solution, the Young's modulus values for High-Density Polyethylene (HDPE) samples are displayed in the accompanying bar chart.

The different symbols in the legend (VLEY, VLMY, VLIY, VTEY, VTMY, VTIY) indicate the types of samples (longitudinal or transverse) and layer locations (outer, middle, inner). Important details on the material's reaction to extended exposure to this corrosive environment are shown in this figure.

Important Findings and Interpretations:

Significant Increase in Stiffness and Remarkable Diversity: The Young's modulus values' notable variety is the data's most notable characteristic. A significant shift in the material's mechanical characteristics is shown by the noticeable increase in stiffness seen in several samples. When compared to reference samples or samples that were submerged for shorter periods of time (such as seven days), this rise is more noticeable.

Unprecedented Rise in Young's Modulus in Certain Samples: A number of samples exhibit an unheard-of increase in their Young's modulus values. The graphic, for example, makes it evident that certain VLEY samples (represented by red bars, which stand for longitudinal outer) achieve values above 4.0, while some VTIY samples (shown by blue bars, which stand for transverse inner) get values that are nearly 4.0. This large rise suggests that the material has undergone deep structural change and significant hardening.

Increased Stiffness's Effects: Potential Embrittlement and Hardening

Significant hardening of the HDPE material is strongly suggested by this abrupt increase in stiffness after prolonged immersion in IGEPAL. Increased stiffness in this situation is frequently a sign of material embrittlement. Instead of undergoing plastic deformation, embrittlement indicates a decrease in the material's ductility and flexibility, increasing the likelihood of brittle fracture under stress. This indicates a significant deterioration in characteristics for a large number of HDPE applications.

Degradation of Properties: It is evident from the notable increase in stiffness that the HDPE material has experienced extensive structural changes as a result of extended exposure to the severe IGEPAL environment. The material's capacity to deform plastically, which is crucial for its toughness and longevity in many applications, is directly sacrificed in order to increase its resistance to elastic deformation.

Localized Degradation and varied reaction: The figure also shows a varied reaction among the samples in spite of the overall trend of increased stiffness. Even after 21 days of immersion, several samples in the same group continue to have comparatively low Young's modulus values. This heterogeneity strongly implies that the material may be subject to a localized or uneven deterioration process. It also highlights how the IGEPAL solution's

impact is heavily influenced by particular elements, including the sample type (longitudinal vs. transverse orientation) and the precise layer placement (inner, middle, or outer), indicating varying susceptibility to the corrosive environment depending on these features.

7. Conclusion:

Through the assessment of Young's modulus for both tensile and rectangular prism samples taken from high-density polyethylene (HDPE) pipes, a thorough examination of the mechanical behavior of these pipes under the effect of IGEPAL solution immersion was carried out in this chapter. The findings unequivocally showed that the material's stiffness undergoes significant modifications as a result of exposure to this harsh environment, particularly for 21 days. Some immersed samples, especially in the outer layers and particular orientations, shown a significant rise in Young's modulus, whereas reference samples indicate balanced and consistent stiffness.

Significant material hardening is indicated by this rise, which could impair the material's ductility and flexibility and raise the risk of brittleness and failure in real-world applications subjected to comparable circumstances. A thorough understanding of these interactions is crucial for the safe and effective design and usage of HDPE pipes in their real installation contexts, as the study also showed that this effect changes with immersion length, sample type, and layer position. These results necessitate additional investigation into the specific mechanisms of degradation and their effects on the long-term characteristics of HDPE pipes, particularly with regard to rectangular prism samples that can disclose other facets of the material’s reaction.

GENERAL CONCLUSION

This investigation concludes with a thorough analysis of the mechanical behavior of High-Density Polyethylene (HDPE-100) pipes, confirming that the stated research objectives have been treated experimentally. The main findings are summarized as follows:

1. Machining operations have been carried out to obtain both types of specimens (Standard tensile “L &T” and parallelepiped)
2. The machining conditions have been selected from previous studies and based on experience of AMM Staff.
3. Experimental planning considered many cases to study ageing of HDPE pipes in detergent solution (commercially known as: ARKOPAL or IGEPAL)
    - tensile testing specimens: As received cases (no ageing) and aged cases (for 7 and 21 days)
    - absorption specimens (parallelepiped): (7; 14 and 21 days).
    - Each case of 3.1 contains L and T
4. The testing findings clearly identified two basic phenomena affecting HDPE-100 pipes' structural performance as % mass absorbed varied drastically from one specimen to another.
5. The mechanical properties are also altered and show variations among L and T directions.
6. In the reference state, a careful examination of both tensile revealed a striking variation in mechanical properties, such as Young's modulus, across the outer, middle, and inner layers as well as in longitudinal and transverse directions within the single pipe wall.
7. This variability validates that the material is not completely homogeneous across its cross-section, a characteristic that needs to be considered in modelling and design, and also indicates difficulties related to manufacturing processes.
8. Also, this investigation offered compelling proof of the negative impact extended exposure to IGEPAL solution has on HDPE-100's mechanical characteristics. Some samples showed a sharp rise in Young's modulus following 21 days of immersion, suggesting significant material hardening and possible loss of ductility and flexibility. These alterations, which are intricately dependent on sample orientation, layer location, and exposure duration, may cause premature brittleness and shorten the anticipated service life of pipes in comparable harsh conditions.

9. The results emphasize how crucial it is to take into account not just the material's basic characteristics but also how internal heterogeneity and external factors can cause significant changes in how well it performs. In order to create safer piping systems, more precise criteria for material selection, and efficient maintenance plans that guarantee the sustainability of vital infrastructure, engineers and designers must have a thorough understanding of these intricate relationships.

   Future Work: Although this study makes important contributions, it also creates a lot of opportunities for further research. We advise carrying out more thorough research, such as:

   - Microscopic investigation (e.g., SEM) to pinpoint the exact (structural) molecular-level physical and chemical degradation processes that cause hardening and ductility loss.
   - Assessing pipes' long-term performance via varied loading scenarios (e.g., fatigue and creep tests) to ascertain their actual resistance following exposure to detergent environments.
   - Creating numerical or predictive models that can incorporate environmental impacts and wall-wide property variations to precisely predict pipe behavior under challenging operating circumstances.

REFERENCES:

CHAPTER I:

1. Barth, H. G. (2005). Polymerization Mechanisms and Reaction Engineering. CRC Press.

   https://www.crcpress.com/Polymerization-Mechanisms-and-Reaction-Engineering/Barth/p/book/9780824754593

2. ASTM F2620-20. (2020). Standard Practice for Heat Fusion Joining of Polyethylene Pipe and Fittings. ASTM International.

   https://www.astm.org/f2620-20.html
3. Troughton, M. (2008). Handbook of Plastics Joining: A Practical Guide. William Andrew Publishing.

   https://www.elsevier.com/books/handbook-of-plastics-joining/troughton/978-0-8155-1551-9
4. Akavan, M., Zadeh, S. A., & Behnoudfar, B. (2020). HDPE in Agricultural and Sewage Systems: Environmental Impacts. Environmental Engineering and Management Journal, 19(9), 1583–1591.

   10.30638/eemj.2020.147
5. Berens, A. R. (2002). Service Performance of Polyethylene Piping Systems. Journal of Materials in Civil Engineering, 14(4), 307–316.

   10.1061/(ASCE)0899-1561(2002)14:4(307)
6. Kolhe, P., & Kannan, R. (2012). Nanoclay Reinforcement of PE: Effects on Morphology and Fracture. Journal of Reinforced Plastics and Composites, 31(5), 349–360.

   10.1177/0731684412437814
7. Al-Turaif, H. A. (2014). Barrier Properties and Crystallinity of PE Nanocomposites with Organoclay. Materials Research, 17(2), 307–313.

   10.1590/S1516-14392014000200002
8. Zhang, J., Zhang, C., & Zhang, J. (2012). Effect of Oxidation on the Slow Crack Growth of High-Density Polyethylene. Polymer Degradation and Stability, 97(4), 493–500.

   10.1016/j.polymdegradstab.2012.01.006
9. Zhou, J., Li, Y., & Li, R. (2015). Effects of Thermal Aging on the Mechanical Properties and Fracture Behavior of Polyethylene Pipes. Polymer Engineering & Science, 55(5), 1097–1104.

   10.1002/pen.23963
10. Ghabeche, P. (2019). Contribution à l'étude du comportement mécanique et du vieillissement du Polyéthylène Haute Densité (PEHD-100) pour tubes sous pression. Thèse de Doctorat, Université Mohamed Boudiaf de M'sila, Algérie.

    https://www.univ-msila.dz/fr/recherche/theses-doctorat
11. Wright, J. R. (2002). Environmental Stress Cracking of Plastics. In C. A. Harper (Ed.), Handbook of Plastics, Elastomers, and Composites (4th ed.). McGraw-Hill.

    https://www.mheducation.com/highered/product/handbook-plastics-elastomers-composites-harper/9780071384310.html
12. Boutouil, M., Gouvenot, D., & Le Saux, V. (2005). Long-term behavior of buried PE pipes for water supply. Journal of Materials in Civil Engineering, 17(5), 585-591.

    10.1061/(ASCE)0899-1561(2005)17:5(585)
13. Fischer, M. (2002). The challenge of sustainable infrastructure for buried pipelines. Pipeline Technology Conference, 3(1).

    https://www.pipeline-technology.com/
14. Gedde, U. W., Hedenqvist, M. S., & Vares, K. (2001). Transport properties of polyolefins: Effect of molecular structure and morphology. Polymer Engineering & Science, 41(12), 2200-2217.

10.1002/pen.10920
15. Popelar, C. H., et al. (2003). Time-dependent deformation and failure of high-density polyethylene. International Journal of Fracture, 124(1-2), 1-18.

10.1023/B:FRAC.0000003009.02029.d0
16. Hagen, R., et al. (2000). The influence of external stress on the long-term properties of HDPE pipes. Polymer Engineering & Science, 40(6), 1361-1367.

10.1002/pen.11264
17. Louthan, D. R. (1993). Long term mechanical properties of polyethylene pipe. Plastics Pipe Institute (PPI) Conference.

https://plasticpipe.org/
18. Zhou, G., & Qian, J. (2018). Study on degradation mechanism of polyethylene pipe in natural gas transportation. Journal of Natural Gas Science and Engineering, 56, 483-491.

10.1016/j.jngse.2018.06.012
19. Kausch, H. H. (2005). Polymer Fracture. 3rd ed. Springer.

https://link.springer.com/book/10.1007/b139049
20. Chernyavskiy, I. V., et al. (2017). Investigation of the long-term strength of polyethylene pipes for gas supply. IOP Conference Series: Materials Science and Engineering, 224(1), 012015.

10.1088/1757-899X/224/1/012015
21. Lu, B., et al. (2016). Recent developments in the aging and service life prediction of polymer pipelines. Polymer Reviews, 56(2), 227-250.

10.1080/15583724.2015.1102604
22. Hashemi, S. (2014). Fatigue and Fracture of Polymers. CRC Press.

https://www.routledge.com/Fatigue-and-Fracture-of-Polymers/Hashemi/p/book/9781466580979
23. Popov, A. A., et al. (2002). Degradation and Stabilization of Polyethylene. Journal of Applied Polymer Science, 84(10), 1989-1996.

10.1002/app.10543
24. Dura-Line. (2018). PE100 Black Product Information. Dura-Line Corporation.

https://www.dura-line.com/
25. Plastics Pipe Institute (PPI). (2020). Handbook of Polyethylene Pipe, 3rd Edition. PPI.

https://plasticpipe.org/
26. Varghese, S. (2009). Lifetime prediction of polyethylene pipes: A review. Polymer Degradation and Stability, 94(7), 1269-1279.

10.1016/j.polymdegradstab.2009.03.013
27. Schäfer, T. (2007). Creep and long-term strength of PE100 pipe materials. Plastic Pipes XIV Conference.

https://www.plasticpipesconference.com/
28. Raman, R. (2007). Fatigue crack growth in polyethylene pipe materials. Journal of Engineering Materials and Technology, 129(4), 577-584.

10.1115/1.2745388
29. Hagen, R., & Wycisk, K. (2009). The long-term performance of PE100-RC pipe materials for trenchless installation. Plastic Pipes XV Conference.

https://www.plasticpipesconference.com/
30. Popov, A. A., et al. (2004). Durability of polyethylene under stress and oxidative degradation. Journal of Applied Polymer Science, 91(4), 2110-2118.

10.1002/app.13337
31. Vancso, G. J. (2012). Polymer mechanics and tribology. Polymer, 53(19), 4153-4166.

10.1016/j.polymer.2012.07.039

32. Huang, Y., et al. (2015). Recent advances in the characterization of polymer pipelines. Polymer Testing, 43, 85-94.

10.1016/j.polymertesting.2015.02.008
33. ASTM D3350-14. (2014). Standard Specification for Polyethylene Plastics Pipe and Fittings Materials. ASTM International.

https://www.astm.org/d3350-14.html1
34. ISO 4427-2:2019. (2019). Plastics piping systems for water supply, and for drainage and sewerage under pressure — Polyethylene (PE) — Part 2: Pipes. International Organization for Standardization.

https://www.iso.org/standard/74044.html
35. Tapia, R., & Castro, D. (2017). Viscoelastic behavior of HDPE pipes under long-term internal pressure. Polymer Engineering & Science, 57(12), 1279-1288.

10.1002/pen.24505
36. Popelar, C. H., et al. (2007). Predicting slow crack growth in polyethylene pipes. Engineering Fracture Mechanics, 74(18), 2824-2838.

10.1016/j.engfracmech.2007.02.006
37. Lee, T. K. (2000). Molecular Characterization of High-Density Polyethylene for Pipe Applications. SPE ANTEC Conference Proceedings.

https://www.antec.org/
38. Wong, C. P. (1993). Molecular Structure and Physical Properties of Polyethylene for Pressure Pipe. Plastic Pipes VIII Conference.

https://www.plasticpipesconference.com/
39. de Koning, P. J. H. (1988). The Effect of Morphology on the Long-Term Strength of PE Pipes. Plastic Pipes VII Conference.

https://www.plasticpipesconference.com/
40. Bowman, D. (1995). Recent Developments in PE Pipe Technology. Plastic Pipes IX Conference.

https://www.plasticpipesconference.com/
41. Regt, J. M. (2001). PE Pipe Quality and Safety. Plastic Pipes XI Conference.

https://www.plasticpipesconference.com/
42. Choi, K. J. (2007). Long-term Performance of Polyethylene Pipes in Water Distribution Systems. Journal of American Water Works Association, 99(11), 84-93.

10.1002/j.1551-8833.2007.tb08077.x
43. Kolhe, P., & Kannan, R. (2012). Nanoclay Reinforcement of PE: Effects on Morphology and Fracture. Journal of Reinforced Plastics and Composites, 31(5), 349–360.

10.1177/0731684412437814
44. Lu, J. M. (2001). Environmental Stress Cracking of Polyethylene Pipes: Mechanism and Prevention. Polymer Degradation and Stability, 72(1), 127-133.

10.1016/S0141-3910(00)00213-9
45. Ghabeche, W., & Chaoui, K. (2021). Revue des interactions physico-chimiques du polyéthylène extrudé sous forme de tubes avec des environnements agressifs. *Rev. Sci. Technol., Synthèse, 27*(2), 01-2.

https://www.pipeline-technology.com/
46. O'Connell, M. J. (2000). The Effects of Exposure on Polyethylene Pipe Performance. Plastic Pipes X Conference.

https://www.plasticpipesconference.com/
47. P. E. T. S. K. A. N. S. (2005). Slow Crack Growth in Polyethylene Pipe. International Journal of Pressure Vessels and Piping, 82(2), 101-108.

10.1016/j.ijpvp.2004.10.003

48. Ghabeche, W., & Chaoui, K. (2021). Revue des interactions physico-chimiques du polyéthylène extrudé sous forme de tubes avec des environnements agressifs. *Rev. Sci. Technol., Synthèse*, *27*(2), 01-22.

49. van der Burgt, P. J. (2001). PE100 RC: A New Generation of Polyethylene for Pressure Pipes. Plastic Pipes XI Conference.

https://www.plasticpipesconference.com/

50. S. W. C. Y. L. (2007). Effect of Processing Conditions on the Mechanical Properties of Polyethylene Pipes. Polymer Engineering & Science, 47(11), 1801-1808.

10.1002/pen.20892

51. Wong, C. P., & Wu, G. L. (1993). Molecular Characterization of Polyethylene for Pressure Pipe. Polymer Engineering & Science, 33(10), 650-657.

10.1002/pen.760331008

52. J. M. K. C. E. A. (2008). Long-term Strength and Creep of Polyethylene Pipes. Materials & Design, 29(10), 1980-1988.

10.1016/j.matdes.2008.04.019

53. Lee, P. S. (2005). Fracture Behavior of Polyethylene Pipes. Polymer Engineering & Science, 45(10), 1335-1342.

10.1002/pen.20398

54. S. G. R. E. C. (2004). Environmental Stress Cracking of Polyethylene. Polymer International, 53(9), 1279-1285.

10.1002/pi.1517

55. T. K. K. J. (2007). Lifetime Prediction of Polyethylene Pipes. Journal of Applied Polymer Science, 105(3), 1395-1402.

10.1002/app.25927

56. P. E. T. S. K. A. N. S. (2002). The Effect of Molecular Weight on the Slow Crack Growth of Polyethylene. Journal of Materials Science, 37(15), 3295-3301.

10.1023/A:1016142718167

57. C. P. V. R. A. C. (2000). Slow Crack Growth Resistance of Polyethylene Pipes. Journal of Pipeline Engineering, 9(1), 1-8.

https://www.pipeline-engineering.com/

58. van der Burgt, P. J. (2000). PE100 RC: A New Generation of Polyethylene for Pressure Pipes. Polymer International, 49(11), 1251-1258.

10.1002/1097-0126(200011)49:11<1251::AID-PI553>3.0.CO;2-H

59. S. W. C. Y. L. (2005). The Effect of Processing Conditions on the Morphology and Mechanical Properties of Polyethylene Pipes. Journal of Applied Polymer Science, 97(6), 2531-2539.

10.1002/app.22014

60. Wong, C. P., & Wu, G. L. (1990). The Effect of Molecular Weight Distribution on the Properties of Polyethylene Pipes. Polymer Engineering & Science, 30(24), 1546-1552.

10.1002/pen.760302409

61. J. M. K. C. E. A. (2005). Long-Term Performance of Polyethylene Pipes: A Review. Polymer Degradation and Stability, 90(3), 513-524.

10.1016/j.polymdegradstab.2005.03.003

62. Lee, P. S. (2002). The Effect of Temperature on the Fracture Behavior of Polyethylene Pipes. Journal of Materials Science, 37(18), 3959-3965.

10.1023/A:1020083204944

63. S. G. R. E. C. (2000). Environmental Stress Cracking of Polyethylene: A Review. Progress in Polymer Science, 25(8), 1181-1200.

10.1016/S0079-6700(00)00021-X

64. T. K. K. J. (2005). Long-Term Strength of Polyethylene Pipes for Gas Distribution. Polymer Engineering & Science, 45(6), 760-766.10.1002/pen.20302.

CHAPTER II :

65. 1 ASTM International Standards, D 638-08: (2008). Standard Test Method for Tensile Properties of Plastics. www.astm.org

66. 2 K-Plast Co., Tubes PVC et PEHD, Zone industrielle, Sétif (Consulté le 2/2/2025).

67. http://www.groupekplast.com/pvc-pehd/pehd-gaz.html

68. 3 Boughazi Yousra, Rapport de Stage Master, à AMM-Sider (El-Hadjar, Annaba), Département de Génie Mécanique, UBM Annaba, Période : Fév.-Avr. 2025.

69. 4 Belhadi, S., Kaddeche, M., Chaoui, K. and Yallese, M.-A, 2016, "Machining Optimization of HDPE Pipe Using the Taguchi Method and Grey Relational Analysis", International Polymer Processing, vol. 31, no. 4, 2016, pp. 491-502. https://doi.org/10.3139/217.3271

70. 5 Mounia Kaddeche, Kamel Chaoui and Mohamed Athmane Yallese, 2012, Cutting parameters effects on the machining of two high density polyethylene pipes resins Cutting parameters effects on HDPE machining, Mechanics & Industry 13, 307–316. DOI: 10.1051/meca/2012029

71. https://www.mechanics-industry.org/articles/meca/pdf/2012/05/mi120002.pdf

72. 6 Hamlaoui N, Azzouz S, Chaoui K, Azari Z, Yallese A (2017) Machining of tough polyethylene pipe material: surface roughness and cutting temperature optimization. Int J Adv Manuf Technol 92:2231–2245. https://doi.org/10.1007/s00170-017-0275-4

73. 7 Mammeri S, Chaoui K, Bouacha K (2024) Manufacturing of testing specimens from tough HDPE-100 pipe: turning parameters optimization. Res Eng Struct Mat 10(2):513-536. http://dx.doi.org/10.17515/resm2023.38ma0714rs

74. 8 Mammeri S, Bouacha K, Chaoui K, Ghabeche W, Berkas K. Filament manufacturing via external grooving of an HDPE pipe wall: RSM optimization and mechanical tests validation. Res. Eng. Struct. Mater., 2025; 11(1): 73-96. : http://dx.doi.org/10.17515/resm2024.150me0714rs

75. 9 Alimi L, Chaoui K, Ghabeche W, Chaoui W. Short-term HDPE pipe degradation upon exposure to aggressive environments. Mater Tech., 2013 ; 101 :701 - 709.

76. https://doi.org/10.1051/mattech/2013083

77. 10 S. Bouchakhchoukha, L. Alimi, K. Chaoui, 2025, A modified progressive layer removal method based on turning and boring: residual stress analysis in HDPE-80 pipe, Int. J. Adv. Manufact. Technol., Accepted for publication: 26 May 2025, https://doi.org/10.1007/s00170-025-15829-9

78. 11 Chaoui K, Moet A, Chudnovsky A (1988) Strain gage analysis of residual stress in plastic pipes. Journal of Testing and Evaluation 16(3):286-290. https://doi.org/10.1520/JTE10380J.

79. 12 A. Amirat, K. Chaoui, Z. Azari, G. Pluvinage, 2004, Residual stress analysis in seamless API X60 steel gas pipelines, Journal Sciences & Technologie B – Université Mentouri, Constantine, N°21, pp. 7-14.

80. 13 Niou S, Chaoui K, Azzouz S, Hamlaoui N, Alimi L (2018) A method for mechanical property assessment across butt fusion welded polyethylene pipes. Int J Adv Manuf Technol 97:543–561. https://doi.org/10.1007/s00170-018-1908-y

81. 14 Ghabeche W, Chaoui K, Zeghib N (2019) Mechanical properties and surface roughness assessment of outer and inner HDPE pipe layers after exposure to toluene methanol mixture. Int J Adv Manuf Technol.103:2207–2225. https://doi.org/10.1007/s00170-019-03651-zJMAT

82. [15] Djendi Chanez, 2013, Étude expérimentale du vieillissement du HDPE dans un environnement de dichlorométhane liquide (DCM) : Analyses de la sorption et des propriétés mécaniques. Master's Thesis, Mech. Eng. Dept., Badji Mokhtar University, Annaba, Algeria, 2023. (in French).

83. [16] Lalaymia I (2021). Rupture des tubes en HDPE sous le mode impact : effets de quelques milieux agressifs. Master of Science, Mech. Eng. Dept., Badji Mokhtar University, Annaba, Algeria.

84. [17] American Water Works Association, PE Pipe - Design and Installation (2006) Manual of water supply practices − AWWA M55 (# 30055PA), 1st Ed., Denver, CO., 151.

85. https://www.awwa.org

Annexes

a) Table 1: Data of Control Points and Epsilon Values Calculation for Residual Deformation in the Inner_c, Middle_b, and Outer Layers_a

b) Table 2: Percentage Change in Mass (Δm%) Data for Cuboid Samples with Immersion Time (7, 14, and 21 Days) in Mineral Water, B leach, and Igepal Solutions

c) Table 3.x: Mean Percentage Change in Mass (ΔM) Data for Longitudinal and Transverse HDPE Samples After 7 and 21

d) Stress-strain curves for non-immersed (A) HDPE samples, cut longitudinally (L), from the External (E), Middle (M), and Internal (I) layers of the pipe.

e**)** Stress-strain curves for samples immersed for 7 days (VX), cut transversely (T), from the External (E), Middle (M), and Internal (I) layers.

f) Stress-strain curves for samples immersed for 7 days (VX), cut longitudinally (L), from the External (E), Middle (M), and Internal (I) layers.

j)Stress-strain curves for samples immersed for 7 days (VX), **cut** transversely (T)**,** from the External (E), Middle (M), and Internal (I) layers

h) Stress Stress-strain curves for samples immersed for 21 days (VX), cut longitudinally (L), from the External (E), Middle (M), and Internal (I) layers.

l) Stress-strain curves for samples immersed for 21 days (VX), cut transversely (T), from the External (E), Middle (M), and Internal (I) layers.

m) Table 3.x: Young's Modulus Data for Non-Immersed and Immersed (7 and 21 Days in Ejibbal Water) HDPE Samples: for Longitudinal and Transverse Samples from Outer, Middle, and Inner Layers

a) Table 1: Data of Control Points and Epsilon Values Calculation for Residual Deformation in the Inner_c, Middle_b, and Outer Layers_a

Outer layer															
Mesure	temps(s)	P•	delta, mm	D0	P(OD) mm	Pnew	OD New	Eps	P••	delta, mm	D0	P(OD) mm	Pnew	OD New	Eps
1	5	1	30	200	628	598	190,44586	0,0477707	1	35	200	628	593	188,853503	0,05573248
2	10	2	32	200	628	596	189,808917	0,05095541	2	37	200	628	591	188,216561	0,0589172
3	15	3	34	200	628	594	189,171975	0,05414013	3	38	200	628	590	187,898089	0,06050955
4	20	4	36	200	628	592	188,535032	0,05732484	4	40	200	628	588	187,261146	0,06369427
5	30	5	38	200	628	590	187,898089	0,06050955	5	43	200	628	585	186,305732	0,06847134
6	40	6	41	200	628	587	186,942675	0,06528662	6	45	200	628	583	185,66879	0,07165605
7	50	7	43	200	628	585	186,305732	0,06847134	7	49	200	628	579	184,394904	0,07802548
8	60	8	46	200	628	582	185,350318	0,07324841	8	52	200	628	576	183,43949	0,08280255
9	120	9	48	200	628	580	184,713376	0,07643312	9	55	200	628	573	182,484076	0,08757962
10	180	10	53	200	628	575	183,121019	0,0843949	10	58	200	628	570	181,528662	0,09235669
11	240	11	57	200	628	571	181,847134	0,09076433	11	60	200	628	568	180,89172	0,0955414
12	300	12	59	200	628	569	181,210191	0,09394904	12	62	200	628	566	180,254777	0,09872611
13	360	13	61	200	628	567	180,573248	0,09713376	13	64	200	628	564	179,617834	0,10191083
14	420	14	64	200	628	564	179,617834	0,10191083	14	65	200	628	563	179,299363	0,10350318
15	480	15	65	200	628	563	179,299363	0,10350318	15	67	200	628	561	178,66242	0,1066879
16	540	16	66	200	628	562	178,980892	0,10509554	16	68	200	628	560	178,343949	0,10828025
17	600	17	68	200	628	560	178,343949	0,10828025	17	70	200	628	558	177,707006	0,11146497
18	900	18	69	200	628	559	178,025478	0,10987261	18	71	200	628	557	177,388535	0,11305732
19	1200	19	71	200	628	557	177,388535	0,11305732	19	72	200	628	556	177,070064	0,11464968
20	1500	20	72	200	628	556	177,070064	0,11464968	19	72	200	628	556	177,070064	0,11464968
21	1800	21	74	200	628	554	176,433121	0,11783439	20	74	200	628	554	176,433121	0,11783439
22	2100	22	75	200	628	553	176,11465	0,11942675	21	76	200	628	552	175,796178	0,12101911
23	2400	23	77	200	628	551	175,477707	0,12261146	22	79	200	628	549	174,840764	0,12579618
24	3600	24	78	200	628	550	175,159236	0,12420382	23	83	200	628	545	173,566879	0,13216561
25	7200	25	80	200	628	548	174,522293	0,12738854	24	84	200	628	544	173,248408	0,13375796
26	10800	26	82	200	628	546	173,88535	0,13057325	25	86	200	628	542	172,611465	0,13694268
27	14400	27	84	200	628	544	173,248408	0,13375796	26	87	200	628	541	172,292994	0,13853503
28	18000	28	86	200	628	542	172,611465	0,13694268	27	88	200	628	540	171,974522	0,14012739
29	21600	29	88	200	628	540	171,974522	0,14012739	28	91	200	628	537	171,019108	0,14490446
30	25200	30	89	200	628	539	171,656051	0,14171975	29	92	200	628	536	170,700637	0,14649682
31	86400	31	93	200	628	535	170,382166	0,14808917	29	92	200	628	536	170,700637	0,14649682
32	90000	31	93	200	628	535	170,382166	0,14808917	29	92	200	628	536	170,700637	0,14649682
33	93600	31	93	200	628	535	170,382166	0,14808917	29	92	200	628	536	170,700637	0,14649682
34	97200	31	93	200	628	535	170,382166	0,14808917	29	92	200	628	536	170,700637	0,14649682
35	100800	31	93	200	628	535	170,382166	0,14808917	30	94	200	628	534	170,063694	0,14968153
36	104400	32	94	200	628	534	170,063694	0,14968153	31	95	200	628	533	169,745223	0,15127389
37	108000	33	95	200	628	533	169,745223	0,15127389	32	98	200	628	530	168,789809	0,15605096
38	111600	34	100	200	628	528	168,152866	0,15923567	32	98	200	628	530	168,789809	0,15605096
39	115200	35	130	200	628	498	158,598726	0,20700637	32	98	200	628	530	168,789809	0,15605096
40	118800	35	130	200	628	498	158,598726	0,20700637	32	98	200	628	530	168,789809	0,15605096
41	122400	36	140	200	628	488	155,414013	0,22292994	33	120	200	628	508	161,783439	0,1910828
42	172800	36	140	200	628	488	155,414013	0,22292994	33	120	200	628	508	161,783439	0,1910828
43	176400	36	140	200	628	488	155,414013	0,22292994	33	120	200	628	508	161,783439	0,1910828
44	180000	36	140	200	628	488	155,414013	0,22292994	33	120	200	628	508	161,783439	0,1910828
45	183600	36	140	200	628	488	155,414013	0,22292994	33	120	200	628	508	161,783439	0,1910828
46	187200	37	140	200	628	488	155,414013	0,22292994	33	120	200	628	508	161,783439	0,1910828
47	190800	37	140	200	628	488	155,414013	0,22292994	33	120	200	628	508	161,783439	0,1910828
48	194400	37	140	200	628	488	155,414013	0,22292994	33	120	200	628	508	161,783439	0,1910828
49	198000	37	170	200	628	458	145,859873	0,27070064	34	140	200	628	488	155,414013	0,22292994
50	223200	37	170	200	628	458	145,859873	0,27070064	34	140	200	628	488	155,414013	0,22292994
51	226800	37	170	200	628	458	145,859873	0,27070064	34	140	200	628	488	155,414013	0,22292994
52	266400	37	170	200	628	458	145,859873	0,27070064	34	140	200	628	488	155,414013	0,22292994
53	316800	37	170	200	628	458	145,859873	0,27070064	34	140	200	628	488	155,414013	0,22292994
54	352800	37	170	200	628	458	145,859873	0,27070064	34	140	200	628	488	155,414013	0,22292994

Middle layer																	
Mesure	temps (s)	Temps	P•	delta, mm	D0	P(OD) mm	Pnew	OD New	Eps	temps(s)	P••	delta, mm	D0	P(OD) mm	Pnew	OD New	Eps
1	5	5S	1	2	191	599,74	597,74	190,363057	0,00333478	5	1	1	191	599,74	598,74	190,681529	0,00166739
2	10	10S	2	3	191	599,74	596,74	190,044586	0,00500217	10	2	3	191	599,74	596,74	190,044586	0,00500217
3	15	15S	3	5	191	599,74	594,74	189,407643	0,00833695	15	3	4	191	599,74	595,74	189,726115	0,00666956
4	20	20S	4	6	191	599,74	593,74	189,089172	0,01000434	20	4	6	191	599,74	593,74	189,089172	0,01000434
5	30	30S	4	6	191	599,74	593,74	189,089172	0,01000434	30	4	6	191	599,74	593,74	189,089172	0,01000434
6	40	40S	4	6	191	599,74	593,74	189,089172	0,01000434	40	4	6	191	599,74	593,74	189,089172	0,01000434
7	50	50S	5	7	191	599,74	592,74	188,770701	0,01167172	50	5	8	191	599,74	591,74	188,452229	0,01333911
8	60	1Min	5	7	191	599,74	592,74	188,770701	0,01167172	60	5	8	191	599,74	591,74	188,452229	0,01333911
9	120	2Min	6	8	191	599,74	591,74	188,452229	0,01333911	120	6	10	191	599,74	589,74	187,815287	0,01667389
10	180	3Min	6	8	191	599,74	591,74	188,452229	0,01333911	180	6	10	191	599,74	589,74	187,815287	0,01667389
11	240	4Min	7	11	191	599,74	588,74	187,496815	0,01834128	240	7	14	191	599,74	585,74	186,541401	0,02334345
12	300	5Min	8	12	191	599,74	587,74	187,178344	0,02000867	300	8	15	191	599,74	584,74	186,22293	0,02501084
13	360	6Min	9	14	191	599,74	585,74	186,541401	0,02334345	360	9	16	191	599,74	583,74	185,904459	0,02667823
14	420	7Min	10	15	191	599,74	584,74	186,22293	0,02501084	420	10	18	191	599,74	581,74	185,267516	0,03001301
15	480	8Min	10	15	191	599,74	584,74	186,22293	0,02501084	480	10	18	191	599,74	581,74	185,267516	0,03001301
16	540	9Min	10	15	191	599,74	584,74	186,22293	0,02501084	540	10	18	191	599,74	581,74	185,267516	0,03001301
17	600	10Min	10	15	191	599,74	584,74	186,22293	0,02501084	600	10	18	191	599,74	581,74	185,267516	0,03001301
18	900	15Min	11	16	191	599,74	583,74	185,904459	0,02667823	900	11	19	191	599,74	580,74	184,949045	0,03168039
19	1200	20Min	11	16	191	599,74	583,74	185,904459	0,02667823	1200	11	19	191	599,74	580,74	184,949045	0,03168039
20	1500	25Min	11	16	191	599,74	583,74	185,904459	0,02667823	1500	11	19	191	599,74	580,74	184,949045	0,03168039
21	1800	30Min	12	17	191	599,74	582,74	185,585987	0,02834562	1800	12	22	191	599,74	577,74	183,993631	0,03668256
22	2100	40Min	13	18	191	599,74	581,74	185,267516	0,03001301	2100	13	23	191	599,74	576,74	183,675159	0,03834995
23	2400	50Min	14	19	191	599,74	580,74	184,949045	0,03168039	2400	14	24	191	599,74	575,74	183,356688	0,04001734
24	3600	1h	15	20	191	599,74	579,74	184,630573	0,03334778	3600	15	25	191	599,74	574,74	183,038217	0,04168473
25	7200	2h	16	23	191	599,74	576,74	183,675159	0,03834995	7200	16	27	191	599,74	572,74	182,401274	0,04501951
26	10800	3h	17	24	191	599,74	575,74	183,356688	0,04001734	10800	17	28	191	599,74	571,74	182,082803	0,0466869
27	14400	4h	18	25	191	599,74	574,74	183,038217	0,04168473	14400	18	29	191	599,74	570,74	181,764331	0,04835429
28	18000	5h	19	27	191	599,74	572,74	182,401274	0,04501951	18000	19	32	191	599,74	567,74	180,808917	0,05335645
29	21600	6h	20	29	191	599,74	570,74	181,764331	0,04835429	21600	20	33	191	599,74	566,74	180,490446	0,05502384
30	25200	7h	20	29	191	599,74	570,74	181,764331	0,04835429	25200	20	33	191	599,74	566,74	180,490446	0,05502384
31	86400	24h	21	34	191	599,74	565,74	180,171975	0,05669123	86400	21	34	191	599,74	565,74	180,171975	0,05669123
32	90000	25h	21	34	191	599,74	565,74	180,171975	0,05669123	90000	21	34	191	599,74	565,74	180,171975	0,05669123
33	93600	26h	21	34	191	599,74	565,74	180,171975	0,05669123	93600	21	34	191	599,74	565,74	180,171975	0,05669123
34	97200	27h	21	34	191	599,74	565,74	180,171975	0,05669123	97200	21	34	191	599,74	565,74	180,171975	0,05669123
35	100800	28h	21	34	191	599,74	565,74	180,171975	0,05669123	100800	21	34	191	599,74	565,74	180,171975	0,05669123
36	104400	29h	21	34	191	599,74	565,74	180,171975	0,05669123	104400	21	34	191	599,74	565,74	180,171975	0,05669123
37	108000	30h	22	35	191	599,74	564,74	179,853503	0,05835862	108000	22	35	191	599,74	564,74	179,853503	0,05835862
38	111600	31h	23	35	191	599,74	564,74	179,853503	0,05835862	111600	23	36	191	599,74	563,74	179,535032	0,06002601
39	115200	32h	23	35	191	599,74	564,74	179,853503	0,05835862	115200	23	36	191	599,74	563,74	179,535032	0,06002601
40	118800	33h	23	35	191	599,74	564,74	179,853503	0,05835862	118800	23	36	191	599,74	563,74	179,535032	0,06002601
41	122400	48h	23	35	191	599,74	564,74	179,853503	0,05835862	122400	23	36	191	599,74	563,74	179,535032	0,06002601
42	172800	49h	23	35	191	599,74	564,74	179,853503	0,05835862	172800	23	36	191	599,74	563,74	179,535032	0,06002601
43	176400	50h	23	35	191	599,74	564,74	179,853503	0,05835862	176400	23	36	191	599,74	563,74	179,535032	0,06002601
44	180000	51h	23	35	191	599,74	564,74	179,853503	0,05835862	180000	23	36	191	599,74	563,74	179,535032	0,06002601
45	183600	52h	23	35	191	599,74	564,74	179,853503	0,05835862	183600	23	36	191	599,74	563,74	179,535032	0,06002601
46	187200	53h	23	35	191	599,74	564,74	179,853503	0,05835862	187200	23	36	191	599,74	563,74	179,535032	0,06002601
47	190800	54h	23	35	191	599,74	564,74	179,853503	0,05835862	190800	23	36	191	599,74	563,74	179,535032	0,06002601
48	194400	55h	23	35	191	599,74	564,74	179,853503	0,05835862	194400	23	36	191	599,74	563,74	179,535032	0,06002601
49	198000	62h	23	35	191	599,74	564,74	179,853503	0,05835862	198000	23	36	191	599,74	563,74	179,535032	0,06002601
50	223200	63h	23	35	191	599,74	564,74	179,853503	0,05835862	223200	23	36	191	599,74	563,74	179,535032	0,06002601
51	226800	74h	23	35	191	599,74	564,74	179,853503	0,05835862	226800	23	36	191	599,74	563,74	179,535032	0,06002601
52	266400	86h	23	35	191	599,74	564,74	179,853503	0,05835862	266400	23	36	191	599,74	563,74	179,535032	0,06002601
53	316800	98h	23	35	191	599,74	564,74	179,853503	0,05835862	316800	23	36	191	599,74	563,74	179,535032	0,06002601
54	352800	110h	23	35	191	599,74	564,74	179,853503	0,05835862	352800	23	36	191	599,74	563,74	179,535032	0,06002601

Inner layer																
Mesure	temps(s)	P•	delta, mm	D0	P(OD) mm	Pnew	OD New	Eps	temps(s)	P••	delta, mm	D0	P(OD) mm	Pnew	OD New	Eps
1	5	1	1,5	187	587,18	585,68	186,522293	0,00255458	5	1	1,5	186	584,04	582,54	185,522293	0,00256832
2	10	2	2	187	587,18	585,18	186,363057	0,00340611	10	2	2	186	584,04	582,04	185,363057	0,00342442
3	15	3	3	187	587,18	584,18	186,044586	0,00510917	15	3	2,5	186	584,04	581,54	185,203822	0,00428053
4	20	3	3	187	587,18	584,18	186,044586	0,00510917	20	4	3	186	584,04	581,04	185,044586	0,00513663
5	30	3	3	187	587,18	584,18	186,044586	0,00510917	30	4	3	186	584,04	581,04	185,044586	0,00513663
6	40	3	3	187	587,18	584,18	186,044586	0,00510917	40	4	3	186	584,04	581,04	185,044586	0,00513663
7	50	3	3	187	587,18	584,18	186,044586	0,00510917	50	4	3	186	584,04	581,04	185,044586	0,00513663
8	60	3	3	187	587,18	584,18	186,044586	0,00510917	60	4	3	186	584,04	581,04	185,044586	0,00513663
9	120	3	3	187	587,18	584,18	186,044586	0,00510917	120	4	3	186	584,04	581,04	185,044586	0,00513663
10	180	3	3	187	587,18	584,18	186,044586	0,00510917	180	4	3	186	584,04	581,04	185,044586	0,00513663
11	240	3	3	187	587,18	584,18	186,044586	0,00510917	240	4	3	186	584,04	581,04	185,044586	0,00513663
12	300	3	3	187	587,18	584,18	186,044586	0,00510917	300	4	3	186	584,04	581,04	185,044586	0,00513663
13	360	3	3	187	587,18	584,18	186,044586	0,00510917	360	5	2	186	584,04	582,04	185,363057	0,00342442
14	420	3	3	187	587,18	584,18	186,044586	0,00510917	420	5	2	186	584,04	582,04	185,363057	0,00342442
15	480	4	2,5	187	587,18	584,68	186,203822	0,00425764	480	5	2	186	584,04	582,04	185,363057	0,00342442
16	540	4	2,5	187	587,18	584,68	186,203822	0,00425764	540	5	2	186	584,04	582,04	185,363057	0,00342442
17	600	5	1,5	187	587,18	585,68	186,522293	0,00255458	600	5	2	186	584,04	582,04	185,363057	0,00342442
18	900	5	1,5	187	587,18	585,68	186,522293	0,00255458	900	5	2	186	584,04	582,04	185,363057	0,00342442
19	1200	6	1	187	587,18	586,18	186,681529	0,00170306	1200	5	2	186	584,04	582,04	185,363057	0,00342442
20	1500	6	1	187	587,18	586,18	186,681529	0,00170306	1500	5	2	186	584,04	582,04	185,363057	0,00342442
21	1800	6	1	187	587,18	586,18	186,681529	0,00170306	1800	5	2	186	584,04	582,04	185,363057	0,00342442
22	2100	6	1	187	587,18	586,18	186,681529	0,00170306	2100	5	2	186	584,04	582,04	185,363057	0,00342442
23	2400	6	1	187	587,18	586,18	186,681529	0,00170306	2400	5	2	186	584,04	582,04	185,363057	0,00342442
24	3600	6	1	187	587,18	586,18	186,681529	0,00170306	3600	5	2	186	584,04	582,04	185,363057	0,00342442
25	7200	6	1	187	587,18	586,18	186,681529	0,00170306	7200	5	2	186	584,04	582,04	185,363057	0,00342442
26	10800	6	1	187	587,18	586,18	186,681529	0,00170306	10800	5	2	186	584,04	582,04	185,363057	0,00342442
27	14400	6	1	187	587,18	586,18	186,681529	0,00170306	14400	5	2	186	584,04	582,04	185,363057	0,00342442
28	18000	6	1	187	587,18	586,18	186,681529	0,00170306	18000	5	2	186	584,04	582,04	185,363057	0,00342442
29	21600	6	1	187	587,18	586,18	186,681529	0,00170306	21600	5	2	186	584,04	582,04	185,363057	0,00342442
30	25200	6	1	187	587,18	586,18	186,681529	0,00170306	25200	5	2	186	584,04	582,04	185,363057	0,00342442
31	86400	6	1	187	587,18	586,18	186,681529	0,00170306	86400	5	2	186	584,04	582,04	185,363057	0,00342442
32	90000	6	1	187	587,18	586,18	186,681529	0,00170306	90000	5	2	186	584,04	582,04	185,363057	0,00342442
33	93600	6	1	187	587,18	586,18	186,681529	0,00170306	93600	5	2	186	584,04	582,04	185,363057	0,00342442
34	97200	6	1	187	587,18	586,18	186,681529	0,00170306	97200	5	2	186	584,04	582,04	185,363057	0,00342442
35	100800	6	1	187	587,18	586,18	186,681529	0,00170306	100800	6	1,5	186	584,04	582,54	185,522293	0,00256832
36	104400	6	1	187	587,18	586,18	186,681529	0,00170306	104400	6	1,5	186	584,04	582,54	185,522293	0,00256832
37	108000	6	1	187	587,18	586,18	186,681529	0,00170306	108000	6	1,5	186	584,04	582,54	185,522293	0,00256832
38	111600	6	1	187	587,18	586,18	186,681529	0,00170306	111600	6	1,5	186	584,04	582,54	185,522293	0,00256832
39	115200	6	1	187	587,18	586,18	186,681529	0,00170306	115200	6	1,5	186	584,04	582,54	185,522293	0,00256832
40	118800	6	1	187	587,18	586,18	186,681529	0,00170306	118800	6	1,5	186	584,04	582,54	185,522293	0,00256832
41	122400	6	1	187	587,18	586,18	186,681529	0,00170306	122400	7	1	186	584,04	583,04	185,681529	0,00171221
42	172800	6	1	187	587,18	586,18	186,681529	0,00170306	172800	7	1	186	584,04	583,04	185,681529	0,00171221
43	176400	6	1	187	587,18	586,18	186,681529	0,00170306	176400	7	1	186	584,04	583,04	185,681529	0,00171221
44	180000	6	1	187	587,18	586,18	186,681529	0,00170306	180000	7	1	186	584,04	583,04	185,681529	0,00171221
45	183600	6	1	187	587,18	586,18	186,681529	0,00170306	183600	7	1	186	584,04	583,04	185,681529	0,00171221
46	187200	6	1	187	587,18	586,18	186,681529	0,00170306	187200	7	1	186	584,04	583,04	185,681529	0,00171221
47	190800	6	1	187	587,18	586,18	186,681529	0,00170306	190800	7	1	186	584,04	583,04	185,681529	0,00171221
48	194400	6	1	187	587,18	586,18	186,681529	0,00170306	194400	7	1	186	584,04	583,04	185,681529	0,00171221
49	198000	6	1	187	587,18	586,18	186,681529	0,00170306	198000	7	1	186	584,04	583,04	185,681529	0,00171221
50	223200	6	1	187	587,18	586,18	186,681529	0,00170306	223200	7	1	186	584,04	583,04	185,681529	0,00171221
51	226800	6	1	187	587,18	586,18	186,681529	0,00170306	226800	7	1	186	584,04	583,04	185,681529	0,00171221
52	266400	6	1	187	587,18	586,18	186,681529	0,00170306	266400	7	1	186	584,04	583,04	185,681529	0,00171221
53	316800	6	1	187	587,18	586,18	186,681529	0,00170306	316800	7	1	186	584,04	583,04	185,681529	0,00171221
54	352800	6	1	187	587,18	586,18	186,681529	0,00170306	352800	7	1	186	584,04	583,04	185,681529	0,00171221

b) Table 2: Percentage Change in Mass (Δm%) Data for Cuboid Samples with Immersion Time (7, 14, and 21 Days) in Mineral Water, B leach, and Igepal Solutions

nitial weight before immersion.						immersion for 7DAYS					
						DISTILLED WATER					
Code	M1	M2	M3	Average	Code	M1	M2	M3	M	Δm%	
63	1,994	1,994	1,994	1,994	63	1,994	1,994	1,994	1,994	0	
56	2,435	2,435	2,434	2,4346667	56	2,435	2,435	2,435	2,435	0,0136911	
59	2,178	2,178	2,178	2,178	59	2,178	2,178	2,178	2,178	0	
57	2,203	2,202	2,202	2,2023333	57	2,203	2,203	2,202	2,2026667	0,0151355	
71	2,15	2,15	2,15	2,15	71	2,15	2,15	2,15	2,15	0	
68	2,395	2,395	2,394	2,3946667	68	2,395	2,395	2,394	2,3946667	0	
Average(moyenne)				2,2256111					2,2257222	0,0048044	
						BLEACH					
Code	M1	M2	M3	Average	Code	M1	M2	M3	M		
37	2,008	2,008	2,008	2,008	37	2,009	2,009	2,009	2,009	0,0498008	
32	2,133	2,133	2,133	2,133	32	2,133	2,133	2,133	2,133	0	
33	2,115	2,114	2,114	2,1143333	33	2,113	2,114	2,113	2,1133333	-0,047296	
30	2,384	2,383	2,383	2,3833333	30	2,384	2,383	2,383	2,3833333	1,399E-07	
44	2,128	2,127	2,127	2,1273333	44	2,128	2,128	2,128	2,128	0,0313383	
47	2,146	2,146	2,146	2,146	47	2,146	2,146	2,146	2,146	0	
Average(moyenne)				2,152					2,1521111	0,0056405	
						IGEPAL					
Code	M1	M2	M3	Average	Code	M1	M2	M3	M		
1	2,156	2,156	2,156	2,156	1	2,157	2,157	2,157	2,157	0,0463822	
17	2,304	2,304	2,304	2,304	17	2,303	2,303	2,303	2,303	-0,043403	
23	2,075	2,075	2,075	2,075	23	2,075	2,075	2,074	2,0746667	-0,016064	
10	2,328	2,328	2,328	2,328	10	2,328	2,327	2,327	2,3273333	-0,028637	
11	2,189	2,189	2,189	2,189	11	2,189	2,189	2,189	2,189	0	
6	2,131	2,131	2,131	2,131	6	2,131	2,131	2,131	2,131	0	
Average(moyenne)				2,1971667					2,197	-0,006954	
						immersion for 14DAYS					
						DISTILLED WATER					
Code	M1	M2	M3	Average	Code	M1	M2	M3	M		
70	2,321	2,32	2,319	2,32	70	2,32	2,321	2,32	2,3203333	0,0143678	
72	1,911	1,912	1,911	1,9113333	72	1,912	1,912	1,911	1,9116667	0,01744	
64	2,005	2,004	2,005	2,0046667	64	2,004	2,004	2,004	2,004	-0,033256	
60	2,121	2,121	2,122	2,1213333	60	2,122	2,122	2,122	2,122	0,0314269	
69	1,917	1,917	1,917	1,917	69	1,918	1,918	1,918	1,918	0,0521648	
52	1,889	1,889	1,889	1,889	52	1,89	1,89	1,89	1,89	0,0529381	
Average(moyenne)				2,0272222					2,0276667	0,0225136	
						BLEACH					
Code	M1	M2	M3	Average	Code	M1	M2	M3	M		
38	2,231	2,23	2,231	2,2306667	38	2,231	2,231	2,231	2,231	0,0149431	
43	2,049	2,047	2,047	2,0476667	43	2,048	2,048	2,048	2,048	0,0162785	
35	2,095	2,094	2,094	2,0943333	35	2,095	2,095	2,095	2,095	0,0318321	
48	2,458	2,458	2,458	2,458	48	2,459	2,459	2,459	2,459	0,0406835	
25	1,973	1,973	1,973	1,973	25	1,973	1,973	1,973	1,973	0	
46	2,223	2,223	2,223	2,223	46	2,224	2,223	2,224	2,2236667	0,0299895	
Average(moyenne)				2,1711111					2,1716111	0,0222878	
						IGEPAL					
Code	M1	M2	M3	Average	Code	M1	M2	M3	M		
2	2,091	2,091	2,091	2,091	2	2,091	2,091	2,091	2,091	0	
12	2,284	2,284	2,284	2,284	12	2,284	2,284	2,284	2,284	0	
14	1,662	1,662	1,662	1,662	14	1,662	1,662	1,662	1,662	0	
20	1,91	1,91	1,91	1,91	20	1,91	1,911	1,91	1,9103333	0,017452	
18	2,416	2,416	2,415	2,4156667	18	2,415	2,415	2,415	2,415	-0,027598	
22	2,195	2,194	2,194	2,1943333	22	2,194	2,195	2,195	2,1946667	0,0151908	
Average(moyenne)				2,0928333					2,0928333	0,0008408	
						immersion for21DAYS					
						DISTILLED WATER					
Code	M1	M2	M3	Average	Code	M1	M2	M3	M		
58	1,938	1,937	1,937	1,9373333	58	1,937	1,938	1,937	1,9373333	1,721E-07	
50	2,593	2,593	2,593	2,593	50	2,594	2,594	2,593	2,5936667	0,0257102	
66	2,395	2,395	2,394	2,3946667	66	2,093	2,093	2,093	2,093	-0,125974	
65	2,037	2,037	2,037	2,037	65	2,037	2,037	2,037	2,037	0	
62	1,967	1,966	1,966	1,9663333	62	1,965	1,965	1,966	1,9653333	-0,050856	
53	2,382	2,383	2,382	2,3823333	53	2,382	2,382	2,381	2,3816667	-0,027984	
Average(moyenne)				2,2184444					2,168	-0,029851	
						BLEACH					
Code	M1	M2	M3	Average	Code	M1	M2	M3	M		
42	2,154	2,155	2,154	2,1543333	42	2,157	2,158	2,158	2,1576667	0,1547271	
39	1,927	1,927	1,927	1,927	39	1,929	1,929	1,929	1,929	0,1037883	
28	2,063	2,063	2,063	2,063	28	2,065	2,065	2,065	2,065	0,0969462	
27	2,272	2,272	2,272	2,272	27	2,274	2,274	2,274	2,274	0,0880282	
36	2,081	2,081	2,081	2,081	36	2,083	2,082	2,083	2,0826667	0,0800897	
34	2,056	2,056	2,056	2,056	34	2,058	2,057	2,056	2,057	0,0486381	
Average(moyenne)				1,7331667					2,0942222	0,0953696	
						IGEPAL					
Code	M1	M2	M3	Average	Code	M1	M2	M3	M		
73	1,98	1,98	1,98	1,98	73	1,98	1,979	1,98	1,9796667	-0,016835	
13	1,855	1,855	1,856	1,8553333	13	1,855	1,855	1,855	1,855	-0,017966	
81	1,979	1,98	1,98	1,9796667	81	1,979	1,98	1,979	1,9793333	-0,016838	
80	2,042	2,042	2,042	2,042	80	2,042	2,042	2,042	2,042	0	
16	2,064	2,064	2,064	2,064	16	2,064	2,064	2,064	2,064	0	
24	2,403	2,403	2,403	2,403	24	2,404	2,403	2,403	2,4033333	0,0138715	
Average(moyenne)				1,724	24				2,0538889	-0,006295	

c) Table 3.x: Mean Percentage Change in Mass (ΔM) Data for Longitudinal and Transverse HDPE Samples After 7 and 21

Code	Mi					Mt				
	M1	M2	M3	MOUY	7 Day	M1	M2	M3	MOUY	ΔM
VLEX1	6,887	6,887	6,887	6,887	VLEX1	6,887	6,886	6,886	6,88633333	0,00968007
VLEX2	7,068	7,068	7,068	7,068	VLEX2	7,067	7,067	7,067	7,067	0,01414827
VLEX3	6,814	6,814	6,813	6,81366667	VLEX3	6,814	6,814	6,813	6,81366667	4,8921E-08
VLEX4	6,768	6,769	6,768	6,76833333	VLEX4	6,769	6,769	6,769	6,769	-0,00984984
VLEX5	6,478	6,479	6,478	6,47833333	VLEX5	6,478	6,478	6,478	6,478	0,0051453
VLMX1	6,015	6,014	6,015	6,01466667	VLMX1	6,013	6,012	6,012	6,01233333	0,03879411
VLMX2	6,828	6,829	6,828	6,82833333	VLMX2	6,827	6,826	6,826	6,82633333	0,02928968
VLMX3	6,828	6,829	6,828	6,82833333	VLMX3	6,043	6,043	6,042	6,04266667	11,5059799
VLMX4	6,044	6,043	6,043	6,04333333	VLMX4	6,727	6,727	6,726	6,72666667	-11,3072257
VLMX5	6,729	6,728	6,728	6,72833333	VLMX5	7,122	7,121	7,121	7,12133333	-5,84097107
VLMX6	7,123	7,123	7,122	7,12266667	VLMX6	5,517	5,517	5,517	5,517	22,5430551
VLIX1	6,374	6,373	6,373	6,37333333	VLIX1	6,373	6,373	6,373	6,373	0,00523007
VLIX2	6,41	6,409	6,41	6,40966667	VLIX2	6,41	6,41	6,409	6,40966667	5,2005E-08
VLIX3	6,493	6,494	6,493	6,49333333	VLIX3	6,491	6,491	6,491	6,491	0,03593424
VLIX4	6,336	6,336	6,335	6,33566667	VLIX4	6,336	6,336	6,336	6,336	-0,00526117
VTEX1	6,583	6,583	6,583	6,583	VTEX1	6,583	6,583	6,583	6,583	-1,3492E-14
VTEX2	6,906	6,906	6,906	6,906	VTEX2	6,906	6,906	6,906	6,906	0
VTEX3	6,615	6,615	6,615	6,615	VTEX3	6,614	6,614	6,614	6,614	0,01511716
VTEX4	6,754	6,754	6,754	6,754	VTEX4	6,754	6,754	6,754	6,754	-1,315E-14
VTEX5	6,667	6,667	6,667	6,667	VTEX5	6,667	6,667	6,667	6,667	1,3322E-14
VTEX6	6,505	6,505	6,505	6,505	VTEX6	6,506	6,506	6,506	6,506	-0,01537279
VTMX1	6,424	6,424	6,424	6,424	VTMX1	6,421	6,421	6,421	6,421	0,04669988
VTMX2	6,825	6,825	6,824	6,82466667	VTMX2	6,916	6,916	6,916	6,916	-1,33828265
VTMX3	5,622	5,622	5,622	5,622	VTMX3	6,382	6,382	6,382	6,382	-13,5183209
VTMX4	5,98	5,98	5,979	5,97966667	VTMX4	5,795	5,795	5,795	5,795	3,08824355
VTIX1	6,381	6,381	6,381	6,381	VTIX1	6,38	6,38	6,38	6,38	0,01567152
VTIX2	5,741	5,74	5,74	5,74033333	VTIX2	5,739	5,74	5,74	5,73966667	0,01161367
VTIX3	5,964	5,963	5,962	5,963	VTIX3	5,963	5,963	5,962	5,96266667	0,00559003
VTIX4	6,11	6,109	6,109	6,10933333	VTIX4	6,109	6,108	6,108	6,10833333	0,01636834
VTIX5	6,244	6,244	6,243	6,24366667	VTIX5	6,242	6,243	6,242	6,24233333	0,02135503
cod	M1	M2	M3	MOUY	21 Day	M1	M2	M3	MOUY	ΔM
VLEY1	7,156	7,156	7,157	7,15633333	VLEY1	7,157	7,157	7,157	7,157	-0,0093158
VLEY2	7,267	7,267	7,267	7,267	VLEY2	7,267	7,267	7,267	7,267	0
VLEY3	6,619	6,619	6,619	6,619	VLEY3	6,619	6,62	6,62	6,61966667	-0,01007201
VLEY4	6,824	6,823	6,823	6,82333333	VLEY4	6,824	6,824	6,824	6,824	-0,00977044
VLEY5	6,984	6,984	6,985	6,98433333	VLEY5	6,985	6,985	6,985	6,985	-0,00954522
VLEY6	6,075	6,075	6,075	6,075	VLEY6	6,076	6,076	6,076	6,076	-0,01646091
VLMY1	6,108	6,108	6,108	6,108	VLMY1	6,108	6,107	6,107	6,10733333	0,01091465
VLMY2	6,27	6,27	6,27	6,27	VLMY2	6,27	6,27	6,269	6,26966667	0,00531632
VLMY3	5,614	5,614	5,613	5,61366667	VLMY3	5,612	5,612	5,612	5,612	0,02968951
VLMY4	5,429	5,428	5,429	5,42866667	VLMY4	5,428	5,428	5,428	5,428	0,01228055
VLMY5	5,393	5,393	5,393	5,393	VLMY5	5,394	5,394	5,393	5,39366667	-0,0123617
VLMY6	6,046	6,046	6,045	6,04566667	VLMY6	6,047	6,047	6,047	6,047	-0,02205431
VLMY7	5,723	5,723	5,723	5,723	VLMY7	5,723	5,723	5,723	5,723	0
VLIY1	5,945	5,945	5,945	5,945	VLTY1	5,946	5,946	5,946	5,946	-0,01682086
VLIY2	6,349	6,349	6,35	6,34933333	VLTY2	6,351	6,351	6,351	6,351	-0,02624953
VLIY3	5,708	5,708	5,707	5,70766667	VLTY3	5,71	5,71	5,71	5,71	-0,04088063
VLIY4	5,494	5,494	5,494	5,494	VLTY4	5,496	5,496	5,496	5,496	-0,03640335
VLIY5	5,947	5,946	5,946	5,94633333	VLTY5	5,948	5,948	5,948	5,948	-0,02802853
VTEY1	6,518	6,518	6,518	6,518	VTEY1	6,518	6,519	6,519	6,51866667	-0,01022809
VTEY2	6,518	6,517	6,517	6,51733333	VTEY2	6,519	6,518	6,518	6,51833333	-0,0153437
VTEY3	7,187	7,187	7,186	7,18666667	VTEY3	7,186	7,186	7,186	7,186	0,00927644
VTEY4	6,91	6,91	6,91	6,91	VTEY4	6,911	6,912	6,912	6,91166667	-0,02411963
VTEY5	6,793	6,793	6,74	6,77533333	VTEY5	6,74	6,739	6,739	6,73933333	0,53133917
VTMY1	6,656	6,656	6,656	6,656	VTMY1	6,825	6,824	6,824	6,82433333	-2,52904647
VTMY2	6,825	6,825	6,825	6,825	VTMY2	6,656	6,656	6,656	6,656	2,47619048
VTMY3	6,656	6,657	6,656	6,65633333	VTMY3	5,979	5,979	5,979	5,979	10,1757724
VTMY4	5,98	5,98	5,98	5,98	VTMY4	5,622	5,622	5,622	5,622	5,98662207
VTIY1	6,363	6,363	6,363	6,363	VTIY1	6,364	6,364	6,364	6,364	-0,01571586
VTIY2	6,371	6,371	6,37	6,37066667	VTIY2	6,372	6,371	6,371	6,37133333	-0,01046458
VTIY3	5,665	5,664	5,665	5,66466667	VTIY3	5,665	5,667	5,665	5,66566667	-0,01765323
VTIY4	6,392	6,391	6,391	6,39133333	VTIY4	6,392	6,392	6,392	6,392	-0,01043084
VTIY5	6,1	6,1	6,101	6,10033333	VTIY5	6,102	6,102	6,102	6,102	-0,02732097
VTIY6	5,566	5,565	5,566	5,56566667	VTIY6	5,567	5,567	5,567	5,567	-0,02395634

d) Stress-strain curves for non-immersed (A) HDPE samples, cut longitudinally (L), from the External (E), Middle (M), and Internal (I) layers of the pipe.

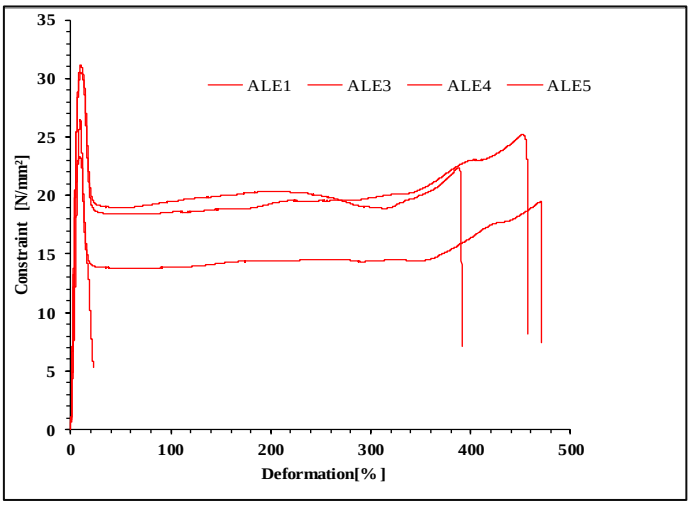

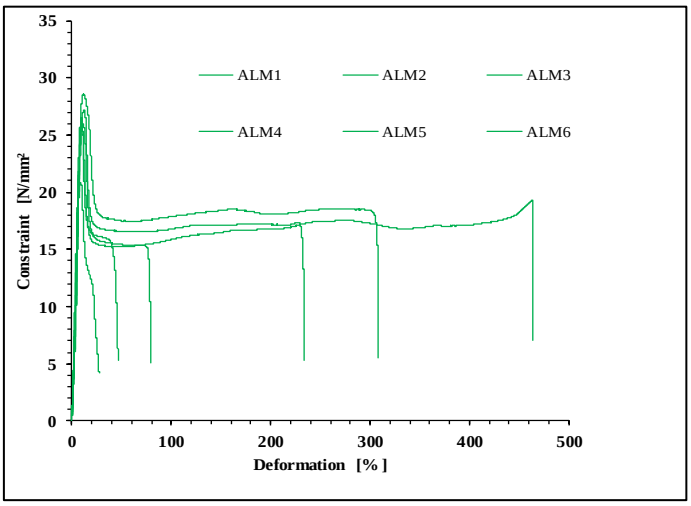

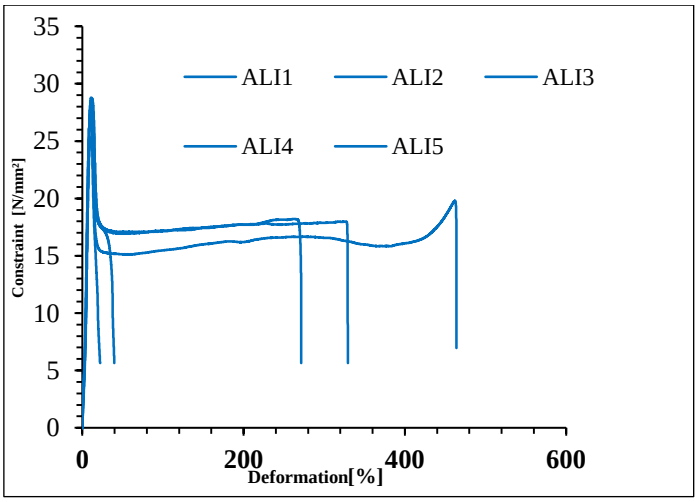

e**)** Stress-strain curves for samples immersed for 7 days (VX), cut transversely (T), from the External (E), Middle (M), and Internal (I) layers.

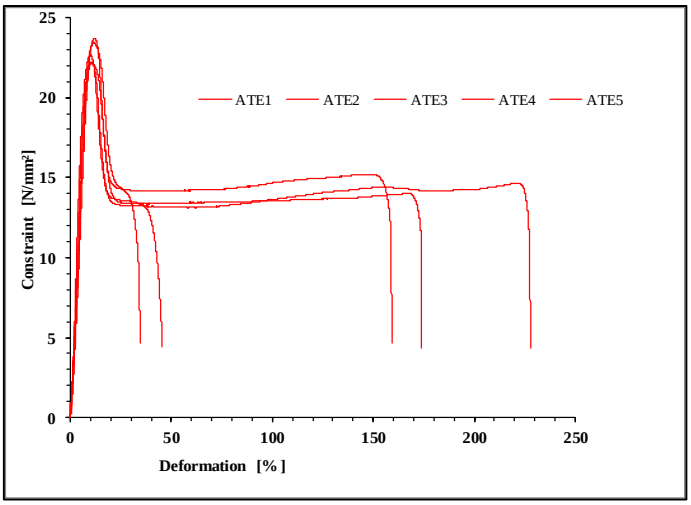

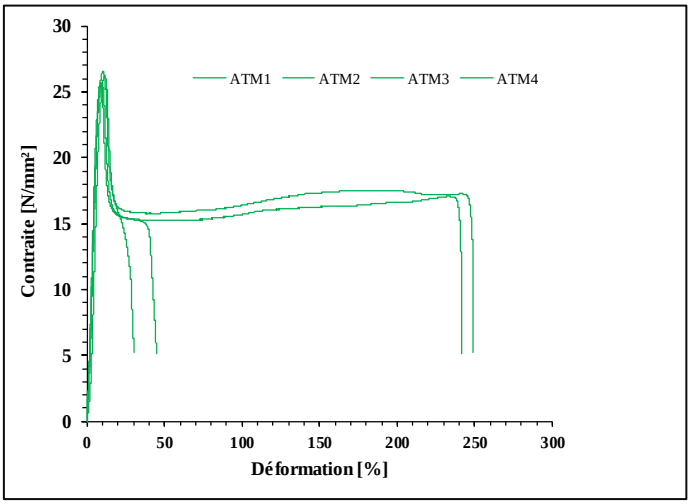

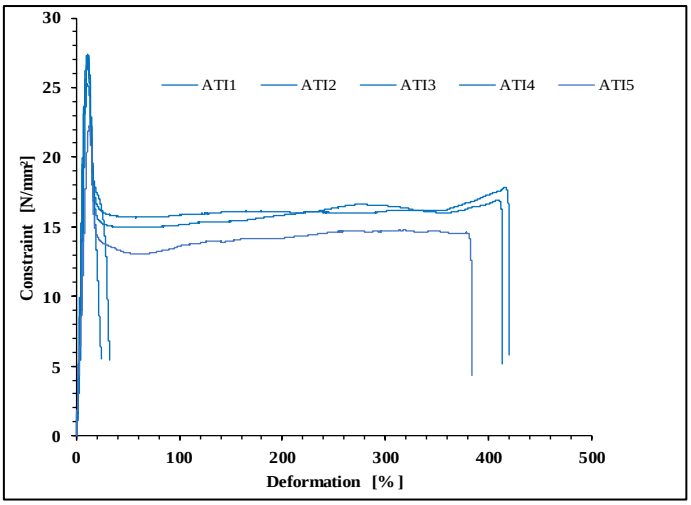

f) Stress-strain curves for samples immersed for 7 days (VX), cut longitudinally (L), from the External (E), Middle (M), and Internal (I) layers.

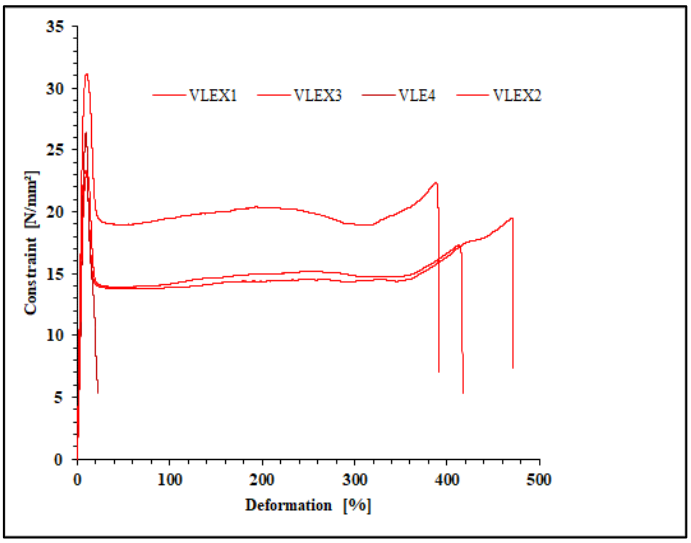

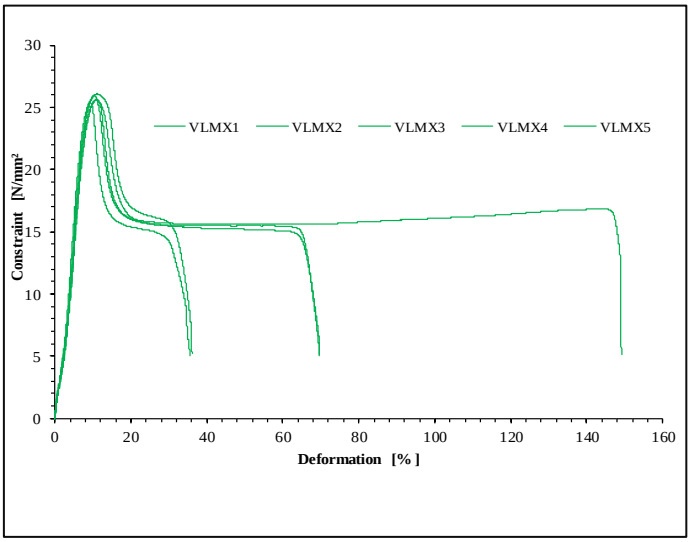

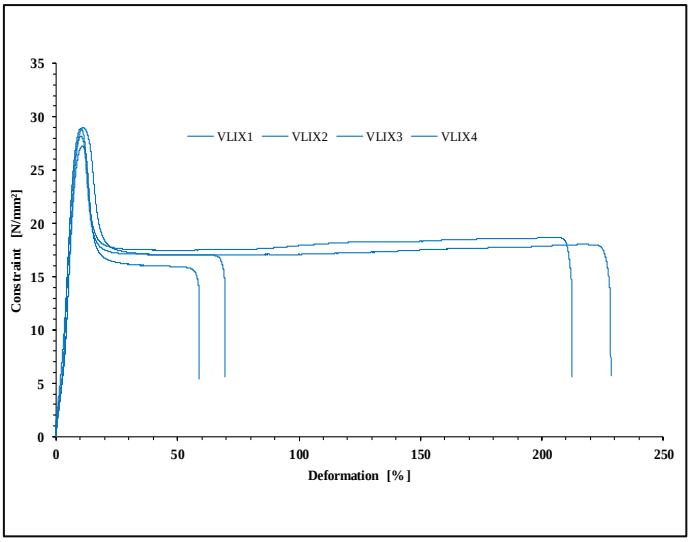

j)Stress-strain curves for samples immersed for 7 days (VX), **cut** transversely (T)**,** from the External (E), Middle (M), and Internal (I) layers

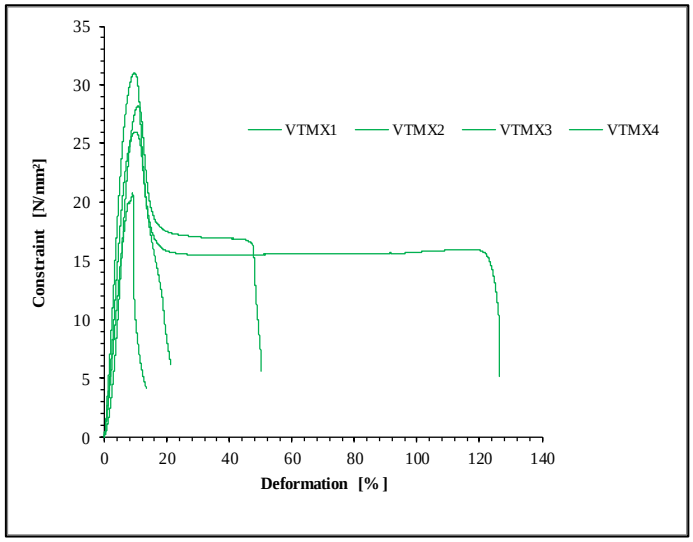

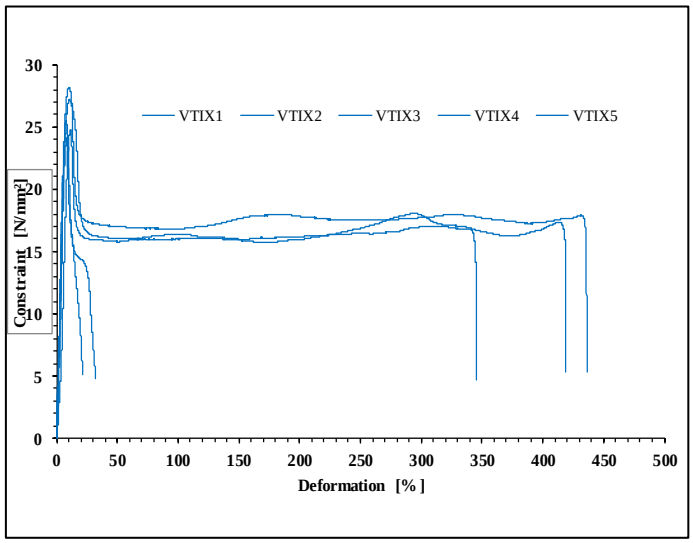

h) Stress Stress-strain curves for samples immersed for 21 days (VX), cut longitudinally (L), from the External (E), Middle (M), and Internal (I) layers.

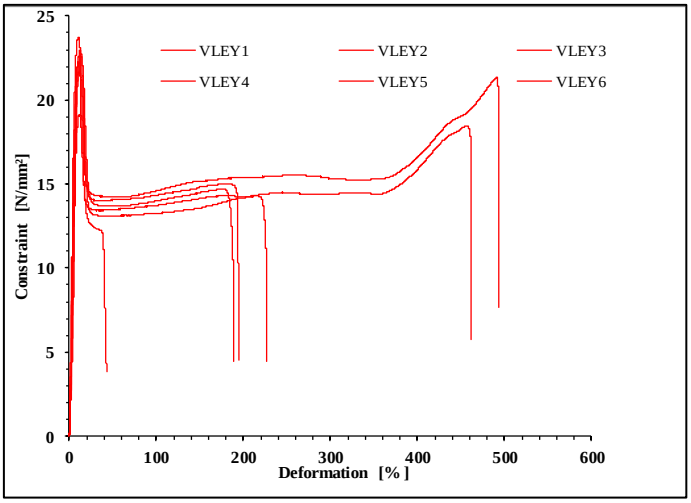

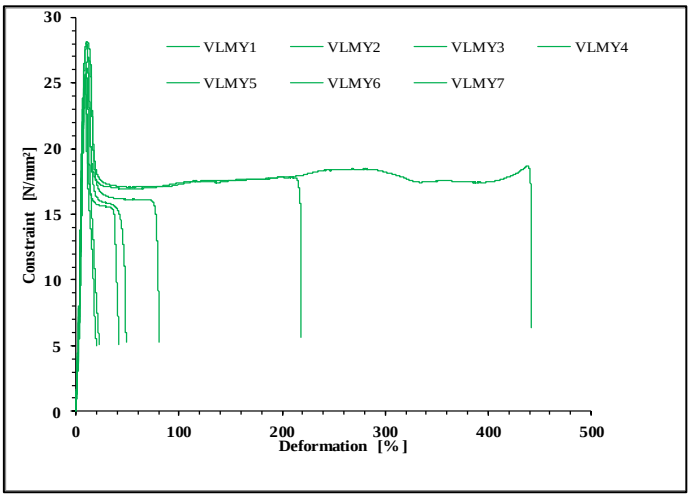

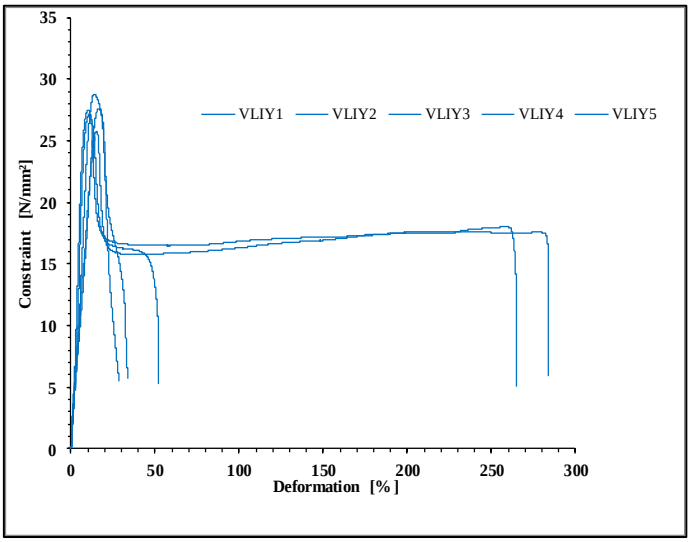

l) Stress-strain curves for samples immersed for 21 days (VX), cut transversely (T), from the External (E), Middle (M), and Internal (I) layers.

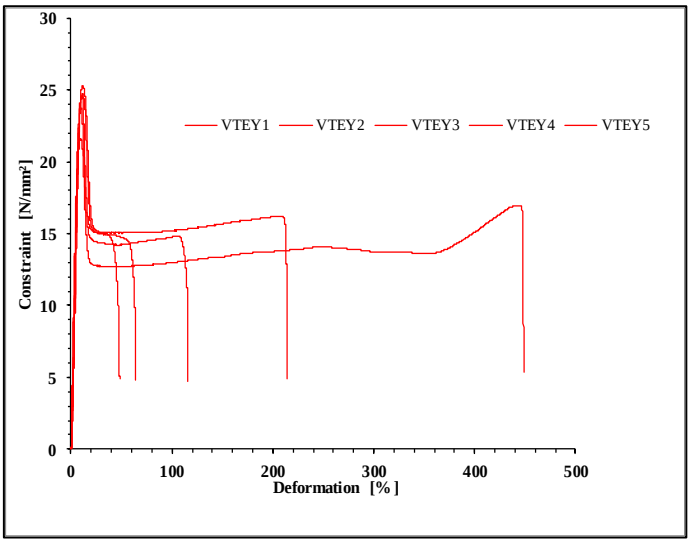

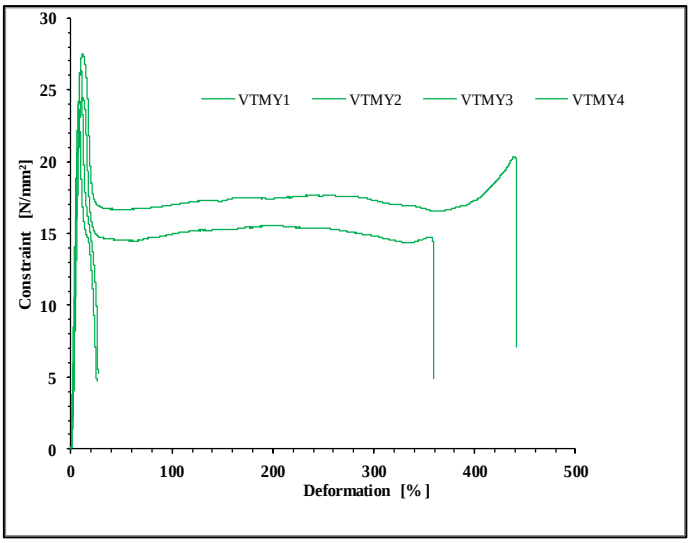

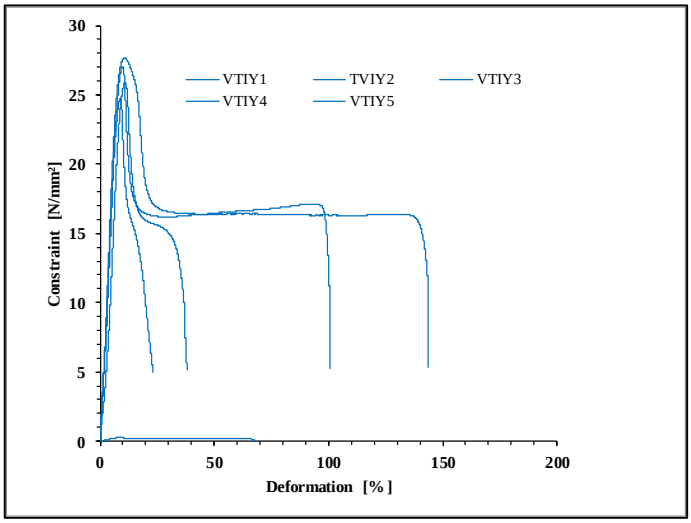

m) Table 3.x: Young's Modulus Data for Non-Immersed and Immersed (7 and 21 Days in Ejibbal Water) HDPE Samples: for Longitudinal and Transverse Samples from Outer, Middle, and Inner Layers

code	AR X1 %	h Y1 N/mm²	X2 %	Y2 N/mm²	ΔX	ΔY	E
ALE1	2,01	9,258	2,697	12,354	0,687	3,096	4,50655022
ALE2	1,994	9,787	2,697	13,18	0,703	3,393	4,82645804
ALE3	2,005	7,077	2,702	10,993	0,697	3,916	5,61836442
ALE4	9,313	25,308	10,543	26,424	1,23	1,116	0,90731707
ALE5	2,005	8,961	2,697	12,685	0,692	3,724	5,38150289
ALM1	1,979	5,406	2,677	7,393	0,698	1,987	2,84670487
ALM2	1,995	5,977	2,697	8,934	0,702	2,957	4,21225071
ALM3	1,995	4,292	2,697	5,766	0,702	1,474	2,0997151
ALM4	2,005	5,467	2,697	7,051	0,692	1,584	2,28901734
ALM5	2,01	4,608	2,697	6,008	0,687	1,4	2,03784571
ALM6	1,979	4,961	2,712	7,026	0,733	2,065	2,81718963
ALI1	2,015	3,58	2,707	4,77	0,692	1,19	1,71965318
ALI2	1,995	4,031	2,697	5,325	0,702	1,294	1,84330484
ALI3	1,985	3,917	2,707	5,144	0,722	1,227	1,69944598
ALI4	2,036	4,321	2,687	5,572	0,651	1,251	1,92165899
ALI5	2	4,519	2,692	5,793	0,692	1,274	1,84104046
ATE1	2,005	3,782	2,697	5,688	0,692	1,906	2,75433526
ATE2	2,005	5,259	2,696	8,143	0,691	2,884	4,17366136
ATE3	1,99	4,124	2,702	5,628	0,712	1,504	2,11235955
ATE4	2	4,607	2,707	6,54	0,707	1,933	2,73408769
ATE5	2,01	5,097	2,717	7,619	0,707	2,522	3,56718529
ATM1	2,005	6,229	2,717	9,026	0,712	2,797	3,92837079
ATM2	1,999	5,835	2,702	8,472	0,703	2,637	3,75106686
ATM3	2	5,175	2,697	7,713	0,697	2,538	3,64131994
ATM4	2,01	2,237	2,702	3,853	0,692	1,616	2,33526012
ATI1	1,995	3,638	2,702	5,659	0,707	2,021	2,85855728
ATI2	2	3,799	2,712	5,66	0,712	1,861	2,61376404
ATI3	2	4,494	2,707	6,758	0,707	2,264	3,20226308
ATI4	2	2,747	2,708	3,774	0,708	1,027	1,45056497
ATI5	2,01	3,919	2,697	5,119	0,687	1,2	1,74672489

code	7Day X1 %	Y1 N/mm²	X2 %	Y2 N/mm²	ΔX	ΔY	E
VLEX1	2	6,174	2,702	9,528	0,702	3,354	4,77777778
VLEX2	2	4,584	2,702	7,19	0,702	2,606	3,71225071
VLEX3	2,005	5,671	2,697	8,608	0,692	2,937	4,24421965
VLEX4	2	4,876	2,702	6,604	0,702	1,728	2,46153846
VLEX5	2,005	4,884	2,702	7,189	0,697	2,305	3,30703013
VLMX1	2	3,995	2,707	5,559	0,707	1,564	2,21216407
VLMX2	2,005	4,448	2,707	5,939	0,702	1,491	2,12393162
VLMX3	2,02	4,304	2,697	5,765	0,677	1,461	2,15805022
VLMX4	2,015	4,387	2,707	5,877	0,692	1,49	2,15317919
VLMX5	1,995	4,706	2,707	6,554	0,712	1,848	2,59550562
VLMX6	2,005	5,471	2,702	7,591	0,697	2,12	3,04160689
VLIX1	2,005	4,761	2,702	6,332	0,697	1,571	2,25394548
VLIX2	2,005	4,249	2,717	5,57	0,712	1,321	1,85533708
VLIX3	2,01	4,194	2,707	5,646	0,697	1,452	2,08321377
VLIX4	2,005	5,999	2,687	7,898	0,682	1,899	2,78445748
VTEX					0	0	#DIV/0!
VTMX1	2,005	2,953	2,697	4,785	0,692	1,832	2,64739884
VTMX2	2,025	6,117	2,702	8,834	0,677	2,717	4,01329394
VTMX3	2,005	8,305	2,697	11,604	0,692	3,299	4,76734104
VTMX4	2	5,123	2,702	7,413	0,702	2,29	3,26210826
VTIX1	2,005	5,487	2,697	7,969	0,692	2,482	3,5867052
VTIX2	2,01	6,289	2,687	9,134	0,677	2,845	4,20236337
VTIX3	2,005	7,904	2,697	10,901	0,692	2,997	4,33092486
VTIX4	2	6,894	2,707	9,776	0,707	2,882	4,07637907
VTIX5	2	2,725	2,707	3,897	0,707	1,172	1,65770863

21Day						
X1 %	Y1 N/mm²	X2 %	Y2 N/mm²	ΔX	ΔY	E
1,995	3,776	2,697	5,901	0,702	2,125	3,02706553
2,01	6,154	2,697	9,111	0,687	2,957	4,30422125
1,984	2,751	2,707	3,84	0,723	1,089	1,50622407
1,979	4,287	2,707	6,754	0,728	2,467	3,38873626
2	3,475	2,707	4,958	0,707	1,483	2,09759547
2	4,717	2,707	6,726	0,707	2,009	2,84158416
2	5,148	2,692	6,995	0,692	1,847	2,66907514
2,01	3,6	2,707	4,917	0,697	1,317	1,88952654
2	4,541	2,692	6,3	0,692	1,759	2,54190751
2,015	4,924	2,702	7,034	0,687	2,11	3,0713246
2,005	4,182	2,707	5,934	0,702	1,752	2,4957265
2,01	4,311	2,712	5,972	0,702	1,661	2,36609687
1,995	4,411	2,702	6,098	0,707	1,687	2,38613861
2	4,58	2,697	6,077	0,697	1,497	2,14777618
2	5,747	2,702	8,253	0,702	2,506	3,56980057
2	4,168	2,697	5,561	0,697	1,393	1,99856528
1,99	4,408	2,712	5,844	0,722	1,436	1,98891967
2	4,681	2,702	6,407	0,702	1,726	2,45868946
1,995	4,27	2,702	6,053	0,707	1,783	2,52192362
1,995	4,807	2,697	6,805	0,702	1,998	2,84615385
2,01	4,072	2,702	6,489	0,692	2,417	3,49277457
1,999	7,038	2,712	9,81	0,713	2,772	3,88779804
1,995	6,82	2,707	9,468	0,712	2,648	3,71910112
1,995	2,683	2,707	4,487	0,712	1,804	2,53370787
2,01	4,052	2,707	6,229	0,697	2,177	3,12338594
2,005	4,426	2,707	6,556	0,702	2,13	3,03418803
2,005	6,303	2,697	9,196	0,692	2,893	4,18063584
2,005	5,835	2,697	8,009	0,692	2,174	3,1416185
2,015	6,043	2,707	8,644	0,692	2,601	3,75867052
2,015	3,455	2,712	4,882	0,697	1,427	2,04734577
1,995	5,846	2,697	8,072	0,702	2,226	3,17094017
2,005	0,063	2,707	0,09	0,702	0,027	0,03846154
2,005	5,472	2,727	8,319	0,722	2,847	3,9432133